Tampere University

JIYEONG KIM

Computational Analysis of Complex Beat-to-Beat Dynamics in Heart Cells

Tampere University Dissertations 742

Tampere University Dissertations 742

JIYEONG KIM

Computational Analysis of Complex Beat-to-Beat Dynamics in Heart Cells

ACADEMIC DISSERTATION
To be presented, with the permission of
the Faculty of Engineering and Natural Sciences
of Tampere University,
for public discussion in the auditorium S2
of the Sähkötalo building, Korkeakoulunkatu 3, Tampere,
on 20 January 2023, at 12 o'clock.

ACADEMIC DISSERTATION
Tampere University, Faculty of Engineering and Natural Sciences
Finland

Responsible supervisor and Custos	Professor Esa Räsänen Tampere University Finland	
Pre-examiners	Professor Mikko Alava Aalto University Finland	Senior Lecturer Steven Williams University of Edinburgh United Kingdom
Opponent	Professor Elaine Chew King's College London United Kingdom	

The originality of this thesis has been checked using the Turnitin OriginalityCheck service.

Cover design: Roihu Inc.

ISBN 978-952-03-2750-7 (print)
ISBN 978-952-03-2751-4 (pdf)
ISSN 2489-9860 (print)
ISSN 2490-0028 (pdf)
http://urn.fi/URN:ISBN:978-952-03-2751-4

Carbon dioxide emissions from printing Tampere University dissertations have been compensated.

PunaMusta Oy – Yliopistopaino
Joensuu 2023

To my baby Lotto,
I cannot wait to welcome you into this world!

PREFACE

The research for this thesis was carried out at the Computational Physics Laboratory in the Faculty of Engineering and Natural Sciences, Tampere University, in close collaboration with the Heart Group at BioMediTech in the Faculty of Medicine and Health Technology, Tampere University.

I am eternally grateful to my supervisor and mentor, Esa Räsänen, who never stopped believing in me and showed me endless support and encouragement that I needed through this challenging but meaningful journey in my career. Thank you for going above and beyond in your support. I could not have come this far without your guidance and positive energy. You have always been such a caring supervisor and I cannot thank you enough.

I would like to acknowledge with gratitude my collaborators at the Heart group for their excellent experimental work. I am deeply grateful to Katriina Aalto-Setälä for her expertise and guidance in the projects, and to Jukka Kuusela, Disheet Shah, and Aliisa Lönnrot for producing and sharing the cell data that was essential to this work.

I also wish to thank all my colleagues in Quantum Control and Dynamics group, whom I had the pleasure to interact every day and to study and work with. I am particularly grateful to Matti Molkkari and Perttu Luukko for all the help in research and technical support, whenever I was stuck in some computer/code-related problems. I am also thankful to Ilya Potapov and Joonas Latukka for valuable collaborations, and to Joonas Keski-Rahkonen, Janne Solanpää, Rostislav Duda, Alexander Odriazola-Diaz for all the helps and good memories I received in my earlier days in the group. In addition, I would like to extend my gratitude to Teemu Pukkila and Matias Kanniainen for the discussions and collaboration in our recent heart projects.

I acknowledge several organizations including Tampere University, the Finnish Academy of Science and Letters, Magnus Ehrnrooth foundation, Orion Research Foundation, and Business Finland, for funding my research. I also thank my pre-examiners, Professor Mikko Alava, Aalto University, and Senior Lecturer Steven Williams, University of Edinburgh, United Kingdom for their detailed feedback on this thesis. I extend my gratitude also to Anna Nykänen for helping me navigate the dissertation-related process.

Special thanks to my family and friends for their faith and support, and especially to Christine, Daniel, Eddie, Lavanya, Mandy, and Paul for proofreading this thesis and having fun together.

Finally, I am grateful to my life partner Mikko Poikkimäki, who has been here for me from the very beginning of this journey. I have received so much love and support from you.

Jiyeong Kim
January 2023, Tampere

ABSTRACT

Contrary to the popular belief that the heart maintains a regular rhythm, healthy heartbeats fluctuate in a chaotic way. We now know that the fluctuations do not display uncorrelated randomness, but they contain long-range correlations and can be characterized by a fractal. This behavior supports the adaptability of the heart and may thus protect it from external stress. The fractal complexity is also found in the smallest parts of the heart: the cells. In the dawn of advanced pluripotent stem cell technology, producing independently beating cardiomyocytes in a laboratory, the beat-rate fluctuations of heart cells can be directly studied.

In this thesis, we investigate the complex fluctuations in the field potentials generated by clusters of human cardiomyocytes. We show that the heart cells exhibit similar correlation properties in the beat-to-beat intervals and field potential durations comparable to RR and QT intervals, i.e., time between consecutive R waves and time from Q wave to the end of T wave, respectively, in an electrocardiogram of a heart. The cells are studied under conditions resembling real-life situations such as cardiac disorders, application of cardioactive drugs, and injuries. The results show significant alteration of the scaling properties in the beat rates, reflecting the changes in the intrinsic mechanism at the cellular level.

By employing a set of nonlinear time series analysis tools, we explore their powerful applicability as well as their limitations. Our main method of choice throughout the work is detrended fluctuation analysis, which is designed to detect the degree of correlation in nonstationary time series. We demonstrate that detrended fluctuation analysis and its extensions are extremely useful in dealing with the field potential data of the heart cells despite the presence of abnormalities and irregular trends. The study of heartbeat dynamics at the cellular level using computational methods has important advantages. In particular, the methods provide non-invasive and versatile ways to improve our understanding of the intrinsic firing patterns of the heart cells, which play a crucial role in the future applications of *in vitro* human cardiomyocytes.

CONTENTS

LIST OF SYMBOLS AND ABBREVIATIONS

α_1	Short-term scaling exponent
α_2	Long-term scaling exponent
ANS	Autonomous nervous system
APD	Action potential duration
ARFIMA	Autoregressive fractionally integrated moving average
ARIMA	Autoregressive integrated moving average
BR	Beat rate
BRV	Beat rate variability
cFPD	Corrected FPD
CM	Cardiomyocyte
DDFA	Dynamical detrended fluctuation analysis
DFA	Detrended fluctuation analysis
ECG	Electrocardiogram
ESC	Embryonic stem cell
FBM	Fractional Brownian motion
FGN	Fractional Gaussian noise
FPD	Field potential duration
hESC	Human embryonic stem cell
HF	High frequency power
hiPSC	Human-induced pluripotent stem cell
hiPSC-CM	Human-induced pluripotent stem cell-derived cardiomyocyte

HR	Heart rate
HRV	Heart rate variability
HYPOX	Hypoxia
IBI	Interbeat interval
iPSC	Induced pluripotent stem cell
LF	Low frequency power
LQTS	Long QT syndrome
LRC	Long-range correlation
MEA	Multielectrode array
MSE	Multiscale entropy
PNS	Parasympathetic nervous system
QT	Time from the start of the Q wave to the end of the T wave of the QRS signal on the electrocardiogram
REOX	Reoxygenation (reperfusion)
RMS	Root-mean-square
RMSSD	Root-mean-square of successive differences
RR	Time between two successive R-waves of the QRS signal on the electrocardiogram
SAN	Sanoatrial node
SDNN	Standard deviation of normal-to-normal beats
SNS	Sympathetic nervous system
SRC	Short-range correlation
WT	Wild type

LIST OF PUBLICATIONS

Publication I — J. Kuusela, J. Kim, E. Räsänen, and K. Aalto-Setälä, "The effects of pharmacological compounds on beat rate variations in human long QT-syndrome cardiomyocytes," *Stem Cell Reviews and Reports*, vol. 12, no. 6, pp. 698–707, 2016. DOI: 10.1007/s12015-016-9686-0.

Publication II — J. Kim, I. Potapov, D. Shah, J. Kuusela, K. Aalto-Setälä, and E. Räsänen, "Intrinsic complexity of RR and QT intervals at the cellular level," in *Computing in Cardiology*, C. Pickett, Ed., vol. 45, IEEE, 2018, pp. 1–4. DOI: 10.22489/CinC.2018.179.

Publication III — J. Kim, D. Shah, I. Potapov, J. Latukka, K. Aalto-Setälä, and E. Räsänen, "Scaling and correlation properties of RR and QT intervals at the cellular level," *Scientific Reports*, vol. 9, no. 1, pp. 1–9, 2019. DOI: 10.1038/s41598-019-40247-9.

Publication IV — J. Kim, D. Shah, M. Molkkari, A. Lönnrot, K. Aalto-Setälä, and E. Räsänen, "Beat rate variability in human cardiomyocytes during hypoxia and reperfusion," *PLOS One*, 2023, Submitted.

Author's contribution

Publication I — J. Kim carried out the computational analysis, visualized the results, and contributed to the writing of the manuscript. J. Kuusela designed and performed the experiments and wrote the first draft of the manuscript. E. Räsänen and K. Aalto-Setälä supervised the work and participated in writing and revising the manuscript.

Publication II — J. Kim wrote the first draft of the manuscript and is the corresponding author. J. Kim carried out the computational analysis and interpreted the results. D. Shah and J. Kuusela provided the experimental data. I. Potapov processed the PhysioNet ECG data and participated in the revision of the manuscript. K. Aalto-Setälä and E. Räsänen supervised and revised the work.

Publication III — J. Kim wrote the first draft of the manuscript and is the corresponding author. J. Kim carried out the computational analysis and interpreted the results. D. Shah performed the experiments and contributed to the writing of the manuscript. I. Potapov and J. Latukka extracted and processed the PhysioNet ECG data and participated in the revision of the manuscript. The work was carried out under the supervision of K. Aalto-Setälä and E. Räsänen.

The publication has been previously included in the doctoral dissertation "Heart disease on a dish" by Disheet Shah, Tampere University, 2020. D. Shah and J. Kim have distinctive contributions to the publication.

Publication IV — J. Kim wrote the first draft of the manuscript and is the corresponding author. J. Kim and M. Molkkari performed the computational analysis and interpreted the results. D. Shah designed the experiment. D. Shah and A. Lönnrot carried out the measurements. All the authors revised the manuscript. The work was carried out under the supervision of K. Aalto-Setälä and E. Räsänen.

1 INTRODUCTION

1.1 Overview

The research presented in this thesis is inspired by the beautiful complexity found in our heartbeats. As elaborated in detail below, a healthy human heart exhibits fractal characteristics, which can be observed even at the cellular level.

A fractal refers to a structure that exhibits self-similar patterns across different scales. Since long before the mathematician Benoît Mandelbrot invented the term "fractal" in 1975 [1], the concept has fascinated and inspired many mathematicians, scientists, and artists alike. Fractals are found everywhere around us, and many complex patterns in nature are best modeled by a fractal geometry as illustrated in Fig. 1.1 [2].

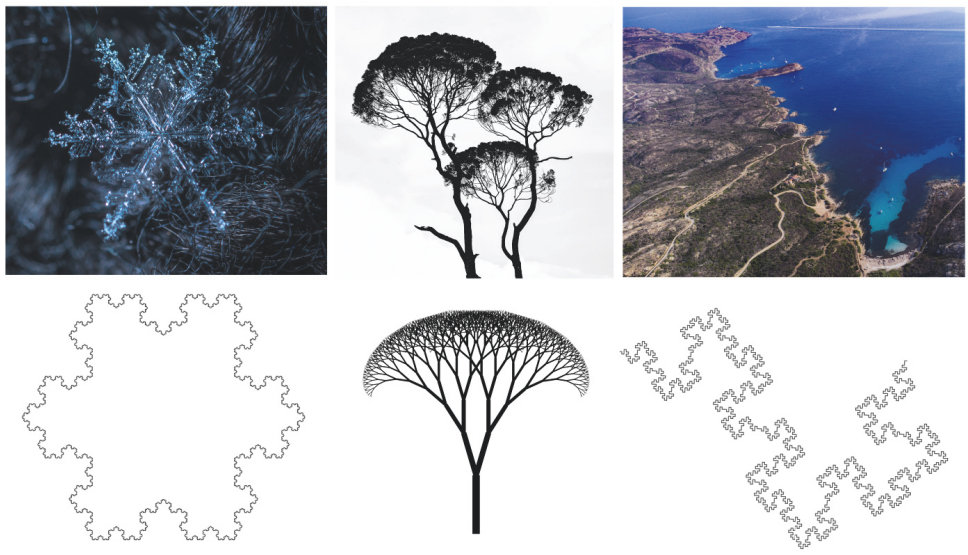

Figure 1.1 Natural and generated fractals. Complex self-similar patterns are found in many places in nature, e.g., snowflakes, tree branches, and coastlines (top). The natural patterns are best modeled by fractal geometries (bottom).

Fractals are also realized in non-geometrical forms. A time series is a sequence of observables measured in time, or time-like, order. A time series generated by a complex system contains important information about the nonlinear dynamics that govern the system. Such time series are often characterized by a scaling law. Following Mandelbrot's pioneering work in fractal analysis of natural time series [3], [4], fractal scaling has been identified in real-world data within numerous complex systems, such as the structure of DNA [5], recordings of rainfall [6] and ozone levels [7], transport in quantum dots [8], fluctuations in human gait [9] and heart rate [10], [11], price fluctuations in financial markets [12], and rhythms of drum beats and musical groove [13], [14]. Fractal analysis and the related methods continue to be applied and refined in numerous studies; according to Google Scholar, in the last decade (2012-2022), more than half a million scientific works related to fractal time series analysis have been published.

Quantification of fractality in a natural complex system is useful for modeling the dynamics and behaviors of the system. Though the origin of the fractal features is not always obvious, it is often suggested that the most optimal and efficient systems are associated with fractals [2], [15], [16]. A well-known example is the branching of the blood vessels in the lung; the fractal branching structure allows a large surface area to fit in a limited space in the lung[1], resulting in the most efficient oxygen delivery. In physiological systems, nonlinear complexity is often related to the autonomous regulation and robustness of the system. For example, the heart, a muscular organ consisting of many parts working in unison through coordinated electrical and mechanical activities, is one of the most complex systems in our body. It is connected to the autonomous nervous system (ANS), of which the sympathetic and parasympathetic branches accelerate and slow the heart rate, respectively. Fractal analysis has been successful in distinguishing sleep stages [18] and identifying the alteration in the fractal scaling due to aging and heart diseases, which reduce the heart's adaptive capacity against external stress [10], [11].

Furthermore, fractal characteristics similar to those found in the functioning heart are also observed in human heart cells without any neural input from ANS [19]. The study of the beat dynamics of isolated human heart cells is made possible today by virtue of recent advancements in stem cell technology. According to the rev-

[1] In fact, a pair of lungs is extremely compact. To be more precise, a surface area of 130 m^2 fits into a volume of 5 liters [17].

olutionary scheme that led to the Nobel Prize in Medicine in 2012, human-induced pluripotent stem cells (hiPSC) can be obtained from adult tissues, such as skin and hair, and give rise to any cell type in the body, such as heart cells [20]. The hiPSC-derived heart muscle cells, or cardiomyocytes (CM), beat spontaneously producing action potential similar to that of the heart. As we will demonstrate throughout this thesis, hiPSC-derived CMs provide an exciting platform to study the fractal properties of the intrinsic firing patterns of the cells and the effects of hereditary diseases, drugs, and other external perturbations.

Because human heart cells are a relatively new realm for fractal analysis, there has been only a limited number of studies available on the topic. However, the surprising and important results so far suggest that fractality in the heart is intrinsic to its nature at the cellular level. This result has motivated further investigation and studies presented in this thesis.

1.2 Research objectives

The goal of this research is to establish a deeper understanding of the fractal dynamics of the heart at the cellular level by quantifying the complexity using advanced, state-of-the-art computational methods. These studies are extremely important in establishing hiPSC-derived CMs as a physiologically valid model of the heart, which, in the long run, can lead to advancements in cardiac disease modeling and drug safety assessments, as well as novel applications, such as biological pacemakers [19]. Our main objectives are:

1. provide detailed descriptions of fractal and other nonlinear properties in beat dynamics of hiPSC-CMs, in comparison to those of the heart
2. investigate the effects of important factors that are known to affect the functionality of the heart, such as (hereditary) cardiac disorders, drug exposure, and hypoxia, on the fractal scaling properties
3. establish a set of advanced computational tools suitable for characterizing the complexity of the cellular level beat rate variability

Objective 1 is addressed in Publications I-III, in which the signals from the cells are studied alongside the signals from human subjects. Objective 2 is addressed in Publication I for the presence of a genetic mutation and application of drugs, in Pub-

lication IV for prolonged hypoxia, and briefly in Publication II for the presence of a genetic mutation using a different method. Objective 3 is addressed across Publications I through IV, in which the conventional and novel computational methods and our newly improved algorithms, are applied to analyze the cell data.

1.3 Structure of the thesis

Chapters 2 and 3 provide painless introductions to the concepts relevant to this thesis. Chapter 2 discusses the basic concepts and characteristics of fractals and long-range correlation, along with historical accounts of how they have developed. We discuss how the concepts are applied to cardiology, highlighting the multidisciplinary character of the research. In Chapter 3, we introduce new stem cell technology and how human heart cells are generated and measured in a laboratory for the studies presented in this thesis. We also discuss the status of research with human CMs that is relevant to this thesis. Next, in Chapter 4, we describe the important methods in nonlinear time series analysis, including conventional and state-of-the-art methods used in this thesis. In Chapter 5, we discuss the key findings from the publications, which are revised and supplemented as necessary. The current limitations of the studies are discussed. We conclude in Chapter 6 with a brief summary and future perspectives.

2 PHYSICS OF FRACTAL TIME SERIES

The study of fractal behaviors has proven to be extremely versatile across multiple disciplinary fields and is deeply rooted in chaos theory. Section 2.1 provides a brief historical account of the development of chaos theory and how the concept of fractals emerged. In the sections that follow, important concepts and characteristics of fractals are introduced.

2.1 Chaos theory and fractals

Most people are familiar with the term "butterfly effect": a flap of a butterfly's wing at a precise moment and location causes a hurricane on a continent across the ocean [21]. This well-known expression captures the complexity and unpredictability of nature, one of the underlying principles of chaos theory. Chaos does not mean randomness. On the contrary, the theory states that in what appears to be a completely irregular and unpredictable system, underlying patterns and order can be found.

Though the word "chaos" had not been used in this context yet, the earliest accounts of chaos theory date back to the 1880s by Henri Poincaré in his study of the three-body problem[1] He discovered that a small change in the initial positions and velocities set the three masses in very different paths, making the long-term prediction of their motions impossible [22]. In the 1950s, when electronic computers became available for lengthy, iterative calculations necessary for the simulations of chaotic systems, chaos theory started to flourish. In 1961, mathematician and meteorologist Edward Lorenz discovered that a certain solution to his model for atmospheric convection formed a curve that continuously spiraled around two points while never crossing its own path [23]. This peculiar solution, later known as the "Lorenz attractor" (Fig. 2.1 (a)), was also highly sensitive to changes in the initial conditions,

[1]The problem of solving the motions of three point masses (e.g., sun, earth, and moon) with their initial positions and velocities, which satisfy Newton's law of motions and Newton's law of universal gravitation.

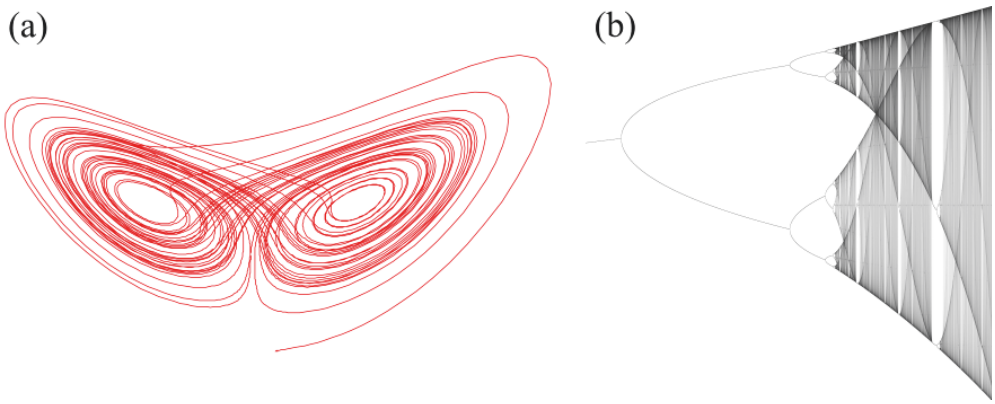

Figure 2.1 An example of (a) the Lorenz attractor and (b) bifurcation diagram. Both belong to chaotic systems that exhibit fractal characteristics.

leading to the conclusion that it could not make precise weather predictions. Around the same time, Robert May, a theoretical ecologist, was reaching similar conclusions during his effort to model animal populations [24]. James Yorke, who saw the potential connection between Lorenz's and May's works, examined May's population model further and presented his bifurcation diagrams (Fig. 2.1 (b)) in 1975, using the words "chaos" and "chaotic" to describe the behavior of the system [25].

The aforementioned Lorenz attractors and bifurcation diagrams, as well as many chaotic systems in nature, share a common feature – *fractals*[2]. A fractal is a geometrical shape consisting of detailed fragments at arbitrarily small scales, that are similar to the whole. They are representable by a fractal set, which is more rigorously defined as having the Hausdorff (fractional) dimension[3] strictly exceeding the topological dimension [2]. Chaos and fractal are not synonyms, but they are closely related. Systems that behave chaotically are often described or visualized by fractal characteristics, in particular, infinitely repeating patterns across different scales, i.e., self-similarity.

[2]It may not be too obvious to recognize why the Lorenz attractor is fractal. It comes from the fact that it consists of an infinite number of surfaces in order for the curves to never intersect, therefore having a non-integer fractal dimension; the interested reader is referred to, e.g., Ref. [2], [26], [27] for more details.

[3]Discussion of fractal dimensions is beyond the scope of the thesis, however, it is very interesting and can be read further in, e.g., Ref. [2], [28].

2.2 Self-similarity and scaling law

Studying scaling properties of a function $f(x)$ involves considering how the function changes under rescaling of the variable x to, e.g., λx. Self-similarity of a fractal indicates scale-invariance, which means that the patterns do not change when the scales are changed, e.g., by magnification. In less strict terms, the concept extends to "statistical self-similarity" in which statistical properties are the same at many scales, as is the case for coastlines [29].

It is also possible for time-dependent functions and probability distributions of stochastic processes to exhibit self-similarity, which may be realized in a time series. A time series is a collection of ordered data points. The values of a time series are produced by an underlying mechanism that drives the system; in other words, by studying a time series, one can learn about the dynamics of the system. However, time series data collected from the real world bring many challenges. Natural systems are governed by nonlinear dynamics, which means they produce complicated and irregular values that appear impossible to extrapolate. However, as we have been enlightened by chaos theory, there are often indeed underlying patterns to be found.

Many such time series are characterized by a scaling law, i.e., a power law with a scaling exponent,

$$F(s) \sim s^{\alpha}, \tag{2.1}$$

which is a characteristic of fractals. Fractal geometry in the context of stochastic processes refers to statistical self-similarity in time scales, rather than in length scales (Fig. 2.2).

Fractal time series, in a more general sense, include those that are self-affine, meaning that they require different rescaling factors for the time axis t and the axis of the values $x(t)$ to achieve statistical self-similarity, described by the relation

$$x(at) \simeq a^{H} x(t) \tag{2.2}$$

for an arbitrary rescale factor a and the Hurst exponent H, named after the hydrologist Harold E. Hurst for his findings of the scaling relation in the river flow of the Nile basin [30]. Therefore, any time series characterized by a reasonable choice of H may be referred to as "fractal" [31].

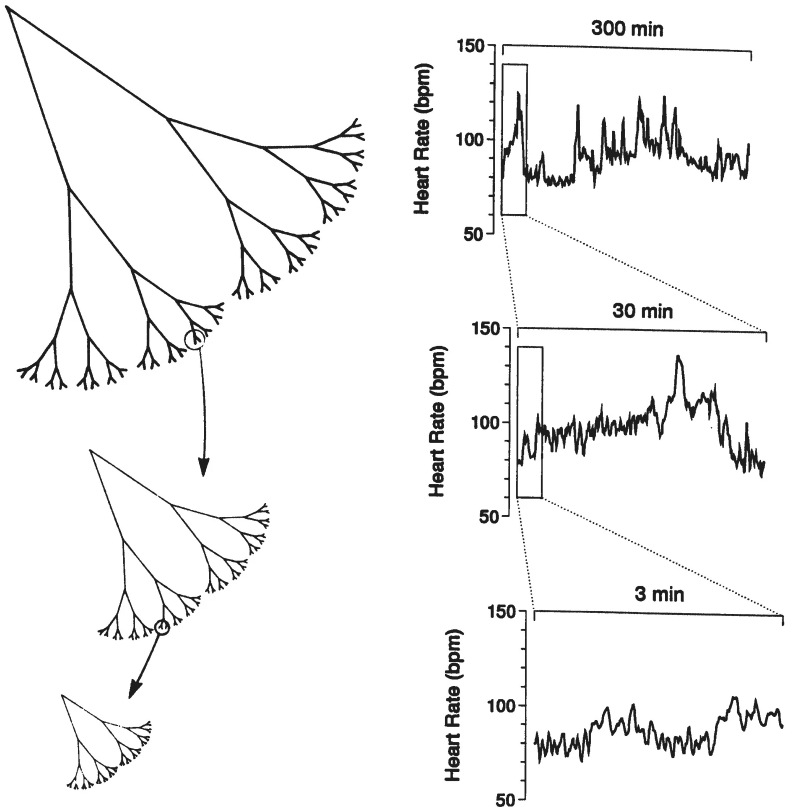

Figure 2.2 Geometrically self-similar structure of a fractal canopy vs. temporal self-similar dynamics of heart rate (Reprinted from Ref. [11], copyright (2002) National Academy of Sciences).

2.3 Long-range correlation

2.3.1 Characterization of long-range correlation

Self-similarity in fractal time series reflects the presence of long-range correlation (LRC). LRC is also commonly known as long-range dependence, long memory, or persistence. LRC describes non-negligible statistical dependence between two data points in a wide range of scales. Consider a discrete scalar series $\{x_i\}$, $i = 1, ..., N$. Increments in the series $\Delta x_i = x_i - x_{i-1}$ may be completely independent of each other or they may be correlated. A formal way to determine the degree of correlation in a stationary time series is by looking at the behavior of the auto-covariance function

of the increments,

$$C(s) = \frac{1}{N-s} \sum_{i=1}^{N-s} \Delta x_i \Delta x_{i+s} \tag{2.3}$$

for the lag s between the increments [31]. For uncorrelated series, $C(s) = 0$ for $s > 0$. For a typical (stationary) stochastic process with short-range correlated increments, the auto-covariance function decays exponentially,

$$C(s) \sim \exp(-s/\tau) \tag{2.4}$$

with a characteristic decay time τ. On the other hand, for long-range correlated (stationary) series, the autocorrelation function (2.3) decays much more slowly, typically displaying power-like decay, i.e.,

$$C(s) \propto s^{-\gamma} \tag{2.5}$$

with the correlation exponent $0 < \gamma < 1$, which is related to the Hurst exponent in Eq. 2.2 by $H = 1 - \gamma/2$. Because the integral $\int_0^\infty C(s)\, \mathrm{d}s$ diverges at infinity, there is no characteristic time scale.

2.3.2 A brief history of long memory

In his study of floods and irregular river flow in the Nile basin in Egypt, H. E. Hurst made an important discovery that led to the concept of long memory [30], [32]. He defined a statistic of the cumulative flows of the river over time, called the adjusted range (R), normalized by the standard deviation (S), to obtain rescaled adjusted range ($R/S(n)$) for the scale n. He observed that these particular statistics empirically followed a power-law,

$$R/S(n) \propto n^k \tag{2.6}$$

for some k, of which the mean was 0.72 ± 0.006. This empirical result was contrary to the prediction of the theoretical model, in which $k = 0.5$ under the assumption of independent Gaussian data[4]. The discrepancy, later named the Hurst phenomenon, remained a riddle until Mandelbrot applied the idea of scaling and self-similarity to

[4]Hurst's data was indeed Gaussian.

develop the fractional Brownian motion (FBM) model and its incremental process, the fractional Gaussian noise (FGN) [33]. Despite being stationary and Gaussian, the FGN model was able to reproduce the Hurst phenomenon. The correlation structure that FGN exhibits, namely, having the auto-correlation function's integral diverge at infinity, became a generally accepted definition of LRC. While Mandelbrot's FGN model was successful in reproducing the Hurst phenomenon, the physical interpretation of the empirical model, i.e., self-similarity, was not popular [32].

A different class of long-memory models, known as autoregressive fractionally integrated moving average (ARFIMA) models, was later established by econometrician Clive Granger [34] and hydrologist Jonathan Hosking [35], who adopted the idea of "fractionally differencing" the simple random walk. The ARFIMA model was an extension of the autoregressive integrated moving average (ARIMA) model, introduced by Box and Jenkins [36], which is more widely accepted for its intuitive interpretation and flexibility. In the present day, ARFIMA models are the most commonly used long memory models [32].

2.3.3 Random walk and detecting long-range correlation

The methods for detecting LRC use the concept of random walk theory. As the name suggests, a random walk refers to a path consisting of a succession of random steps. A time series $\{x_i\}$, $i = 1, \cdots, N$, can be considered as increments of a one-dimensional random walk so that its cumulative sum is the net displacement after n steps of the walker:

$$X_n = \sum_{i=1}^{n} x_i - \mu \,, \tag{2.7}$$

where μ is the mean of the time series $\{x_i\}$, which is subtracted to remove the constant offset. The root-mean-square (RMS) displacement of a random walker is an important statistical quantity for characterizing the walk [37]. For the special case where step sizes vary according to a normal distribution, in which each step in the walk is independent, the RMS displacement after n steps is

$$\sqrt{\mathrm{E}[X_n^2]} = \sigma\sqrt{n} \,, \tag{2.8}$$

where E indicates the expectation value and σ the standard deviation of the step size distribution. Therefore, the RMS displacement of an uncorrelated walk follows a

power law with the scaling exponent 1/2. For a correlated walk, the scaling exponent is greater than 1/2, and for an anticorrelated walk, less than 1/2 [38].

Later, standard fluctuation analysis and detrended fluctuation analysis were introduced by C-K Peng et al. [5], [37] to detect long-range correlation in real-world data (see the following Chapter 4). Both methods use the RMS displacement of a walker to define the fluctuation in the time series as a function of the scale, which corresponds to the number of steps taken (n in Eq. 2.8).

2.4 Application to cardiology

A natural complex system readily found in our environment is the heart. Its complex dynamics can be observed in the recordings of heart rates or heartbeat intervals. A human heart is an example of a chaotic system that exhibits abrupt changes and periodic and irregular patterns that are physiologically meaningful. For example, it may exhibit a type of bifurcation, in which there is a sudden transition between irregular and periodic fluctuations or oscillation of alternating values, known as cardiac alternans [39], [40]. Such nonstationary fluctuations are considered as the output of collective behaviors arising from a network of pacemaker cells that interact in nonlinear ways, meaning that they cannot be defined by a simple summation of individual interactions between the cells. They are also largely influenced by neural input signals from external and internal stimuli [41]. Sympathetic stimulation, such as responding to stress and exercise, increases the firing rate of the action potentials of pacemaker cells in the heart's sinoatrial node (SAN), while parasympathetic stimulation, such as from internal organ functions, trauma, or allergic reactions, decreases the firing rate. It has been widely accepted that autonomic neural control of the heart gives rise to variations in the beat-to-beat intervals, commonly known as heart rate variability (HRV) [42]–[44].

Contrary to the archaic belief that the healthy human heart rate should consist of regular sinus rhythms, aimed at maintaining constant equilibrium, a healthy heart exhibits very complex and nonstationary fluctuations in beat-to-beat intervals, which are neither regular nor completely random, i.e., uncorrelated (Fig. 2.3). A modern interpretation is that such behavior is necessary to keep the heart protected against external stress. Its breakdown into strong periodic oscillations or uncorrelated fluctuations, as seen in Fig. 2.3, indicates the presence of a cardiac problem. In other

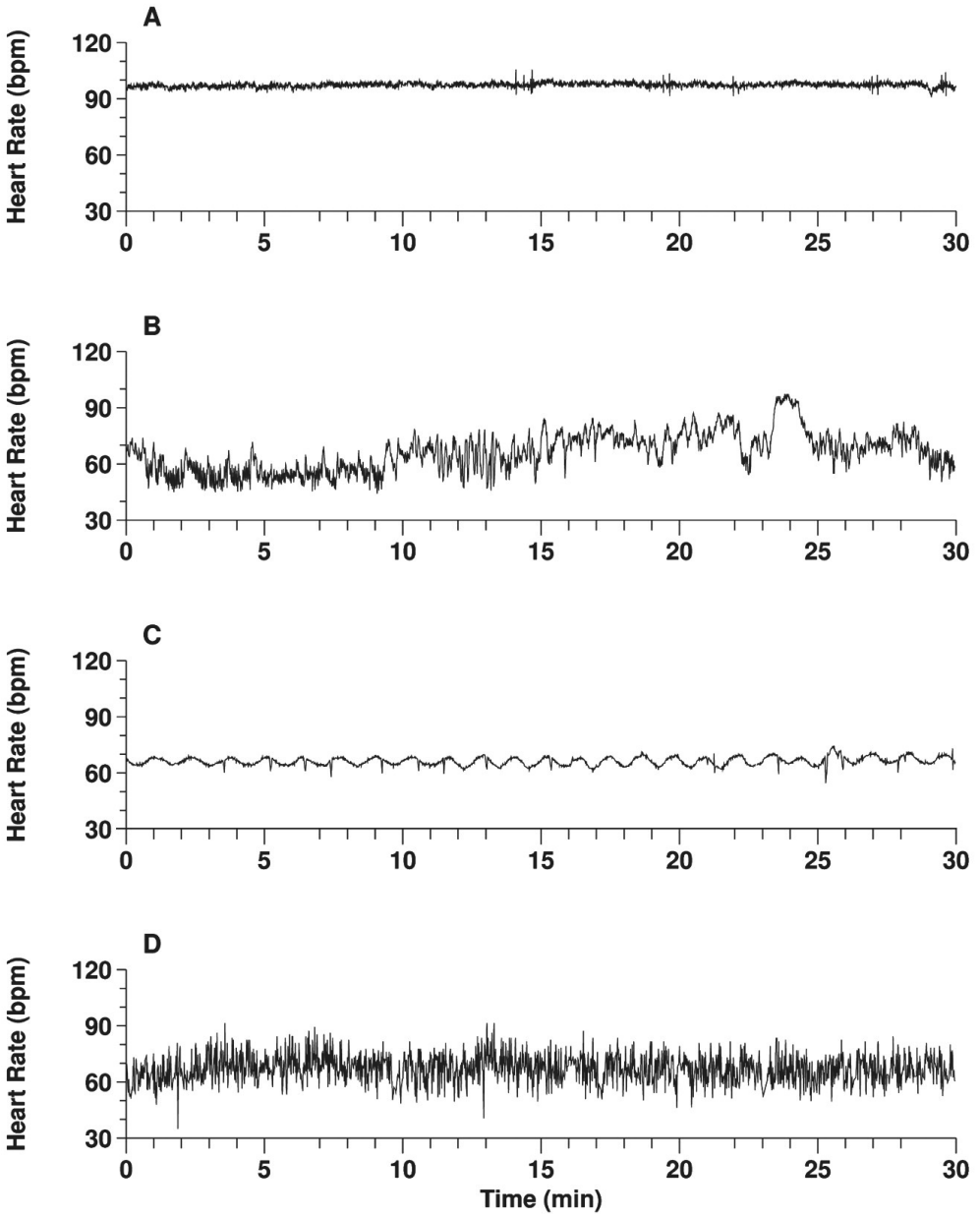

Figure 2.3 Heart rate recordings of a healthy individual and those with cardiac disorders. A, C: severe congestive heart failure; B: healthy; D: atrial fibrillation (Reprinted from Ref. [11], copyright (2002) National Academy of Sciences).

words, the degree of complexity in HRV provides important insights into cardiac health. Numerous papers in the past, e.g., [45]–[47], have shown that HRV, along with heart rate, can be a powerful marker of cardiac health. Ref. [44] provides a comprehensive list of reported cases of the known association between HRV and health factors, as well as various HRV analysis methods.

Nonlinear measures of HRV have been of great interest and there have been many efforts toward a better understanding of the dynamics, e.g., [48]–[51]. In particular, fractal-like scaling properties of HRV and its implications in cardiac health have been well established; many have studied the alteration of scaling properties in HRV with heart diseases, such as congestive heart failure [10], [52], myocardial infarction [53], [54], and dilated cardiomyopathy [55], as well as the effects of age and gender [56], sleep [57], [58], and exercise [59], [60] on the scaling behavior.

The studies also extend to a more fundamental level by investigating the variability at the cellular level, called beat rate variability (BRV). In a human heart, pacemaker cells in SAN tissue are responsible for producing an electric impulse through the heart, making the heart contract. It has already been shown that even in the denervated state, i.e., cut off from any neural inputs, the pacemaker cells exhibit irregular beat-to-beat variations, e.g., [61]. In search of the origin of the power-law behavior in HRV, studies have investigated intrinsic fractal properties of the pacemaker cells in animal models. In particular, it was shown that spontaneously beating heart cells of neonatal rats exhibited fractal self-similarity as a result of nonlinear dynamics of cellular processes [62]. This was further explored using a mathematical model, which showed that the turnover of ion channels induced the variability patterns with power-law behaviors [63]. The experiments using isolated rabbit SAN cells linked the variation in the periodicity in local Ca^{2+} release, which affects the cycle length, to the resulting BRV [64]. So far, studies suggest the importance of quantifying thee fractal-like properties at the cellular level, and clearly indicate that both the intrinsic properties of cellular processes and the inputs from the autonomic nervous system play roles in BRV [65].

3 HUMAN HEART CELLS AS A PLATFORM

This chapter covers the basic background information on the hiPSC-CMs, how they are made and measured, their advantages and disadvantages as a research platform, and some perspectives on their future applications.

3.1 How to make human heart cells

3.1.1 Rise of induced pluripotent stem cells

All the cells with designated roles in our body are derived from stem cells. The process of stem cells becoming specialized cells, such as blood, nerve, and cardiac cells, is called differentiation. Stem cells can be obtained from embryos (embryonic stem cells: ESCs) or, today, from mature adult cells (induced pluripotent stem cells: iPSCs). Both types of stem cells are pluripotent, meaning that they are capable of giving rise to any cell type.

While stem cells offer great potential to advance medical research, because of the origin of embryonic stem cells[1], there has been controversy about the ethics of the research ever since they came onto the scene. When the novel idea of inducing pluripotency in somatic cells to produce pluripotent stem cells (iPSCs) was introduced, it became a game changer in the field.

In 1962, British developmental biologist John B. Gurdon discovered that replacing the immature cell nucleus in an egg cell of a frog with that of a mature intestinal cell resulted in normal development [66]. The result essentially showed that the mature, already specialized cells have all the information necessary to develop all the cells in the frog. In 2006, Japanese stem cell researcher Shinya Yamanaka discovered that mature cells in mice could become pluripotent stem cells by introducing and

[1] They are obtained from fertilized embryos in their early stages, and are either destroyed or at least manipulated in the process.

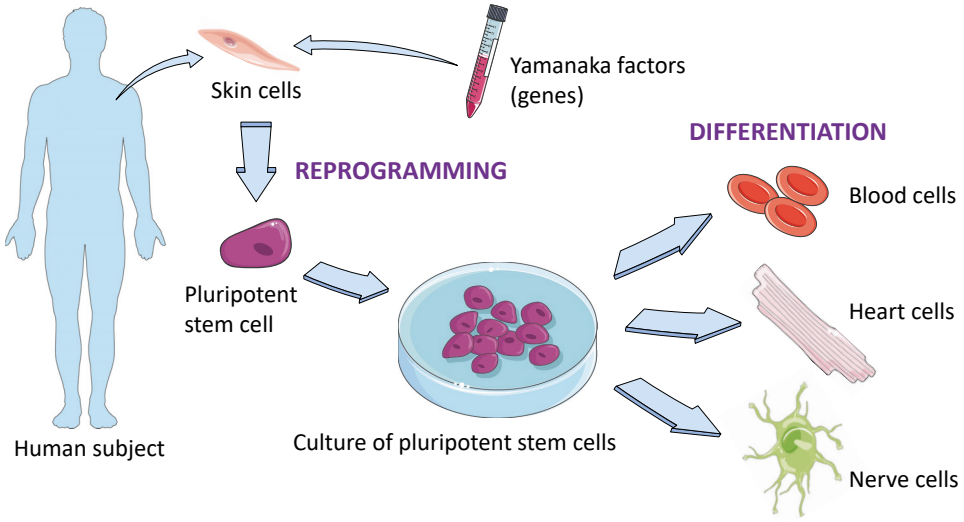

Figure 3.1 Schematics of human-induced pluripotent stem cell generation and differentiation into various types of somatic cells. A special selection of genes, known as Yamanaka factors, are added to the adult skin cells to reprogram them to be pluripotent. The resulting stem cells are then cultured and differentiated into all types of cells in the body. The figure is created using the images from Servier Medical Art, provided by Servier, licensed under a Creative Commons Attribution 3.0 unported license.

activating only a few genes [20]. For the scientific breakthrough, Gurdon and Yamanaka were awarded the Nobel Prize in Medicine in 2012. Since the discovery, the iPSC technology has been further studied and developed; it was shown that iPSC can give rise to all kinds of cell types in the body, and that iPSC can be generated also from mature *human* cells.

3.1.2 Generation and differentiation of human-induced pluripotent stem cells

In practice, there are several approaches of generating human-induced pluripotent stem cells (hiPSCs) with different efficiencies and advantages [67]. The technical details are beyond the scope of the thesis, however, it is briefly outlined how hiPSCs are generated. First, a small sample of skin from a human subject is taken, and the skin cells (dermal fibroblasts) are isolated and cultured. Next, a specific set of genes are then added to the cells; these genes contain factors (proteins) that can reprogram the cells to revert to their embryonic state. After about a month, a subset of the reprogrammed cells turns into pluripotent stem cells, which can be harvested and

cultured separately. The successfully generated hiPSCs are validated by characterization of their features, functionality, and genetic profiles.

Once hiPSCs are generated and characterized, they are ready to be differentiated, i.e., to become any type of cell we choose, such as heart cells. The hiPSCs undergo directed differentiation, guided by physical and chemical stimuli that mimic the embryonic development and signal the cells to take a particular developmental pathway. For the studies discussed in this thesis, we focus on cardiomyocytes (CMs), which reside in the cardiac muscle tissue and are responsible for the pumping function of the heart.

3.2 Measurement of cardiac field potentials

The most apparent feature of hiPSC-derived CMs (hiPSC-CMs) is their spontaneous contraction [68], [69]. Each hiPSC-CM generates an action potential, and an aggregate of hiPSC-CMs produces a collective field potential that can be measured.

3.2.1 Electrophysiology of cardiomyocytes

An action potential of a CM indicates the changes in the cell's membrane potential, which is the driving force for the cell's mechanical contraction. The membrane potential changes due to the movement of ions, namely Na^+, Ca^{2+}, and K^+, through different ion channels. CMs are categorized into three subtypes: nodal-, atrial-, and ventricular-like cells. The subtypes exhibit different action potentials possibly due to different ion channel compositions [70]. The hiPSC-CM aggregates used in the experiments in the thesis were not tested explicitly for their subtypes [71], but it has been suggested that the particular differentiation method, known as END-2, tends to generate mostly ventricular CMs [69]. A schematic of a ventricular cardiac action potential is shown in Fig. 3.2. Ventricular action potentials consist of five distinct phases (see, e.g., Ref. [72] for more details):

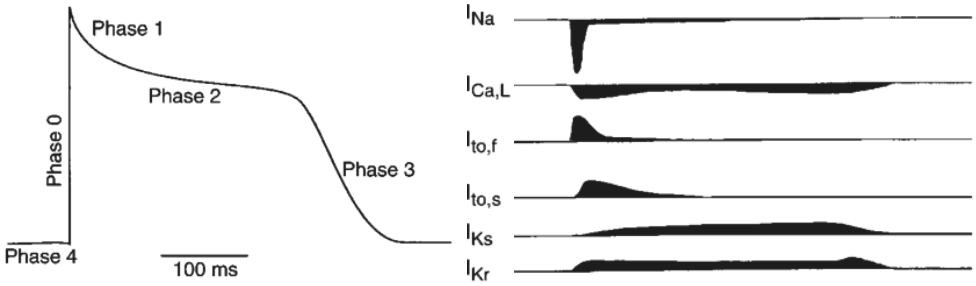

Figure 3.2 A schematic of a ventricular cardiac action potential and the underlying ionic currents. Adapted from Ref. [73], copyright (2005) American Physiological Society.

Phase 0 Onset of action potential. Rapid influx of Na^+ ions into the cells depolarizes the membrane potential.

Phase 1 Transient repolarization. Na^+ channel deactivates and fast transient outward K^+ current activates.

Phase 2 Plateau. Ca^{2+} flows into the cell and balances out with the delayed, outward rectifying K^+ currents.

Phase 3 Repolarization. Ca^{2+} channel closes and the outward K^+ currents bring the potential back to the resting potential.

Phase 4 Resting potential. The potential is maintained at about -90 mV by different ion pumps and the inward rectifying K^+ current.

The activities of the ion channels are summed up to produce the action potential shown in Fig. 3.2, which is converted into mechanical contraction.

3.2.2 Comparison to electrical activity of the heart

The collective extracellular field potential generated by an aggregate of hiPSC-CMs is measured using a multielectrode array (MEA). MEA is a non-invasive method, in which the cells are plated in a culture well on top of the embedded electrodes, as shown in Fig. 3.3.

MEA, while it cannot measure individual ion currents, has many advantages over the traditional patch-clamp method [74]. MEA does not require a high level of technical skills. It allows measurements of a colony of cells with spatial and temporal resolution, as several electrodes measure a cluster, and the cells are continuously cultured and can stay viable over an extended period [75], [76].

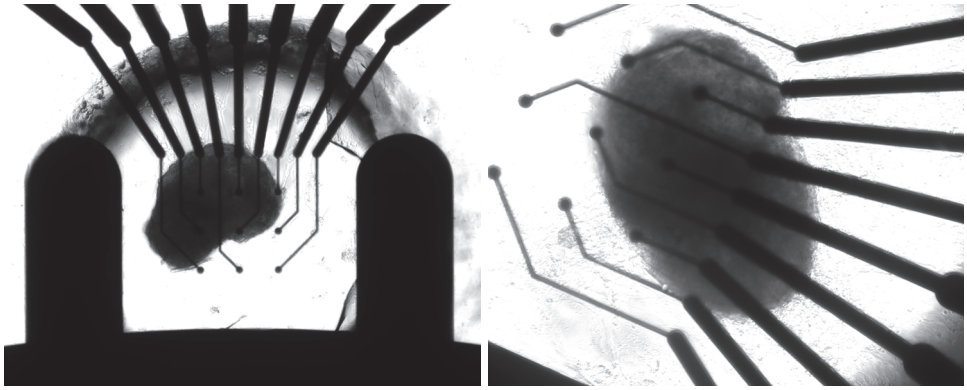

Figure 3.3 Magnified pictures of hiPSC-CM clusters plated in a well of a multielectrode array with electrodes measuring the electrical activity of the cluster.

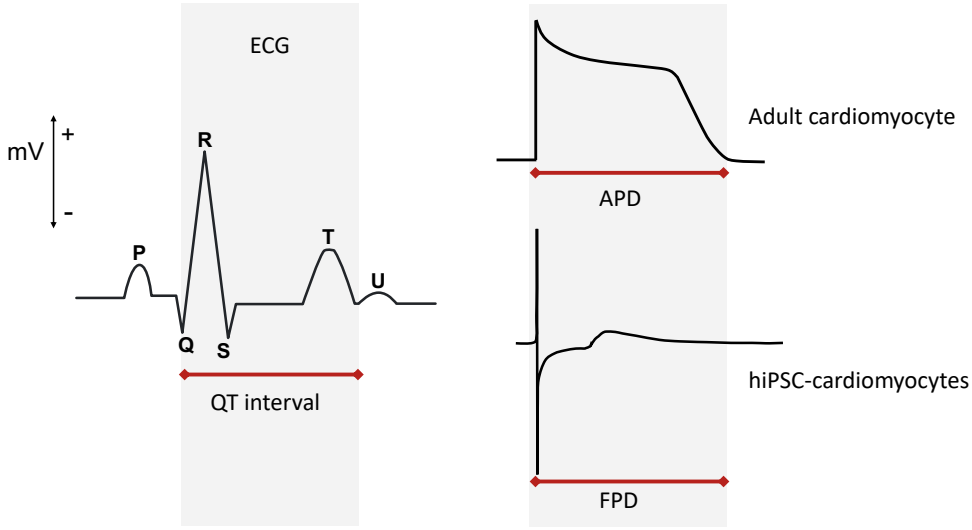

Figure 3.4 Schematics of human ECG, an action potential of an adult CM, and the field potential generated by a cluster of hiPSC-CMs. QT intervals, action potential duration (APD), and field potential duration (FPD) are comparable with each other. Modified from Ref. [75]. The ECG schematic is downloaded from Servier Medical Art, provided by Servier, licensed under a Creative Commons Attribution 3.0 unported license.

The field potential produced by an aggregate of hiPSC-CMs, measured by MEA, consists of a depolarizing Na^+ peak, a plateau phase by Ca^{2+}, and a repolarizing K^+ wave, as shown in the bottom of Fig. 3.4.

A parallel can be drawn among the field potential of a cluster of CMs, an action potential of a single CM, and a human ECG as depicted in Fig. 3.4. The two most commonly considered measures in ECG are RR and QT intervals. Interbeat interval (IBI) in the action potential of a CM and the field potential of a cluster of CMs correspond to the RR intervals in ECG. Similarly, QT intervals in ECG correlate highly with the action potential duration (APD) of a CM and with the field potential duration (FPD) of a cluster of CMs [77], [78].

3.3 Advantages of using human-induced pluripotent stem cell-derived cardiomyocytes

hiPSC-derived cells, including hiPSC-CMs, offer an *in vitro* platform for disease modeling, i.e., the study of how diseases develop at the cellular level. In particular, the hiPSC-CMs carry the exact genetic information of the patient from which they were derived; they are particularly suitable for the study of patient-specific mutations. They are also useful in testing new drug candidates for their effectiveness, any adverse effects, and how the (patient-specific) cells respond to certain drugs [79], [80].

Though not yet used in clinical practice, hiPSCs offer great potential in the development of individual-specific therapies and medicines. For example, stem cells can become healthy, specialized cells that can replace the diseased ones; such treatment is known as regenerative medicine. With the iPSC technology, the stem cells are generated from the patient, and thus the cells are genetically identical to the patient, reducing the risk of transplant refusal. Although practical challenges still remain, exciting possibilities of regenerative medicine and biological pacemakers have been suggested; cells that are cardiomyocyte-like in functionality were generated from human skin and used to partially re-muscularize affected areas of the heart in immunodeficient mice [81]; pacemaker cells derived from hiPSCs were able to pace the host tissues when transplanted in rat hearts [82]; and a biological pacemaker made with iPSC-CMs was demonstrated in a canine model [83].

The advantages mentioned so far can be applied to human ESCs (hESCs) as well,

but, as mentioned earlier, hiPSCs are preferred to hESCs in research because their sources, matured somatic cells, are much more available than the embryos needed to generate hESCs. They are also less controversial, even though the new technology brings its own ethical questions and challenges[2].

There are a few disadvantages to using hiPSC-CMs, including inefficiency in their production, e.g., [67], and their relative immaturity compared to adult CMs [79]. Despite the current limitations, hiPSC-CMs have already proven useful as an *in vitro* model for drug assessments. In recent years, the use of hiPSC-CMs has been implemented in pre-clinical drug screening as a part of the Comprehensive in vitro Proarrhythmia Assay (CiPA) protocol by the US Food and Drug Administration (FDA) [84].

3.4 Beat rate variability of human cardiomyocytes

In Sec. 2.4, applications of time series analysis to study the variations in heartbeats, or HRV, are discussed. Just like a beating heart, spontaneously beating clusters of hiPSC-CMs also exhibit beat-to-beat variations. BRV and its fractal-like characteristics in human *in vitro* heart cells were first reported by Mandel et al. [19]. The study successfully demonstrated that hESC-CMs and hiPSC-CMs exhibit complex BRV and fractal scaling properties, even in the absence of autonomic neural inputs from the ANS, reflecting the presence of intrinsic cardiac regulatory mechanisms. The results are in line with previous animal studies using denervated pacemaker cells in SAN [62]–[64].

The complex nature of BRV is so far considered as a collective phenomenon arising from a network of independently beating cells that are coupled with each other [85]. Studies based on rat and human CMs [19], [63] have postulated that the intrinsic BRV due to stochastic cellular functions contributes to the overall nonlinear characteristics of HRV. In several follow-up studies [86]–[88], the idea is discussed further. In particular, Ref. [86] and [87] hypothesized and tested multiscale interaction in three levels: (a) single pacemaker cells, (b) network of pacemaker cells, and (c) *in situ* SAN, which all exhibit similar fractal BRV/HRV. We summarize the key points as follows:

[2]For example, it is theoretically possible to generate sperm and eggs that can be fertilized from cells from skin or hair using the iPSC technology.

(a) At the single-cell level, magnitude of BRV is the largest. Possible sources of BRV and fractality include nonlinear dynamics from ion-channel gating, intracellular Ca^{2+} cycling, mitochondrial function, and other intracellular processes.

(b) In an ensemble network of electrically coupled pacemaker cells in SAN, BRV is significantly reduced as the single-cell noise is dampened. A few studies have modeled the cardiac network [63], [85], [89] to uncover the origin of BRV at this level and suggested the intracellular coupling of the cells and long-term correlated processes as strong factors responsible for the observed complexity in BRV. In particular, mitochondrial function and intracellular Ca^{2+} cycling, as well as the cross-talk between the sarcoplasmic reticulum and mitochondria exhibit fractal behaviors, which may contribute to that of the network.

(c) Finally, it is hypothesized that complex spatial and temporal integration of intrinsic components from first and second levels as well as external factors in the organ level, such as ANS, humoral factors, thermoregulatory, and circadian inputs, form the overall HRV properties at the third level.

The level that is most relevant to the studies presented in this thesis is (b). We study the BRV of hiPSC-CM clusters using various time series analysis methods introduced in the following chapter. While it is important to consider the physiological origin of the observed BRV, the details of the intracellular processes are beyond the scope of this thesis, and thus are not discussed further in the current work. However, the interested reader may find more information in, e.g., Ref. [86].

4 METHODS OF NONLINEAR TIME SERIES ANALYSIS

Important concepts and methods in nonlinear time series analysis that are relevant to Publications I-IV are presented in this chapter.

4.1 Challenges with the real-world data

Nonlinear systems can produce outputs that are seemingly unpredictable; depending on a single parameter, the behavior may change drastically from regular to erratic. Any attempts to simplify are futile because these systems are so complex that they cannot be split into subsystems. Furthermore, the mechanisms that drive the system can rarely be assumed a priori.

In general, time series data are considered a realization of a stochastic process, i.e., a sequence of random variables produced by an underlying probabilistic mechanism of the system [36], [90]. A common assumption in the study of stochastic processes is *stationarity*, meaning the process remains in a "statistical equilibrium" throughout the series, which requires relevant statistical parameters, such as mean and variance, to remain constant, and the phenomena of interest to be present frequently enough [91]. Therefore, the most common methods in time series analysis require stationarity of the data; however, real-world data is rarely stationary. Nonstationarities are almost always present due to external effects, such as trends, seasonality, and changes in the dynamics of the system over time, which may or may not be known [31]. In an effort to deal with nonstationarities, popular methods to make nonstationary time series (quasi-) stationary include using time derivatives or increments of the series as inputs and detrending; though, the trends need to be known to be independent of the dynamics [91].

4.2 Detrended fluctuation analysis

Detrended fluctuation analysis (DFA), one of the standard tools for the detection of LRC across different fields, was introduced by Peng et al. [5]. Based on the random walk theory, it is similar to its predecessor, standard fluctuation analysis (FA) [37], but DFA incorporates linear detrending into FA to remove monotonic local trends and was later extended to further consider polynomial detrending [18]. The steps for the basic DFA algorithm, based on Ref. [92], are summarized as follows:

1. For a given times series $\{x_i\}$ of length N, the profile, or the cumulative sum is defined:

$$Y(i) = \sum_{k=1}^{i} x_k - \langle x \rangle , \tag{4.1}$$

   where $\langle\rangle$ indicates the mean. Note that the subtraction by the mean is not strictly necessary for DFA [92].

2. The profile $Y(i)$ is divided into N_s non-overlapping segments of equal length s. Since s does not always divide N evenly, the same procedure is performed from both ends of the time series. Thus we obtain $2N_s$ segments in total.

3. For each segment ν, the local trend p_ν is calculated by a least-squares fit. The trend is subtracted from the profile:

$$Y_s(i) = Y(i) - p_\nu(i). \tag{4.2}$$

   p_ν is a linear polynomial in the basic DFA, but it may also be a higher-order polynomial.

4. The variance of the detrended series $Y_s(i)$ each segment is calculated by averaging over all data points i in the ν-th segment:

$$\left\langle Y_s^2 \right\rangle = \frac{1}{s} \sum_{i=1}^{s} Y_s^2[(\nu-1)s + i] = F_s^2(\nu). \tag{4.3}$$

5. By averaging the variance and taking the square root (equivalent to root-mean-square deviation around the local trend), the DFA fluctuation function $F(s)$ as

a function of the segment size s ("scale") is obtained:

$$F(s) = \sqrt{\frac{1}{2N_s} \sum_{\nu=1}^{2N_s} F_s^2(\nu)}. \tag{4.4}$$

The fluctuation function follows a power law,

$$F(s) \propto s^{\alpha}, \tag{4.5}$$

where the scaling exponent α is related to the correlation exponent (in Eq. 2.5) by

$$\alpha = 1 - \frac{\gamma}{2} \quad \text{for} \quad 0 < \gamma < 1. \tag{4.6}$$

The DFA scaling exponent α is determined by plotting the fluctuation F as a function of the scale s in the log-log scale and measuring the linear slope. Depending on the application, it may require more than one scaling exponent to describe the dynamics due to, e.g., crossover phenomenon [10], [93]. It is a common practice to assign two scale regimes for each of which a scaling exponent is calculated; for a range of small scales, the scaling exponent is referred to as "short-term" scaling exponent or α_1, and for a range of large scales, "long-term" scaling exponent or α_2. The scale regimes for α_1 and α_2 are not defined strictly. The scaling exponents are interpreted as in Table 4.1.

DFA's simple interpretation and ability to deal with (unknown) nonstationarity due to local trends are very desirable, hence the method has become extremely popular in diverse fields, such as cardiology [10], [11], [18], meteorology [6], [94],

Table 4.1 Interpretation of the DFA scaling exponent α.

Scaling exponent	Interpretation
$0 < \alpha < 0.5$	Anti-correlation
$\alpha \simeq 0.5$	Uncorrelated (White noise)
$0.5 < \alpha \leq 1$	Correlated
$\alpha \simeq 1$	$1/f$ noise (Pink noise)
$\alpha > 1$	Nonstationary
$\alpha \simeq 1.5$	Brownian noise

finance [95], and physics [8], [96]. However, one must also be aware of the common pitfalls when interpreting the results. While DFA is sensitive to LRC, it is not specific, i.e., the presence of scaling exponent $\alpha > 0.5$ does not always imply LRC, especially for time series with finite lengths [97].

Effects of different types of nonstationarities, namely, discontinuous signals, outliers, different local behaviors, and different types of trends, such as sinusoidal, and power-law trends, have been studied through empirical studies with simulated data [98], [99]. The studies show that, in reality, DFA cannot fully account for nonstationarities, but there are strategies to minimize the effects of nonstationarities. Some also argue that it does not provide even generic protection against nonstationarities [100]. Therefore, we must employ the method with a grain of salt, yet the success and the benefit of the method in identifying important insights in many complex systems, most notably in the field of physiology, cannot be denied.

4.3 Extensions of detrended fluctuation analysis

There have been significant progress in analytical derivations and theoretical understanding of DFA [101]–[104], as well as many extensions of the method. For example, multifractal DFA offers a generalization of DFA to characterize the multifractality [105], and detrended cross-correlation analysis extends DFA to analyze long-range cross-correlation between coupled time series [106]. This section describes the extensions to DFA for a more robust determination of the scaling exponents beyond the conventional methods and to account for the time and scale dependency of the scaling behavior.

4.3.1 Maximally overlapping segments

In the conventional DFA algorithm, non-overlapping segments are utilized to calculate the fluctuation function [Eq. (4.4)]. As a result, the largest possible scale is recommended not to exceed a quarter of the length of the time series [92]. Furthermore, as noted earlier in Sec. 4.2, non-overlapping segments do not allow even division of the time series, hence it is accommodated by division is performed twice from both ends of the time series.

One solution to enhance the statistical properties of the fluctuation function is to allow the segments to overlap and thus increasing the sample size [38] and en-

suring the uniformly weighted estimation of the RMS deviation [102]. Using the overlapping segments yields smaller local slope variability of the scaling exponent due to intermittent bursts and strong LRC in the time series data than that of the conventional non-overlapping segments. We utilize maximally overlapping segments whenever suitable, but not always, due to its high computational cost.

4.3.2 Scaling exponents as a function of scale

A conventional approach to determine the scaling exponent in DFA is using a linear least-squares fit on the fluctuation function in a double-log scale, i.e., $\log_{10}F(s)$ as a function of $\log_{10}s$, which has a linear relationship with the slope α. However, in many complex real-world data, one or more scaling exponents are required to describe the correlation. One common example is the presence of a crossover in the fluctuation function. A crossover refers to the phenomenon, in which the power-law changes after a certain scale, dividing the scale into two regimes that are described with different scaling exponents [10], [93]. The existence of a crossover is usually not a priori but may provide important insights into the underlying dynamical process.

In some cases, it may be difficult to determine one or two suitable regimes in the fluctuation function to apply the normal linear regression. Instead of arbitrarily choosing scale regimes to perform linear regression, these cases can benefit from a different approach of determining scaling exponent as a function of scale, $\alpha(s)$, also known as a "spectrum" of scaling exponents or "local" scaling exponents, which is basically a derivative of the logarithmic fluctuation function,

$$\alpha(s) = \frac{\mathrm{d}[\log_{10} F(s)]}{\mathrm{d}[\log_{10} s]}. \tag{4.7}$$

There are several ways to estimate a smooth derivative, such as applying $\alpha\beta$ filter [107] and parameter-free Kalman smoother [38]. Alternatively, when the fluctuation function possesses a good statistical property, that is, when the data is sufficiently long or maximally overlapping segments (Sec. 4.3.1) are used, a simple numerical differentiation may be used.

4.3.3 Dynamic detrended fluctuation analysis

So far, we have assumed the system or the dynamic under study to be unchanging in time. Dynamic detrended fluctuation analysis (DDFA), first introduced in Ref. [60], successfully detects real-time changes in the correlation properties in a time series. DDFA measures the DFA scaling exponents as a function of time and scale. The dynamical approach is especially powerful when investigating real-world conditions, in which the system changes over time, for example, the heartbeats in high-intensity interval training or in a marathon.

The basic idea of DDFA is to perform DFA in a moving temporal segment. The execution of the method is, however, not so trivial. In order to ensure high temporal resolution, the segment in time must be sufficiently small, but a segment that is too small suffers from high statistical noise in the fluctuation function. In other words, the biggest challenge of DDFA is minimizing the statistical noise while maximizing temporal resolution. DDFA resolves the problem by employing a procedure called "dynamic segmentation", in which the temporal segment length is varied as a function of the scale, e.g.,

$$l(s) = as, \tag{4.8}$$

where a is a constant dynamic length factor. A suitable value is chosen according to the problem in hand. Therefore, for each scale the time series is divided into segments of length $l(s)$. In each temporal segment, the dynamic scaling exponent $\alpha(t,\ s)$ is computed by the finite difference approximation:

$$\alpha(t,\ s) \approx \frac{h_-^2 \tilde{F}_t(s+1) + (h_+^2 - h_-^2)\tilde{F}_t(s) - h_+^2 \tilde{F}_t(s-1)}{h_- h_+ (h_+ + h_-)}, \tag{4.9}$$

where $\tilde{F}_t = \log_{10} F_t,$ (4.10)

$$h_- = \log_{10}(s) - \log_{10}(s-1), \tag{4.11}$$

$$h_+ = \log_{10}(s-1) - \log_{10}(s). \tag{4.12}$$

The full and detailed description of the algorithm and validation are found in Ref. [60].

4.4 Other nonlinear measures

This section introduces a few important nonlinear measures and methods that are complementary to DFA in determining the complexity of a time series, especially in the context of applications in cardiology.

4.4.1 Poincaré plots

A Poincaré plot is a simple visualization tool to quantify short-scale temporal correlation in a time series. For a given time series $\{x_i\}$ for $i = 1, \cdots, N$, each value x_{i+1} is plotted against its preceding value x_i in the time series. The beat-to-beat variability and long-term variability are quantified by measuring the standard deviation perpendicular and along the line $x_i = x_{i+1}$ and denoted as SD1 and SD2, respectively. SD1 and SD2 are computed by an ellipse fitting technique [108]. The two measures are closely related to the overall standard deviation σ by

$$\mathrm{SD1}^2 + \mathrm{SD2}^2 = 2\sigma^2. \tag{4.13}$$

SD1 and SD2, and in particular, the ratio of the two SD1/SD2, have become popular heart rate variability measures that can be potential classifiers of cardiac diseases [44].

4.4.2 Multiscale entropy

Entropy is a measure that originates from statistical physics and information theory and reflects the disorder of a system. In a time series, the concept of entropy is used to quantify complexity and regularity in a statistical sense. Popular entropy measures include approximate entropy (ApEn) [109] and sample entropy (SampEn) [110]. Both measures are aimed at finding how similar a segment is to other segments of equal length in the time series. The problem with such measures is that it is limited to the rudimentary definition of complexity being simply the opposite of regularity and thus cannot portray the *meaningful* complexity that lies between regularity and randomness.

Multiscale entropy (MSE) developed by Costa et al. [111], is developed to address the limitations by considering the scale-dependency of entropy, in particular, that of SampEn. The method successfully distinguishes the correlated complex signals from

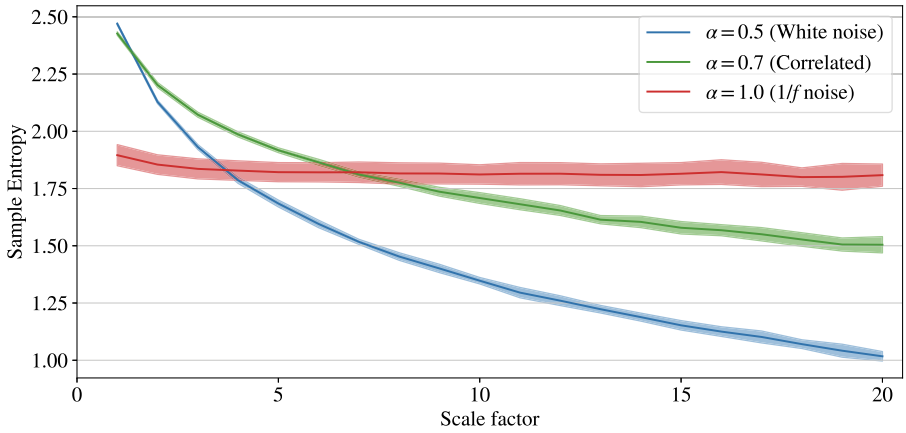

Figure 4.1 Multiscale entropy analysis of generated signals of sufficient lengths with various scaling exponents: $\alpha = 0.5,\ 0.7,\ 1.0$. The sample entropy values are averaged over 20 iterations and the mean (solid lines) and standard deviation (colored bands) are plotted over the scale factor.

the uncorrelated random signals (Fig. 4.1). Furthermore, it has the advantage of being useful for time series of finite lengths, but the finite length also introduces high uncertainty in the entropy measurement, especially for long-range correlated signals. The procedure for MSE is as follows.

1. Given a time series $\{x_i\}$ for $i = 1,\ \cdots,\ N$, a set of consecutive coarse-grained series with the scale factors τ is constructed, for each of which contains the elements:
$$y_j^{(\tau)} = \frac{1}{\tau} \sum_{i=(j-1)\tau+1}^{j\tau} x_i, \qquad 1 \le j \le N/\tau. \tag{4.14}$$

2. For each coarse-grained time series, the SampEn is calculated and plotted as a function of the scale factor τ to produce an MSE curve.

MSE algorithm depends on two parameters, the epoch length m and the tolerance level r, and we use the default values ($m = 2,\ r = 0.15$) as in Ref. [111], [112].

In practice, SampEn behaves differently as a function of the scale for long-range correlated signals compared to uncorrelated white noise, allowing the comparison of the scale dependency between various states and conditions, such as cardiac diseases and sleep stages [111].

5 RESULTS

The common theme in Publications I-IV is the study of complexity exhibited by independently beating clusters of human heart cells. Important findings that contribute to state-of-the-art knowledge of the intrinsic beat rate variability of the heart cells are summarized in Sec. 5.1-5.3. When appropriate, we update the results using newer preprocessing schemes and computational methods. The limitations of the current studies are discussed in Sec. 5.4.

5.1 Beat rate variability and fractal scaling in human cardiomyocytes

In Publications I, III, and IV, we first confirm that clusters of healthy hiPSC-CMs indeed exhibit spontaneous contraction in intervals having fractal scaling similar to that of a functioning human heart. Previous findings and discussions are found in Sec. 3.4. The following subsections summarize the results from Publications I and IV in particular.

5.1.1 Effects of genetic mutation

We investigate how the beat rate properties are altered in the presence of genetic mutations that cause hereditary cardiac disorders, such as Long QT Syndrome (LQTS), which is the main focus of Publication I. LQTS is a disease, characterized by prolonged cardiac repolarization, represented by QT intervals in ECGs. It can lead to fatal arrhythmias, i.e., fast and irregular heartbeats and even a special type of ventricular tachycardia, Torsades de Pointes. Inherited forms of LQTS[1] are classified into subtypes based on which genes are affected by the mutation. The most prevalent subtypes are LQTS type 1 (LQT1) and type 2 (LQT2), caused by mutations in the KCNQ1 and KCNH2 genes, respectively [113], [114]. In the study conducted

[1] LQTS can also be acquired later in life.

Table 5.1 Patient/subject characteristics of the healthy individual, asymptomatic LQT1 mutation carrier, and symptomatic LQT1 mutation carrier. The heart rate is written in mean ± standard deviation.

	Healthy	LQT1 (asymptomatic)	LQT1 (symptomatic)
Age (year)	55	28	41
Gender (M/F)	F	F	F
Heart rate (bpm)	115 ± 26	112 ± 15	99 ± 11
QT_c (ms)	406	428	456

in Publication I, healthy control, denoted as wild type (WT), and LQT1-specific hiPSC-CMs are derived from a healthy individual and two LQT1 mutation carriers, respectively. The characteristics of the subjects are summarized in Table 5.1. One LQT1 mutation carrier is symptomatic and the other, asymptomatic. A previous study has shown that the baseline beat rates of WT- and LQT1-CMs do not differ significantly, but the LQT1-CMs show significantly more prolonged (beat rate-corrected) FPDs [71].

In Publication I, we perform the most basic DFA to detect long-range correlation in the IBI series and find that (i) the average DFA scaling exponents range between $0.9 - 1.1$ for both WT and LQT1-CMs, without any notable differences between the groups, and (ii) the scaling exponents are comparable to those computed from ECGs: $\alpha = 1.21$, 1.07, and 1.08 for the healthy individual, asymptomatic LQT1 mutation carrier, and symptomatic LQT1 mutation carrier, respectively. Later, a follow-up study [115] using two scale ranges to define short- and long-term scaling exponents, α_1 and α_2, rather than a single α, supplements Publication I with the finding that (iii) each group exhibits significantly different short- and long-term behaviors. The results from Publication I and the supplementary study [115] lead to the conclusion that the scaling behaviors are not altered by the presence of a LQT1-specific mutation.

We believe, however, that the results may benefit from clarifying and revising of the analysis procedures. The IBI data used in the analyses in Publication I and the supplementary study underwent several steps of preprocessing, in which large portions of the data were discarded; however, the procedure is not described in the publications. In general, hiPSC-CMs exhibit a wide range of beat rates and their IBI series often contain large fluctuations and nontrivial trends, which means that deciding whether a recording is suitable for the analysis is often an ambiguous and

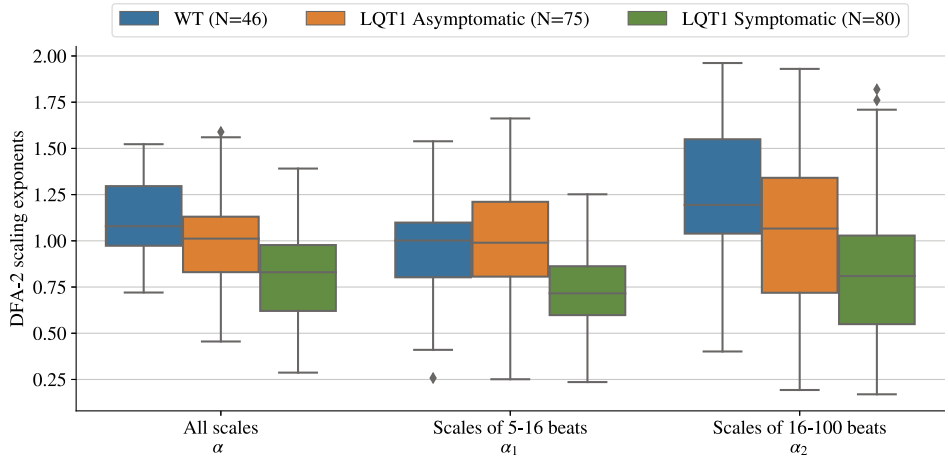

Figure 5.1 DFA-2 scaling exponents for healthy cells (WT), and LQT1-specific hiPSC-CMs, computed over different scale ranges.

subjective process. Therefore, in the following, we include recordings of varying quality to better reflect reality. We revisit the results by first employing a simpler filtering scheme to remove only the most obvious outliers; we set constant cut-off thresholds for each recording so that the data points below 1/2 of the median and above 3/2 of the median are discarded. If more than 20% of the IBI series is removed, then the whole series is discarded. We also use DFA-2 to address any nontrivial trends that are hard to remove with conventional linear detrending of DFA-1. Distributions of the overall α (calculated over all available scales) and of the short- and long-term scaling exponents, α_1 and α_2, are shown in Fig. 5.1.

Figure 5.1, which uses revised analysis procedures, suggests a conclusion contrary to that of Publication I. DFA scaling exponents computed over all available scales are significantly different between the WT- and LQT1-CMs, and also between asymptomatic and symptomatic LQT1-CMs. When only the short-term scale range is considered, the WT- and asymptomatic LQT1-CMs exhibit similar scaling properties, while the scaling exponent for symptomatic LQT1-CMs is notably reduced. Therefore, according to the results, the presence of a LQT1 mutation in the genes reduces the degree of LRC in the IBI. When the LQT1-CMs are derived from a symptomatic patient, correlation properties of the IBI are also affected in the short range.

There is a single 24-hour ECG recording for each subject (i.e., the healthy in-

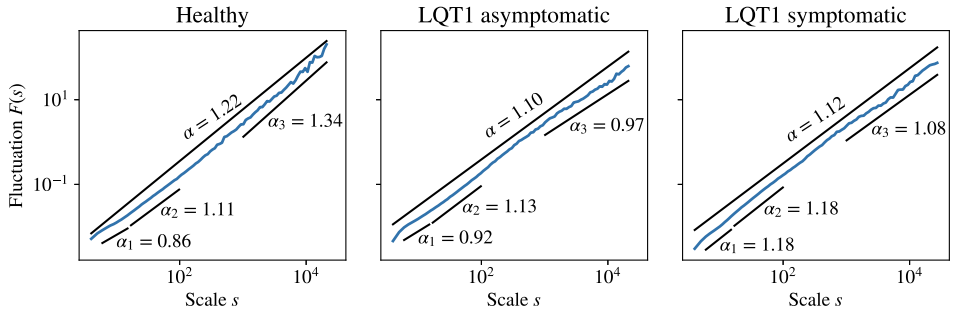

Figure 5.2 Fluctuation function computed by DFA-2 in double-log scale for the 24-hour ECG data of the healthy individual and LQT1 mutation carriers. Short- and long-term scaling exponents α_1 and α_2 are defined in the same scale ranges as in Fig. 5.1. In addition, α_3 is defined for an even longer scale range (>1000 beats).

dividual and LQT1 mutation carriers) from whom the hiPSC-CMs were derived. Analysis of the ECG recordings is shown in Fig. 5.2. The α_1 and α_2 are computed from the same scale ranges as for the cell data. In these scales, the healthy individual and the asymptomatic LQT1 mutation carrier exhibit similar scaling behaviors. Since the ECG recordings are much longer than the 30-minute recordings of the CMs, we are able to define an additional scaling exponent α_3 for larger scales, e.g., longer than 1000 beats. Over the longer range, the healthy individual exhibits a scaling property closer to that of Brownian noise, while no notable change is detected for the asymptomatic LQT1 carrier at the same scale. The surprising case is of the symptomatic LQT1 mutation carrier, whose ECG recording exhibits a "normal" scaling behavior, i.e., the scaling exponents are notably larger compared to those of the cellular counterpart. One may attribute the result to the fact that the symptomatic LQT1 mutation carrier is on the beta blocker treatment, but a previous human study has suggested that the fractal scaling is not altered by the beta blocker treatments [116]. It is not possible to make any strong conclusive interpretations with a single ECG recording for each subject, but we may safely state that there are extra mechanisms in the heart that control the heart rate and its variability that are absent in the isolated clusters of heart cells.

In summary, the scaling properties in the ECG data are approximately comparable to those in the cellular field potentials. However, in the presence of LQT1 mutations and symptoms, the heart rate dynamics are altered, resulting in significantly reduced correlations at the cellular level, which may not be visible in the

Table 5.2 Characteristics of the drugs tested on WT- and LQT1-CMs. A more detailed description is found in Publication I. CM: cardiomyocytes, M: molar unit, BR: beat rate, cFPD: (Fridericia) corrected FPD, -: no physiologically significant effect.

Name	Type	Concentration	Effects on CMs
Bisoprolol	Beta blocker	260, 530 nM	BR -, cFPD -
ML277	I_{Ks} channel activator	1, 2 μM	BR ↑, cFPD ↓
JNJ303	I_{Ks} channel blocker	300, 1000 nM	BR -, cFPD ↑

ECGs. The finding is supported further by MSE analysis, as we discuss in Sec. 5.2. Effects of the age of and medication taken by the subjects and characteristics of the CMs were not examined in the study, but are potential factors that can alter the beat dynamics.

5.1.2 Effects of pharmacological compounds

Another main objective of Publication I is to investigate the effects of exposure to different drugs on the functionality and scaling properties of the healthy and LQT1-specific hiPSC-CMs. Drugs chosen for the study include a type of beta blocker, which is the most commonly used standard medication for LQTS. The results are of particular interest for disease modeling and applications in drug safety assessments.

The list of drugs that are applied to the WT- and LQT1-CMs and their descriptions are found in Table 5.2. Experimental details of how the drugs were applied are found in Publication I. The key findings of Publication I are that (i) all the drugs (Bisoprolol, ML277, and JNJ303) lead to an increase in the DFA scaling exponent α in WT- and LQT1-CMs, and (ii) an increase in the drug concentration does not affect the scaling exponent further. The results have been revised for the reasons described in the previous section (Sec. 5.1.1).

As we have seen in Sec. 5.1.1, the fractal scaling is reduced in the case of symptomatic LQT1-CMs. Figure 5.3 clearly shows that the alteration of the scaling exponents due to a LQT1-specific mutation is more significant than that due to drug exposure. It is also important to notice the large discrepancy between the mean baseline α for different drugs. The reasons behind the discrepancy are not yet clear. Since the variation is rather large even in the same baseline condition, we do not combine the baseline measurements but keep them separate for each drug exposure test. This

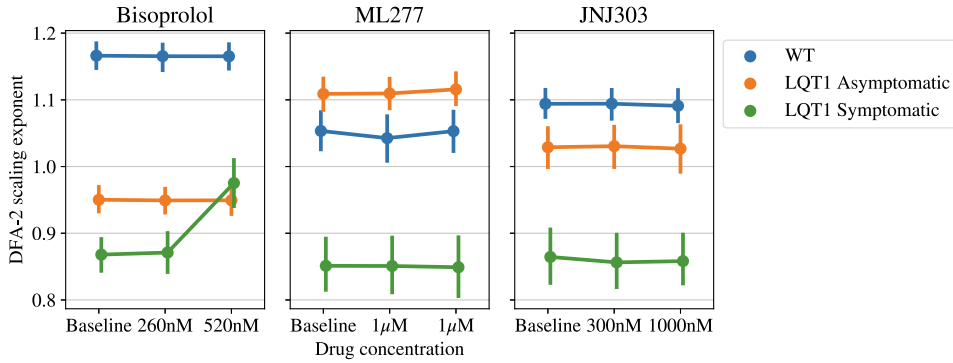

Figure 5.3 DFA-2 scaling exponents as a function of drug concentrations.

way, the relative change in the average scaling exponent due to the drugs is prioritized over the values of the exponents themselves at each drug concentration. The distributions of all baseline scaling exponents are found in Fig. 5.1.

With the updated analysis procedure, we find that Bisoprolol, ML277, and JNJ303, in general, have no meaningful effect on the long-range correlation in the hiPSC-CMs (see Fig. 5.3). One exception is found in the LQT1-CMs derived from the *symptomatic* mutation carrier with the larger dosage of Bisoprolol, which increased the scaling exponent toward $\alpha \sim 1$ ($p \ll 0.001$ with Welch's t-test). Figure 5.3 shows only the average behaviors over all cell lines of symptomatic LQT1-CMs, but we also note that the effect is prominent in one symptomatic cell line, but not in the other. The analysis using two scaling regimes yields similar results, though the enhancement of α_1 is not as prominent as that of α_2.

Based on this result, we may infer that the acute application of the drugs that regulate the K^+ ion channel does not affect the scaling behaviors in hiPSC-CMs. However, the beta blocker bisoprolol, while not having a physiologically significant effect on the beat rate or FPD, seems to increase the correlation in the beats of LQT-CMs derived from the symptomatic LQT1 subject towards fractality, which is associated with a healthy heart. The mechanism behind the effect remains unclear, but the result suggests the reduced fractality in the LQT1-CMs can be recovered by acute applications of bisoprolol at a sufficient dosage. However, further systematic studies are in order, as the results clearly show that the baseline scaling behaviors and the responses to the drugs may depend on the characteristics of the hiPSC-CMs, such as the cell lines and the age of the culture.

Table 5.3 Definitions used to describe stable and transient phases with different partial oxygen pressure (pO_2) in the hypoxia experiment in Publication IV.

Phase	pO_2	Duration	Description
BASELINE	19%	10-12 hours	Stable normoxia
HYPOX-I	19% → 1%	8 hours	Transient hypoxia
HYPOX-II	1%	14 hours	Stable hypoxia
REOX-I	1% → 19%	6 hours	Transient reoxygenation
REOX-II	19%	6 hours	Stable reoxygenation

5.1.3 Effects of hypoxia and reperfusion

Publication IV studies the cellular response to the physiological stress caused by prolonged hypoxia, i.e., low concentration of oxygen in the environment. The study has physiological significance as a cycle of hypoxia and reperfusion mimics the ischemia-reperfusion injury[2] in humans. Despite the hiPSC-CMs being immature in their structure, functionality, and metabolism [79], [117], and being more resistant to hypoxia than adult CMs [118], they have been a popular *in vitro* model for cardiac ischemia (e.g., [118]–[120]). In the experiments, six clusters of healthy hiPSC-CMs are exposed to a hypoxic environment (1% O_2) for up to 24 hours in a custom-built hypoxia chamber [121] and the field potentials are measured on MEA. Experimental details are found in Publication IV.

The most obvious effects of hypoxia and reperfusion on the functionality of the hiPSC-CMs are the changes in the beat rates [119], [120]. As shown in Fig. 5.4, we find that the cell aggregates reduce their beat rates to approximately 61-69% of the baseline values during stable hypoxia. On the other hand, during reperfusion, while three aggregate samples recover about 84% of the baseline levels, the other three samples with the higher baseline beat rates remain at the suppressed beat rates. This is due to a decline in the beat rate independent of hypoxia and reperfusion in the more *active* cells, which leads to the aggregates' inability to fully recover from hypoxia.

In Publication IV, we investigate the effects of prolonged hypoxia and reperfusion on the time- and frequency-domain BRV measures and the scaling properties. The

[2]Ischemia-reperfusion injury refers to the (cardiac) tissue damage caused by ischemia, i.e., shortage of oxygen due to restriction of blood flow, followed by restoration of the blood supply to the tissue.

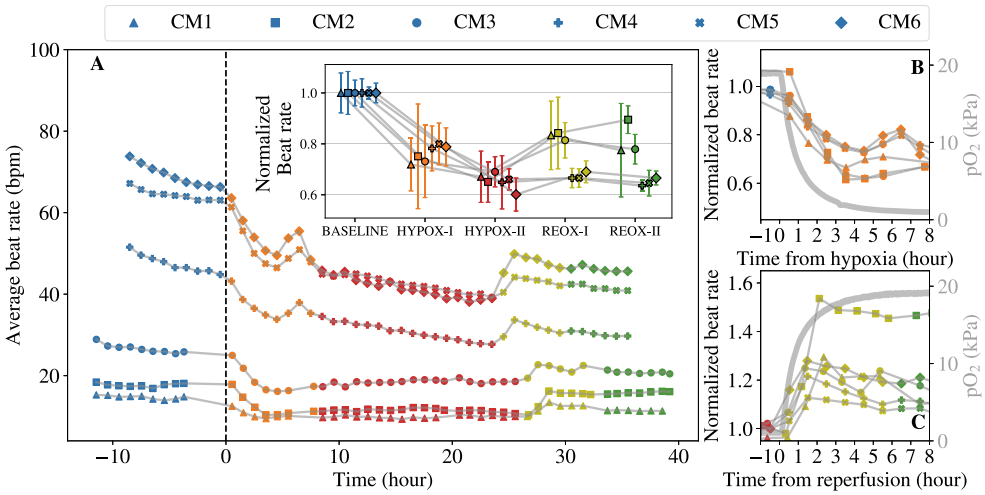

Figure 5.4 Average beat rates of the six hiPSC-CM aggregates in a cycle of normoxia-hypoxia-reperfusion. A: Mean instantaneous beat rates over 1-hour segments. Inset shows the mean beat rates and standard deviations over the entire phases, normalized to the baseline values. B, C: Average beat rates during transient phases, each normalized to the mean beat rates at the onset of hypoxia and reperfusion, respectively, with partial oxygen pressure (pO_2) in gray. Reprinted from Publication IV.

basic time- and frequency-domain measures are discussed along with their relationship with the beat rates in Sec. 5.3. In this present section, we summarize the scaling (correlation) properties at each oxygen phase. In the following discussion, we refer to different oxygen (sub-) phases as defined in Table 5.3.

We compute the DFA-2 scaling exponents α_1 and α_2 over the complete phases for each aggregate. The results are shown in Fig. 5.5. We first note that the baseline behaviors are in line with previous findings, e.g., in Publication III, that most of the cells exhibit long-range correlation and crossover phenomena, in which the short- and long-term DFA scaling exponents are distinctively different. One of the key results is that on average α_1 and α_2 are reduced during hypoxia. However, while average α_1 recovers to the baseline value during reperfusion, average α_2 is not restored to its baseline value. This result suggests that hypoxia affects long-range correlation more than it does short-range correlation, and may indicate possible long-term damage by hypoxia in the cellular mechanisms that affect the intrinsic beat dynamics. The results are, however, far from conclusive, due to the wide variation and strong

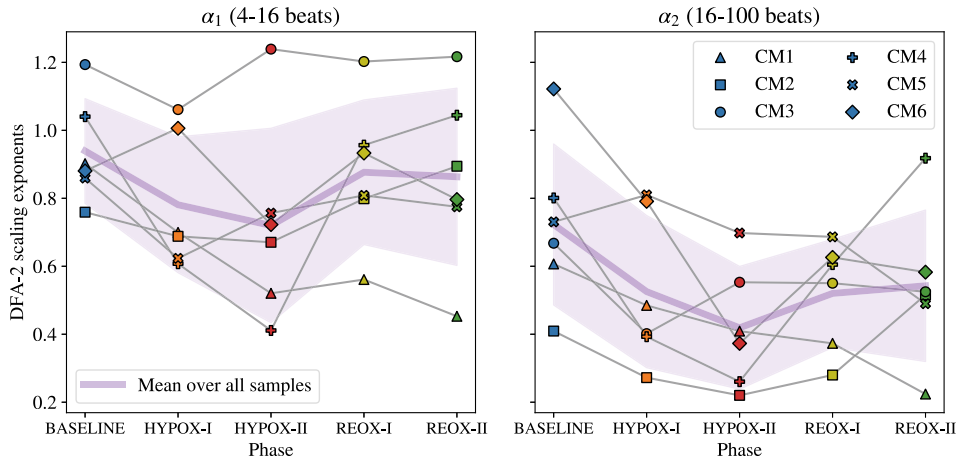

Figure 5.5 DFA-2 scaling exponents α_1 and α_2 as a function of the hypoxia phase. The thicker colored line indicates the average over all samples with standard deviation. Reprinted from Publication IV.

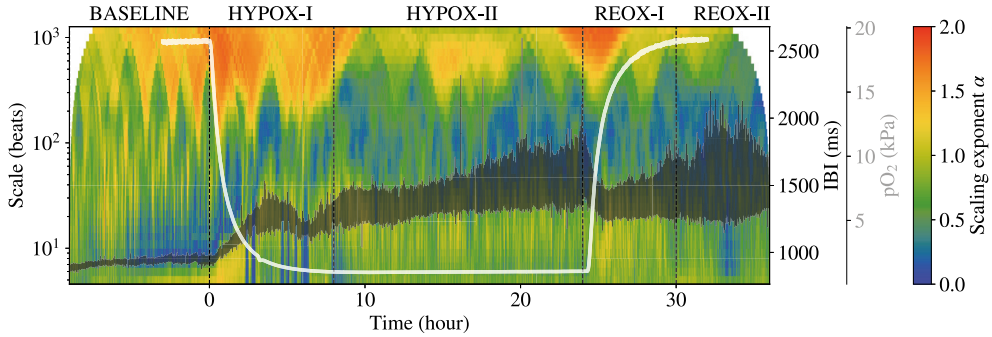

Figure 5.6 An example of the landscape of scaling exponents of CM5 as a function of time and scale computed by dynamical DFA. The real-time changes in the scaling exponent can be seen in relation to the beat rate and oxygen concentration. Modified from Publication IV.

individuality among such a small number of samples, as shown in Fig. 5.5.

While α_1 and α_2 have been widely accepted as standard HRV measures due to the ease of interpretation of the correlation properties, they cannot fully portray the complexity of the scaling properties in real-world data. DDFA can address the possibly missing details in the information by computing the scaling exponent as a function of time and scale, with emphasis on the temporal changes in the correlation properties. The application of DDFA on the cell data is rather preliminary at present, but the example of the DDFA landscape for the aggregate sample CM5

(Fig. 5.6) offers a powerful future perspective.

The particular example contains a number of interesting features. In the landscape of the scaling exponent, the values are represented in different colors, as shown in the color bar in Fig. 5.6, which are interpreted in the same manner as in Table 4.1. For example, the red-orange regions indicate nonstationarity, reflecting the "abrupt" changes in IBI during the transient phases, i.e., HYPOX-I and REOX-I. On the other hand, the blue regions indicate anticorrelation, which reflects periodic modulation and appears at various points in time and scale. The green regions reflect correlated, stationary behaviors. The preliminary results provide novel insights into the local dynamics of the beats; the interplay of anticorrelated, correlated, and nonstationary behaviors across different scales are studied in high temporal resolution at various chosen times, as demonstrated in detail in Publication IV.

5.2 Intrinsic complexity in IBI and FPD variability

Publications II and III explore the scaling properties and the complexity present in the fluctuations of beat-to-beat intervals and the durations of the field potential generated by hiPSC-CMs. While HRV has been studied extensively, relatively few studies are available on QT variability, especially in terms of LRC and nonlinear measures [18], [122], [123]. However, QT intervals also exhibit spontaneous beat-to-beat fluctuations [124] and QT variability is potentially a critical measure to quantify, as QT intervals are often used in assessing risk factors in cardiac safety and drug development. To our best knowledge, Publication II and III are the first to report MSE and DFA results on FPD of human CMs.

In Publication II, we first perform MSE analysis on RR and QT intervals recorded for healthy individuals and IBI and FPD series from healthy WT-CMs (Fig. 5.7). We interpret the results by examining the magnitude of entropy values and the profile of MSE curves between the data and shuffled data. When shuffled, the data is essentially randomized and thus correlation in the data is lost. Hence, the MSE curves of the shuffled series provide a reference behavior of the uncorrelated signal. As mentioned in Sec. 4.4.2, entropy values reflect irregularity in the signal. The values alone are not meaningful in determining the complexity of the signal, but the scale-dependency of the values provides insights into the persistent complexity that does not diminish

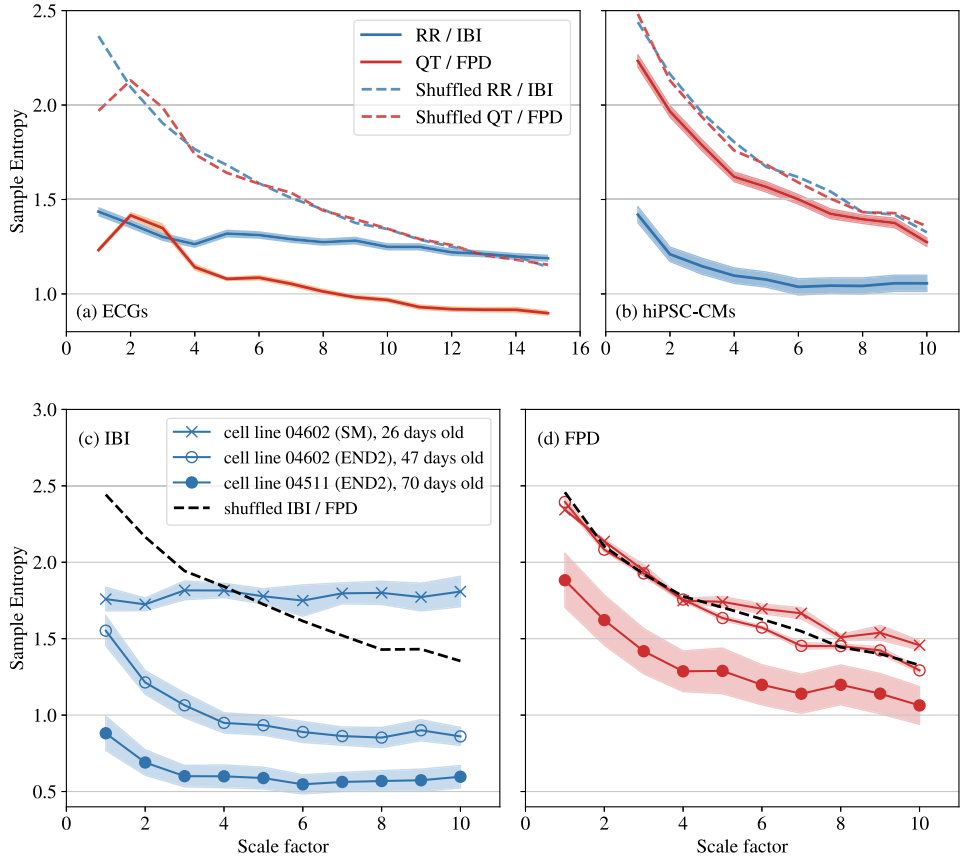

Figure 5.7 Multiscale entropy profiles of (a) RR and QT intervals of healthy individuals and (b) IBI and FPD of healthy hiPSC-CMs. In (c) and (d), IBI and FPD of healthy hiPSC-CMs are grouped according to their cell line, differentiation methods (SM and END2), and the age of the CMs at the time of the measurement. Each profile represents the average over the samples with standard error shown as colored bands. Multiscale entropy profiles of shuffled series with no correlation are added as a reference. Adapted from Publication II.

over a long period.

The MSE of RR intervals has a relatively flat profile, similar to that of $1/f$ noise (see Fig. 4.1), as one would expect. On the other hand, the MSE profile of QT intervals is notably different from that of RR intervals, which is in agreement with a previous report that studied QT intervals of pregnant women [112]. The SampEn values decrease monotonically until the scale factor $\tau \sim 11$ (Fig. 5.7 (a)), indicating the degradation of the control mechanism that drives QT variability, namely the heart rate, in the scale smaller than 11 beats. Coarse-graining process in the MSE

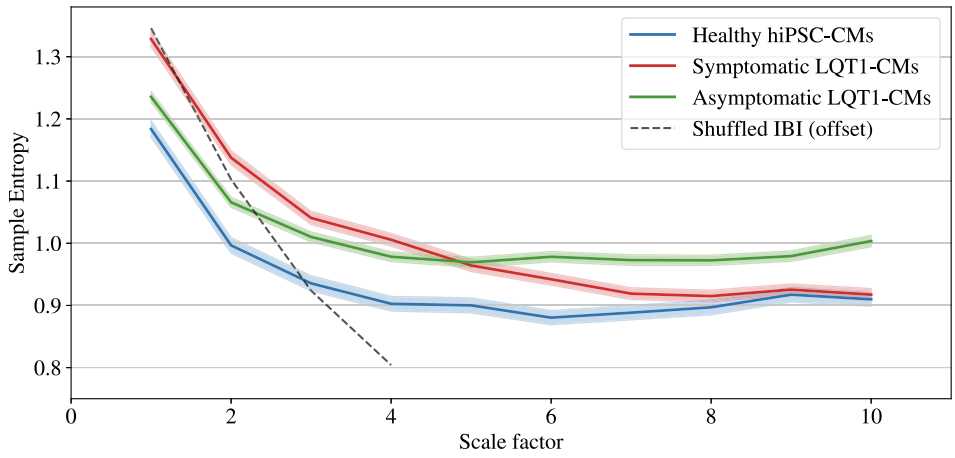

Figure 5.8 Multiscale entropy (MSE) analysis of IBIs of WT- and symptomatic and asymptomatic LQT1-CMs. Each MSE entropy profile shows the mean and the standard error. The MSE profile of the shuffled series is added as a reference.

analysis progressively filters out the uncorrelated components in the QT intervals in the small scales; hence, the flat profile in the larger scales reflects the correlation innate to QT intervals. The MSE curve of the QT intervals staying significantly below that of the shuffled series indicates a deterministic component of the QT variability, which sustains a level of regularity in QT interval.

Figure 5.7 (b) shows the result for the cellular equivalents. Due to the length of each field potential recording, we are limited to a scale factor of up to 10 beats. Similar to RR intervals, IBIs reaches a plateau around $\tau \sim 6$, indicative of LRC. The average MSE curve for IBI lies far below that of the shuffled series for all the available scales, contrary to what we observe for the RR intervals in Fig. 5.7 (a). This appears to be due to the variation among different hiPSC-CMs; some cell lines produce more 'regular' IBI than others (Fig. 5.7 (c)). On the other hand, we observe that FPDs have almost the same profile as the shuffled FPDs. In other words, in the scale range available, FPDs show characteristics of white noise. The average MSE profiles are consistent among the cell aggregates, even though their magnitudes vary and the profiles in the smallest scale regimes < 5 beats may be different, as seen in Fig. 5.7 (c) and (d). Presently it is not clear why there is large variation in the entropy values between cell lines, differentiation methods, and the age of the CMs.

We briefly add here the MSE analysis result on IBI series of LQT1-CMs com-

pared to the healthy CMs. Figure 5.8 shows that WT- and asymptomatic LQT1-CMs exhibit comparable MSE curves, while the entropy continues to decrease for symptomatic LQT1-CMs for longer scales than the other two. The result aligns well with our findings in Sec. 5.1.1 that the scaling properties in the small scales, quantified by DFA-2 α_1, are comparable between WT- and asymptomatic LQT1-CMs, but symptomatic LQT1-CMs exhibit reduction in the correlation towards that of white noise.

In Publication III, we investigate the correlation properties in FPD series of healthy hiPSC-CMs by Poincaré plots and DFA. We first review the Poincaré plots of RR and QT, shown in Fig. 1 in Publication III. For RR intervals, we see a clear positive beat-to-beat correlation. The fan-like shape of the Poincaré plot reflects the heart rate dependence of beat-to-beat variation (we discuss the relationship further in Sec. 5.3), as RR interval increases. The QT variability is relatively smaller in magnitude but also generally exhibits a positive correlation between two consecutive beats similar to RR intervals. We note that the fan-like shape (increasing variation with increasing interval) in (b) is not reciprocated in the QT intervals.

Poincaré plots for the cellular equivalence from a 6-well MEA are shown in Fig. 5.9. While IBIs have very similar positively elongated shapes, the positive correlation is not too obvious in FPDs. The round shapes of Poincaré plots reflect no correlation between two consecutive FPDs, which is in agreement with the MSE results, showing white-noise-like behavior, in small-scale regimes. In some cases, for example, the well C-E in Fig. 5.9, FPDs also exhibit a (weak) positive correlation.

So far, MSE analysis and Poincaré plots provide only small hints of meaningful (long-range) correlation in the FPDs of hiPSC-CMs. DFA allows us to check the correlation and scaling properties in the larger scale regime. We first perform a conventional DFA with two scale regimes to compute α_1 and α_2, then the scale-dependent α spectra to provide a more complete description of the scaling behaviors of IBI and FPD in comparison to their ECG counterparts.

Based on the results so far, it should come as no surprise that RR and IBI exhibit similar fractal scaling properties (see Publication III or Ref. [19] for more details). We now focus more on the QT variability and its equivalence, FPD variability. QT intervals have significantly different mean α_1 and α_2. The mean α_1 is close to 0.5, indicating the scaling property of uncorrelated white noise in the short time scale. On the other hand, the mean α_2 is close to 1, indicating the presence of long-

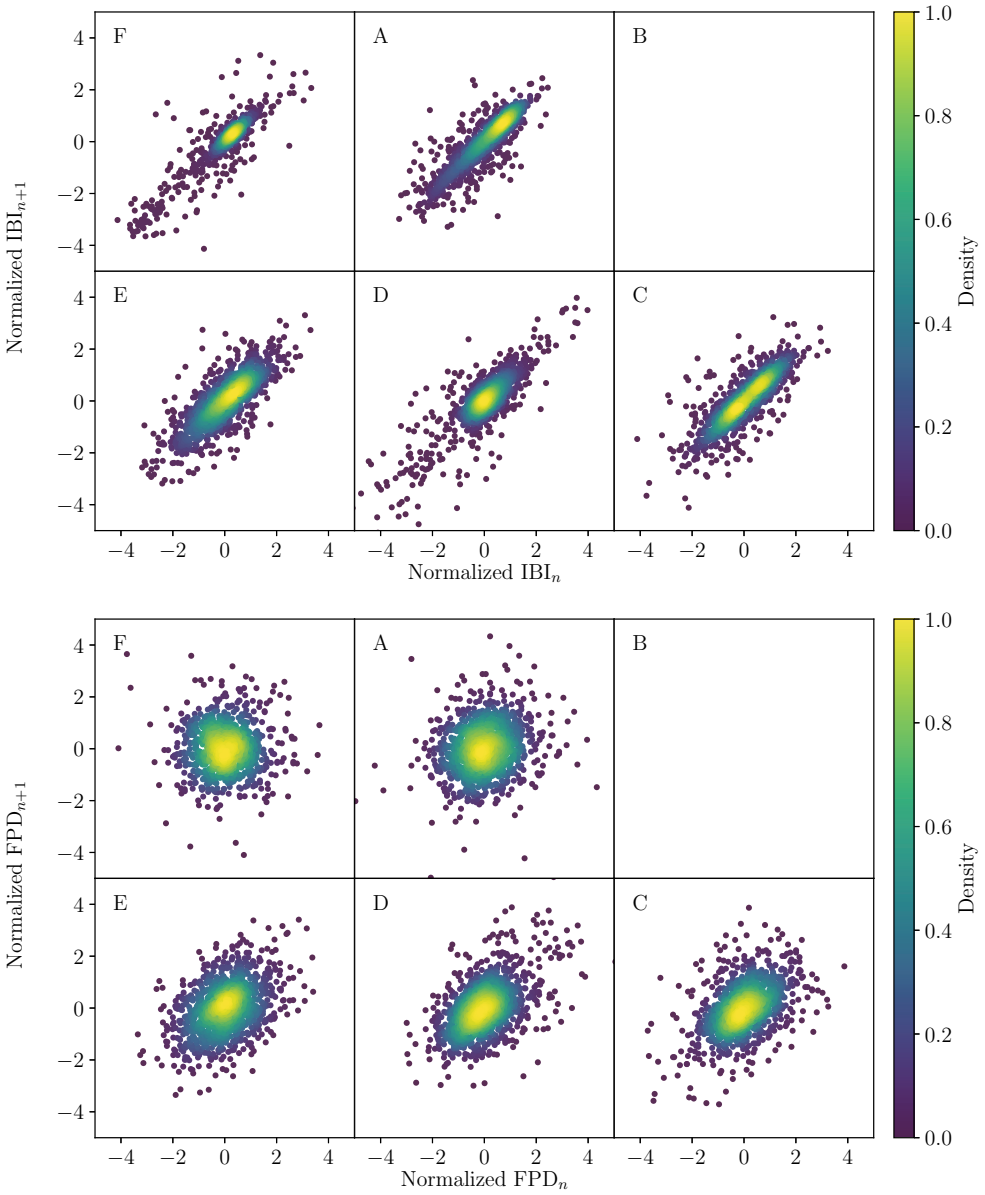

Figure 5.9 Poincaré plots for IBI and FPD series generated by a sample hiPSC-CM aggregate. Each window, labeled with A-F, represents a well in a six-well MEA. Reprinted from Publication III.

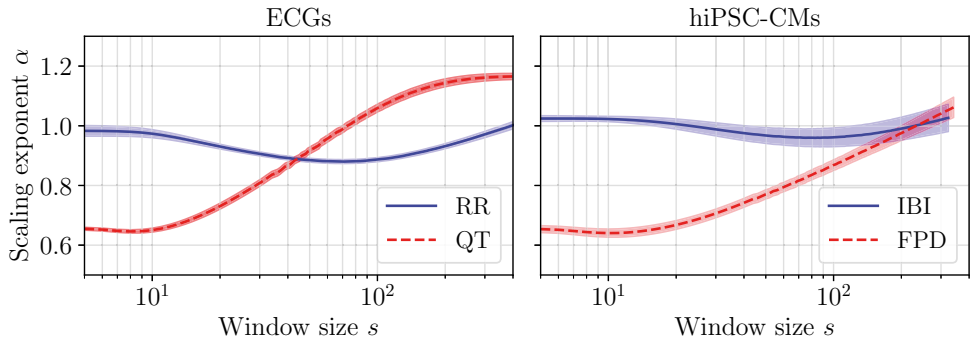

Figure 5.10 Average scaling exponents of RR and QT intervals and IBI and FPD series, as functions of the scale. An updated version of Fig. 4 in Publication III.

range correlation as the RR intervals. FPDs also have very similar average scaling exponents, with only a small discrepancy that α_2 is slightly smaller than that of the QT intervals (p-value ~ 0.09). The results clearly show that QT intervals and FPDs are indeed long-range correlated. The full spectra of scaling exponents are shown in Fig. 5.10. They provide a more complete description of the scaling properties as a function of the scale (more generalized). Again, the overall resemblance between the ECGs and the cell data is clear. The scaling exponent of QT intervals has a very distinctive scaling dependency compared to RR; it increases steadily for the scales longer than 10 beats until it reaches $\alpha \sim 1$. The $\alpha(s)$ of FPD behaves similarly but the increase in the exponent is slower than that of QT intervals.

To summarize, hiPSC-CMs exhibit similar correlation properties as RR and QT intervals, especially in small scales. The scaling exponents of IBI and FPD evolve in a comparable manner to those of RR and FPD, but the long-range correlation is attenuated for FPDs of the cells. In Publication III, we discuss possible explanations for the discrepancy. One such reason is the different RR-QT relationship at the cellular level in the absence of autonomic regulation of the nervous system. In this study, we did not account for the beat-rate dependence of QT intervals and FPDs; in other words, we did not use the beat-rate "corrected" values. While there have been many studies on the response of QT intervals to changes in RR intervals [125], [126], the relationship is not too clear at the cellular level; in fact, as Fig. 5 in Publication III shows, FPDs do not necessarily have a positive correlation with IBIs.

5.3 Relationship between beat rate and beat rate variability

Heart rate is regulated by two branches of the autonomic nervous system; the sympathetic nervous system (SNS) promotes acceleration of the heart rate, while the parasympathetic nervous system (PNS) causes deceleration of the heart rate. And HRV, which measures the degree of variation in the heart rate, reflects the balance between the SNS and PNS and serves as a good marker of cardiac morbidity and mortality [44]. Therefore HRV measures have become popular in assessing cardiac health, in addition to the heart rate. However, some argue that HRV is driven solely by the heart rate, making it a surrogate of the heart rate rather than a mirror of the ANS [127], while others believe that there are independent effects of the ANS on HRV apart from the obvious influence from the heart rate [128].

Many conventional HRV metrics indeed exhibit clear relationship with the heart rate, especially in a chronotropic state, that is, when the heart rate is changing. In the case of the standard deviation of RR intervals (SDNN), a universal beat rate dependence is observed also in denervated hearts and sinoatrial nodal cells of animals, as well as in a functioning human heart [127], which motivated us to examine the relationship between the beat rate and the BRV in the hiPSC-CMs in Publication IV.

In Publication IV, we induce chronotropic states for the independently beating clusters of healthy hiPSC-CMs by reducing and restoring the oxygen in the environment. The beat rate changes due to the changing oxygen state are very clear in each sample of cell aggregates and they happen over an extended period of 6-8 hours. Therefore they provide an excellent platform to observe the dynamical effect of hypoxia and reperfusion on BRV, despite the small number of samples. The results are summarized as follows.

5.3.1 Time- and frequency-domain BRV

Beat rate dependence is most evident and intuitive in the time-domain BRV measures. As RR intervals and heart rate are inversely proportional, changes in higher heart rate naturally correspond to a smaller difference in the RR intervals. For example, while the increase in heart rate by 20 bpm at 60 bpm is equivalent to a decrease in RR interval by 250 ms, the same increase by 20 bpm at 100 bpm corresponds to a decrease in RR by 100 ms. A negative exponential relationship of SDNN and the

root-mean-square of successive differences (RMSSD) with respect to the heart rate has been reported and attempts to correct the measures for the beat rate have been made [129], [130].

We observe the negative exponential relationship between SDNN and the beat rate also in hiPSC-CMs and establish an exponential model similar that that of Monfredi et al. [127],

$$\mathrm{SDNN} = \mathrm{SDNN}_{\mathrm{ref}} \exp\left[\frac{\mathrm{BR}_{\mathrm{ref}} - \mathrm{BR}}{8.7}\right], \tag{5.1}$$

which predicts the changes in SDNN as a function of the beat rate (BR). As shown in Fig. 7 in Publication IV, when each average baseline beat rate and SDNN are used as the reference values, aggregate samples with higher baseline beat rates follow the universal exponential model closely, especially during hypoxia. Others are less conclusive; though the model may be suitable within the standard deviation of the SDNN, and SDNN during stable hypoxia and reperfusion phases deviate from the model in some samples. The results may be an indication of the need for sample-specific models or a possibility of the hypoxia-induced changes beyond the simple beat rate dependence. Due to the limited number of samples, however, it is not sufficient to make a clear conclusion.

Frequency domain measures, low-frequency (LF) and high-frequency (HF) powers, exhibit a strong negative exponential relationship. In Publication IV, we conclude that the strong dependence is more likely to be an artifact of a trivial inverse relationship between IBI and beat rate, rather than something physiologically meaningful. Because the beat rate dependence is comparable between LF and HF powers, when we take the ratio of the two, LF/HF, the dependence is essentially eliminated. Similarly, normalizing the LF and HF measures by the total power (LF + HF) would be another way to remove the strong beat-rate dependence. We observe that the LF/HF computed over the complete phases tends to decrease during HYPOX-I (see Table 5.3 for definitions) and on average does not recover, as shown in Fig. 8 of Publication IV. There are no consistent behaviors among the aggregates, thus the results are largely inconclusive.

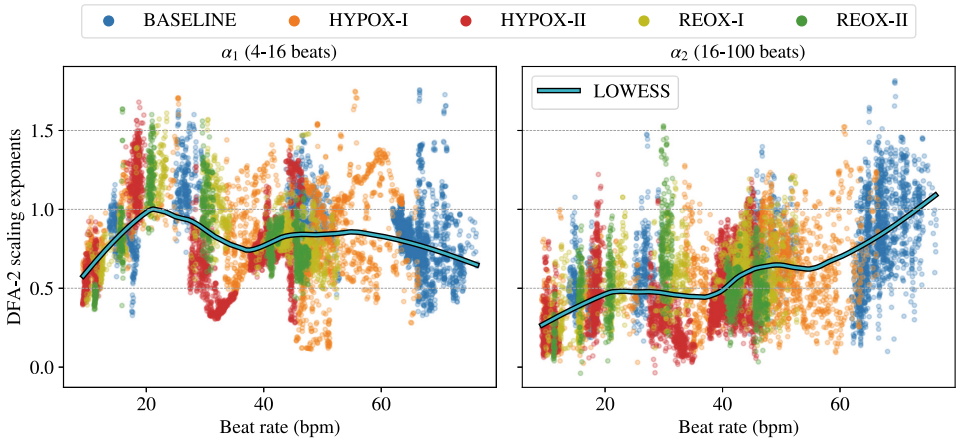

Figure 5.11 DFA-2 scaling exponents α_1 and α_2 as a function of beat rate. The scaling exponents are calculated for a moving window of 300 beats and are plotted over the mean beat rate of the window. Different colors indicate the oxygen phases. The locally weighted scatterplot smoothing (LOWESS) curves are added to show the local trend in the data.

5.3.2 DFA scaling exponents

Discussions on the effects of hypoxia and reperfusion on the scaling exponents are found in Sec. 5.1.3. In this section, we describe the relationship between DFA scaling exponents and the beat rate discussed in Publication IV. Unlike the time- and frequency-domain measures, the beat rate dependence is not so obvious (Fig. 5.11); while the average α_2 appears to increase uniformly from 0.5 to 1.0, α_1 seems to fluctuate with increasing beat rates. These initial observations suggest that the beat rate dependence is not characterized easily by a simple relation as for the basic time- and frequency-domain measures. However, we must note that the strong local behaviors are most likely due to sample-specific characteristics since the aggregates have wildly varying beat rate ranges. One solution is to use the beat rate relative to the baseline mean beat rate, rather than the absolute mean beat rate. The results are shown in Fig. 10 in Publication IV. In summary, α_1 exhibit weaker correlation with the beat rate, while α_2 show in general a more prominent positive correlation. Analysis with the relative beat rate reveals that the scaling exponents exhibit trends with opposite slopes during hypoxia compared to the other phases. While the current result is not yet sufficient to draw a definitive conclusion, it suggests that hypoxia has an effect on the scaling exponents that cannot be explained by the changes in the beat rate alone.

The nonlinear correlation between the scaling exponents and the beat rate has

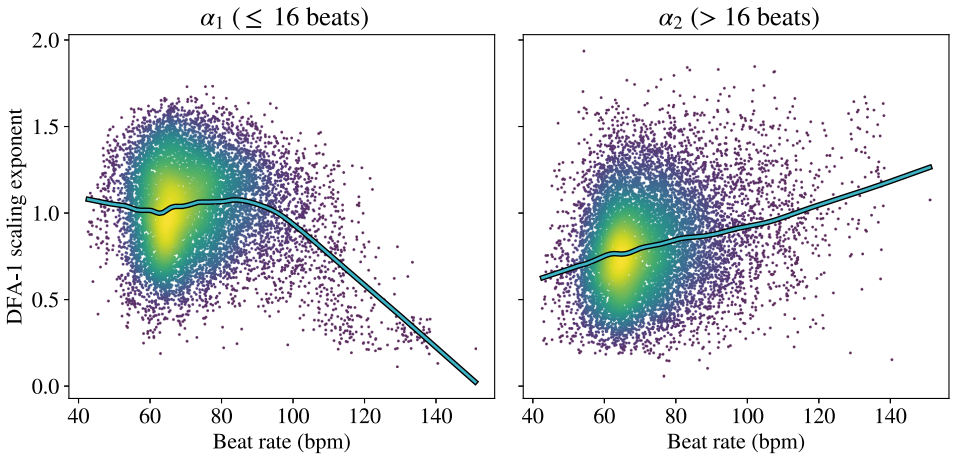

Figure 5.12 DFA-1 scaling exponents α_1 and α_2 of RR interval segments of 100 beats as a function of beat rate. RR intervals are extracted from 24 subjects in Physionet ECG databank [131]. The segments of RR intervals with beat rates ranging over 10 bpm are omitted. Locally Weighted Scatterplot Smoothing (LOWESS) curves are added to show the local trend in the data.

been also seen in the ECG data [60]. We also check the relationship in RR intervals, extracted from PhysioNet ECG databases [131] (Fig. 5.12). Since the beat rate naturally varies over the 24-hour recordings, we use the moving window of 100 beats and omit those that have a large variation of the beat rate (> 10 bpm). Most windows of RR intervals fall roughly between 50 - 90 bpm, in which the α_1 is roughly constant, and α_2 has a positive trend. The rapid decline in α_1 towards anti-correlation for beat rates over 100 bpm may reflect the person's reaching a heart rate threshold in the exercise intensity, which has been studied in detail in recent years [60]. Overall, the beat rate dependence in the resting condition has a comparable trend with the results from the cells. In summary, the results so far suggest that on average the short-range correlation is independent of the beat rate, while the LRC shows on average a positive linear relationship with the beat rates.

In general, it is not possible to separate the effects of chronotropic factors from the effects of beat rate on BRV. For example, in Publication IV, we observe changes in the mean scaling exponents when the oxygen is reduced or restored (see Sec. 5.1.3), however, it is unclear whether those changes reflect the alteration of the intrinsic mechanism due to hypoxia or is purely a result of beat rate dependence, independent of the environment. In order to tackle this challenge, a much larger sample

number representing a wide range of baseline beat rates is required. At present, the baseline data in Publication IV is too sparse over the beat rate to model a meaningful relationship between beat rate and BRV measures. An important takeaway is that, whether we study cells or ECG signals, the beat rate dependence must be taken into account when the changes in the LRC are detected.

5.4 Limitations

The time series analysis methods used in the studies of this thesis have many advantages in the applications to cardiology; they offer non-invasive, cost-effective, and versatile solutions to detect diseases and monitor cardiac health. Even though the study of HRV has been extremely popular in research, they are not yet used in clinical settings. Despite the potentially powerful ability of time series analysis methods, there are also several limitations that need to be addressed.

There are clearly limitations coming from nonstationarities in real-world data. Time-series analysis methods require at least quasi-stationarity more often than not, and even those that are designed to deal with nonstationarities, such as DFA, are limited in their ability to deal with features, such as slowly varying trends, thus requiring a careful preprocessing of the data. Throughout the studies, we have found that the results are often very sensitive to preprocessing, yet a common protocol or a standard guideline is lacking. As we discuss in Sec. 5.1.1 and 5.1.2, the outcome of the study can be very different depending on the severity of the preprocessing schemes. The problem becomes even more challenging when there are many unknowns about the systems of interest, i.e., in our case, the clusters of heart cells. For ECG recordings, a variety of measurement devices, large databases, a good physiological understanding of existing trends, e.g., circadian rhythm, and advanced algorithms to detect important parameters, such as RR and QT intervals, are readily available and constantly improved. On the other hand, hiPSC-CMs are more delicate to work with; they naturally have large variations in their functionality and their measurements are easily influenced by factors, such as the movement of the aggregates and changes in the coupling between the electrodes and the aggregates. Furthermore, it is often ambiguous to determine whether an outlier or underlying trend reflects a physical effect or a spurious feature. In the studies presented in this thesis, we keep the preprocessing steps minimal so that we may not discard the real features of the data.

Another limitation to consider is the state-of-the-art methods to produce hiPSC-CMs. It has been known that hiPSC-CMs are different from mature adult CMs in electrophysiology, and thus their functionality. The hiPSC-CMs used in the studies of this thesis are not tested for their subtypes, and the effects of different factors, such as the cell lines, age, differentiation methods, size, and the number of cells in the aggregates are not considered. The inefficiency in the production also leads to a small sample size, which all the studies have suffered from, but especially the work in Publication IV; even though each recording is exceptionally long, only six aggregate samples were available in total.

6 CONCLUSION AND OUTLOOK

In this thesis, we investigate the complexity in the beating of human heart cells, i.e., cardiomyocytes generated by human-induced pluripotent stem cell technology (hiPSC-CMs). Our computational approach focuses on advanced time series analysis methods, especially nonlinear tools to examine the scaling properties of the beats.

We build upon the state-of-the-art knowledge that hiPSC-CMs exhibit fractal power-law scaling in the beat-to-beat fluctuations, or beat rate variability. In all the studies presented in this thesis, we first confirm that the spontaneous beat rates of hiPSC-CM aggregates exhibit long-range correlations similar to those found in the functioning human heart. We demonstrate that the fractal scaling can be altered by the presence of genetic mutations, exposure to drugs, and external stress in the environment. Understanding these factors is important in establishing hiPSC-CMs as an *in vitro* model of the heart for future studies, as well as for applications in drug safety assessments.

We find that the fractal scaling in interbeat intervals (IBIs) is fairly robust. It is altered by the LQT1-specific mutation, only in some cases, in particular, when the CMs are derived from the symptomatic LQT1-specific mutation carrier. When the hiPSC-CMs are exposed to three pharmacological compounds that are known to influence the beat rates and potassium ion channel, we detect the change in scaling behavior. The change was only notable for a large dose of a beta-blocker on symptomatic LQT1-CMs, though the beta-blocker did not alter the beat rates of the CMs. On the other hand, we observe that hiPSC-CMs respond to hypoxia by drastically reducing their beat rates, and our analysis suggests alteration of the short- and long-range correlations. On average, the correlation found in the short-scale regime recovers while that of the long-scale regime appears to be hindered even after the oxygen is restored. Based on the findings, we conclude that short-range correlations in the beat rates of hiPSC-CMs tend to be more robust than long-range correlations in the presence of LQT1-specific mutations, exposure to drugs, and hypoxia.

When they undergo a chronotropic condition, which alters the beat rates drastically, correlation may also be affected to a larger degree.

There are continuous efforts to reliably produce hiPSC-CMs that can overcome the current limitations of low efficiency and their relative immaturity. Time series analysis can potentially contribute to the development of the reliable establishment of the baseline cell models, by studying different characteristics of the hiPSC-CMs. One aspect to investigate further may be the abnormal peaks and decay effects in the cellular field potential (as shown in Publication IV) and their effects on IBI properties. While this thesis only discusses the effects of LQT1-specific mutations, it would be extremely beneficial to include other hereditary diseases, such as dilated cardiomyopathy, as well as various forms of arrhythmia that are common in hiPSC-CMs.

We also investigate the field-potential durations (FPDs), which are measured to assess the functionality of the CMs. Their nonlinear correlation properties have not yet been widely studied despite their important analogue in the human electrocardiogram, that is, the QT interval. We apply Poincaré plots and detrended fluctuation analysis (DFA) on IBI and FPD series from healthy hiPSC-CMs and compare the results with RR and QT intervals from electrocardiograms. We find that FPDs appear to behave similarly to uncorrelated signals, but in the long-scale regime they exhibit intrinsic correlations. The scaling properties are comparable to that of QT intervals, though it is attenuated for FPDs. The findings give rise to important research questions about the relationship between RR and QT intervals at the cellular level. RR and QT intervals have a nontrivial relationship and less is known about the relationship between IBI and FPD, especially in the absence of autonomic neural control. Further studies exploring (long-range) cross-correlation and transfer entropy between IBIs and FPDs are natural next steps following this thesis.

REFERENCES

[1] F. Dyson, "Characterizing irregularity: Fractals. Form, Chance, and Dimension. Benoit B. Mandelbrot. Translation and revision of French edition (Paris, 1975). Freeman, San Francisco, 1977. xviii, 366 pp," *Science*, vol. 200, no. 4342, pp. 677–678, 1978.

[2] B. B. Mandelbrot and B. B. Mandelbrot, *The fractal geometry of nature*. WH Freeman New York, 1982, vol. 1.

[3] B. B. Mandelbrot and J. W. Van Ness, "Fractional brownian motions, fractional noises and applications," *SIAM review*, vol. 10, no. 4, pp. 422–437, 1968.

[4] B. B. Mandelbrot and J. R. Wallis, "Some long-run properties of geophysical records," *Water Resources Research*, vol. 5, no. 2, pp. 321–340, 1969.

[5] C.-K. Peng, S. V. Buldyrev, S. Havlin, M. Simons, H. E. Stanley, and A. L. Goldberger, "Mosaic organization of DNA nucleotides," *Physical Review E*, vol. 49, no. 2, p. 1685, 1994.

[6] C. Matsoukas, S. Islam, and I. Rodriguez-Iturbe, "Detrended fluctuation analysis of rainfall and streamflow time series," *Journal of Geophysical Research: Atmospheres*, vol. 105, no. D23, pp. 29 165–29 172, 2000.

[7] A. Tuck and S. Hovde, "Fractal behavior of ozone, wind and temperature in the lower stratosphere," *Geophysical Research Letters*, vol. 26, no. 9, pp. 1271–1274, 1999.

[8] V. Kotimäki, E. Räsänen, H. Hennig, and E. J. Heller, "Fractal dynamics in chaotic quantum transport," *Physical Review E*, vol. 88, no. 2, p. 022 913, 2013.

[9] J. M. Hausdorff, P. L. Purdon, C.-K. Peng, Z. Ladin, J. Y. Wei, and A. L. Goldberger, "Fractal dynamics of human gait: Stability of long-range correlations in stride interval fluctuations," *Journal of Applied Physiology*, vol. 80, no. 5, pp. 1448–1457, 1996.

[10] C.-K. Peng, S. Havlin, H. E. Stanley, and A. L. Goldberger, "Quantification of scaling exponents and crossover phenomena in nonstationary heartbeat time series," *Chaos: An Interdisciplinary Journal of Nonlinear Science*, vol. 5, no. 1, pp. 82–87, 1995.

[11] A. L. Goldberger, L. A. Amaral, J. M. Hausdorff, P. C. Ivanov, C.-K. Peng, and H. E. Stanley, "Fractal dynamics in physiology: Alterations with disease and aging," *Proceedings of the National Academy of Sciences*, vol. 99, no. suppl_1, pp. 2466–2472, 2002.

[12] C. J. Evertsz, "Fractal geometry of financial time series," *Fractals*, vol. 3, no. 03, pp. 609–616, 1995.

[13] H. Hennig, R. Fleischmann, A. Fredebohm, *et al.*, "The nature and perception of fluctuations in human musical rhythms," *PLOS One*, vol. 6, no. 10, e26457, 2011.

[14] E. Räsänen, O. Pulkkinen, T. Virtanen, M. Zollner, and H. Hennig, "Fluctuations of hi-hat timing and dynamics in a virtuoso drum track of a popular music recording," *PLOS One*, vol. 10, no. 6, e0127902, 2015.

[15] J. B. Bassingthwaighte, L. S. Liebovitch, and B. J. West, *Fractal physiology*. Springer, 2013.

[16] P. M. Iannaccone and M. Khokha, *Fractal geometry in biological systems: an analytical approach*. CRC Press, 1996.

[17] E. R. Weibel, "What makes a good lung?" *Swiss Medical Weekly*, vol. 139, no. 2728, 2009.

[18] A. Bunde, S. Havlin, J. W. Kantelhardt, T. Penzel, J.-H. Peter, and K. Voigt, "Correlated and uncorrelated regions in heart-rate fluctuations during sleep," *Physical Review Letters*, vol. 85, no. 17, p. 3736, 2000.

[19] Y. Mandel, A. Weissman, R. Schick, *et al.*, "Human embryonic and induced pluripotent stem cell–derived cardiomyocytes exhibit beat rate variability and power-law behavior," *Circulation*, vol. 125, no. 7, pp. 883–893, 2012.

[20] K. Takahashi and S. Yamanaka, "Induction of pluripotent stem cells from mouse embryonic and adult fibroblast cultures by defined factors," *Cell*, vol. 126, no. 4, pp. 663–676, 2006.

[21] E. Lorenz, *Predictability: does the flap of a butterfly's wing in Brazil set off a tornado in Texas?* na, 1972.

[22] H. Poincaré, *The three-body problem and the equations of dynamics: Poincaré's foundational work on dynamical systems theory*. Springer, 2017, vol. 443.

[23] E. N. Lorenz, "Deterministic nonperiodic flow," *Journal of Atmospheric Sciences*, vol. 20, no. 2, pp. 130–141, 1963.

[24] R. M. May, "Simple mathematical models with very complicated dynamics," in *The Theory of Chaotic Attractors*, Springer, 2004, pp. 85–93.

[25] T.-Y. Li and J. A. Yorke, "Period three implies chaos," in *The theory of chaotic attractors*, Springer, 2004, pp. 77–84.

[26] E. N. Lorenz and K. Haman, "The essence of chaos," *Pure and Applied Geophysics*, vol. 147, no. 3, pp. 598–599, 1996.

[27] D. Viswanath, "The fractal property of the lorenz attractor," *Physica D: Nonlinear Phenomena*, vol. 190, no. 1-2, pp. 115–128, 2004.

[28] K. Falconer, *Fractal geometry: mathematical foundations and applications*. John Wiley & Sons, 2004.

[29] B. Mandelbrot, "How long is the coast of Britain? Statistical self-similarity and fractional dimension," *Science*, vol. 156, no. 3775, pp. 636–638, 1967.

[30] H. E. Hurst, "Long-term storage capacity of reservoirs," *Transactions of the American Society of Civil Engineers*, vol. 116, no. 1, pp. 770–799, 1951.

[31] J. W. Kantelhardt, "Fractal and multifractal time series," *arXiv:0804.0747*, 2008.

[32] T. Graves, R. Gramacy, N. Watkins, and C. Franzke, "A brief history of long memory: Hurst, Mandelbrot and the road to ARFIMA, 1951–1980," *Entropy*, vol. 19, no. 9, p. 437, 2017.

[33] B. Mandelbrot, "Une classe de processus stochastiques homothetiques a soi-application a la loi climatologique de he hurst," *Comptes Rendus Hebdomadaires des Seances de l Academie des Sciences*, vol. 260, no. 12, pp. 3274–+, 1965.

[34] C. Granger, "New classes of time series models," *Journal of the Royal Statistical Society. Series D (The Statistician)*, vol. 27, no. 3/4, pp. 237–253, 1978.

[35] J. R. M. Hosking, "Fractional differencing," *Biometrika*, vol. 68, no. 1, pp. 165–176, Apr. 1981.

[36] G. E. Box, G. M. Jenkins, G. C. Reinsel, and G. M. Ljung, *Time series analysis: forecasting and control*. John Wiley & Sons, 2015.

[37] C.-K. Peng, S. V. Buldyrev, A. L. Goldberger, *et al.*, "Long-range correlations in nucleotide sequences," *Nature*, vol. 356, no. 6365, pp. 168–170, 1992.

[38] M. Molkkari, "Advanced methods in detrended fluctuation analysis with applications in computational cardiology," M.S. thesis, Tampere University, 2019.

[39] J. Licinio, C. Bolis, W. H. Organization, *et al.*, "The autonomic nervous system/edited by CL Bolis and J. Licinio," in *The autonomic nervous system/edited by CL Bolis and J. Licinio*, 1999.

[40] L. Glass, M. R. Guevara, and A. Shrier, "Universal Bifurcations and the Classification of Cardiac Arrhythmias," *Annals of the New York Academy of Sciences*, vol. 504, no. 1, pp. 168–178, 1987.

[41] J. P. Saul, "Beat-to-beat variations of heart rate reflect modulation of cardiac autonomic outflow," *Physiology*, vol. 5, no. 1, pp. 32–37, 1990.

[42] M. N. Levy, "Brief reviews: Sympathetic-parasympathetic interactions in the heart," *Circulation Research*, vol. 29, no. 5, pp. 437–445, 1971.

[43] R. Kitney and O. Rompelman, *The study of heart-rate variability*. Oxford University Press, USA, 1980.

[44] U. Rajendra Acharya, K. Paul Joseph, N. Kannathal, C. M. Lim, and J. S. Suri, "Heart rate variability: A review," *Medical and Biological Engineering and Computing*, vol. 44, no. 12, pp. 1031–1051, 2006.

[45] S. Akselrod, D. Gordon, F. A. Ubel, D. C. Shannon, A. C. Berger, and R. J. Cohen, "Power spectrum analysis of heart rate fluctuation: A quantitative probe of beat-to-beat cardiovascular control," *Science*, vol. 213, no. 4504, pp. 220–222, 1981.

[46] B. Pomeranz, R. Macaulay, M. A. Caudill, *et al.*, "Assessment of autonomic function in humans by heart rate spectral analysis," *American Journal of Physiology, Heart and Circulatory Physiology*, vol. 248, no. 1, H151–H153, 1985.

[47] M. Malik, "Heart rate variability: Standards of measurement, physiological interpretation, and clinical use: Task force of the european society of cardiology and the north american society for pacing and electrophysiology," *Annals of Noninvasive Electrocardiology*, vol. 1, no. 2, pp. 151–181, 1996.

[48] D. T. Kaplan and R. J. Cohen, "Searching for Chaos in Fibrillation," *Annals of the New York Academy of Sciences*, vol. 591, no. 1, pp. 367–374, 1990.

[49] M. E. Cohen, D. L. Hudson, and P. C. Deedwania, "Applying continuous chaotic modeling to cardiac signal analysis," *IEEE Engineering in Medicine and Biology Magazine*, vol. 15, no. 5, pp. 97–102, 1996.

[50] D. N. Dutt and S. Krishnan, "Application of phase space technique to the analysis of cardiovascular signals," in *Proceedings of the First Joint BMES/EMBS Conference. 1999 IEEE Engineering in Medicine and Biology 21st Annual Conference and the 1999 Annual Fall Meeting of the Biomedical Engineering Society*, IEEE, vol. 2, 1999, 914–vol.

[51] D. Lin and R. Hughson, "Modeling heart rate variability in healthy humans: A turbulence analogy," *Physical Review Letters*, vol. 86, no. 8, p. 1650, 2001.

[52] K. K. Ho, G. B. Moody, C.-K. Peng, *et al.*, "Predicting survival in heart failure case and control subjects by use of fully automated methods for deriving nonlinear and conventional indices of heart rate dynamics," *Circulation*, vol. 96, no. 3, pp. 842–848, 1997.

[53] T. H. Mäkikallio, J. Koistinen, L. Jordaens, *et al.*, "Heart rate dynamics before spontaneous onset of ventricular fibrillation in patients with healed myocardial infarcts," *The American Journal of Cardiology*, vol. 83, no. 6, pp. 880–884, 1999.

[54] H. V. Huikuri, T. H. Mäkikallio, C.-K. Peng, A. L. Goldberger, U. Hintze, and M. Møller, "Fractal correlation properties of RR interval dynamics and mortality in patients with depressed left ventricular function after an acute myocardial infarction," *Circulation*, vol. 101, no. 1, pp. 47–53, 2000.

[55] N. G. Mahon, A. E. Hedman, M. Padula, *et al.*, "Fractal correlation properties of R-R interval dynamics in asymptomatic relatives of patients with dilated cardiomyopathy," *European Journal of Heart Failure*, vol. 4, no. 2, pp. 151–158, 2002.

[56] K. Otsuka, G. Cornelissen, and F. Halberg, "Age, gender and fractal scaling in heart rate variability," *Clinical Science*, vol. 93, no. 4, pp. 299–308, 1997.

[57] P. C. Ivanov, A. Bunde, L. N. Amaral, *et al.*, "Sleep-wake differences in scaling behavior of the human heartbeat: Analysis of terrestrial and long-term space flight data," *Europhysics Letters*, vol. 48, no. 5, p. 594, 1999.

[58] T. Penzel, J. W. Kantelhardt, L. Grote, J.-H. Peter, and A. Bunde, "Comparison of detrended fluctuation analysis and spectral analysis for heart rate variability in sleep and sleep apnea," *IEEE Transactions on Biomedical Engineering*, vol. 50, no. 10, pp. 1143–1151, 2003.

[59] M. P. Tulppo, R. L. Hughson, T. H. Mäkikallio, K. J. Airaksinen, T. Seppänen, and H. V. Huikuri, "Effects of exercise and passive head-up tilt on fractal and complexity properties of heart rate dynamics," *American Journal of Physiology-Heart and Circulatory Physiology*, vol. 280, no. 3, H1081–H1087, 2001.

[60] M. Molkkari, G. Angelotti, T. Emig, and E. Räsänen, "Dynamical heart beat correlations during running," *Scientific Reports*, vol. 10, no. 1, pp. 1–9, 2020.

[61] R. Wilders and H. J. Jongsma, "Beating irregularity of single pacemaker cells isolated from the rabbit sinoatrial node," *Biophysical Journal*, vol. 65, no. 6, pp. 2601–2613, 1993.

[62] J. P. Kucera, M. O. Heuschkel, P. Renaud, and S. Rohr, "Power-law behavior of beat-rate variability in monolayer cultures of neonatal rat ventricular myocytes," *Circulation Research*, vol. 86, no. 11, pp. 1140–1145, 2000.

[63] J. G. Ponard, A. A. Kondratyev, and J. P. Kucera, "Mechanisms of intrinsic beating variability in cardiac cell cultures and model pacemaker networks," *Biophysical Journal*, vol. 92, no. 10, pp. 3734–3752, 2007.

[64] O. Monfredi, L. A. Maltseva, H. A. Spurgeon, M. R. Boyett, E. G. Lakatta, and V. A. Maltsev, "Beat-to-beat variation in periodicity of local calcium releases contributes to intrinsic variations of spontaneous cycle length in isolated single sinoatrial node cells," *PLOS One*, vol. 8, no. 6, e67247, 2013.

[65] Y. Yaniv, A. E. Lyashkov, and E. G. Lakatta, "The fractal-like complexity of heart rate variability beyond neurotransmitters and autonomic receptors:

Signaling intrinsic to sinoatrial node pacemaker cells," *Cardiovascular Pharmacology: Open Access*, vol. 2, 2013.

[66] J. B. Gurdon, *The developmental capacity of nuclei taken from intestinal epithelium cells of feeding tadpoles*. Oxford University Press for The Company of Biologists Limited, 1962.

[67] M. Brouwer, H. Zhou, and N. Nadif Kasri, "Choices for induction of pluripotency: Recent developments in human induced pluripotent stem cell reprogramming strategies," *Stem Cell Reviews and Reports*, vol. 12, no. 1, pp. 54–72, 2016.

[68] I. Kehat, D. Kenyagin-Karsenti, M. Snir, *et al.*, "Human embryonic stem cells can differentiate into myocytes with structural and functional properties of cardiomyocytes," *The Journal of Clinical Investigation*, vol. 108, no. 3, pp. 407–414, 2001.

[69] C. Mummery, D. Ward-van Oostwaard, P. Doevendans, *et al.*, "Differentiation of human embryonic stem cells to cardiomyocytes: Role of coculture with visceral endoderm-like cells," *Circulation*, vol. 107, no. 21, pp. 2733–2740, 2003.

[70] N. Gaborit, S. Le Bouter, V. Szuts, *et al.*, "Regional and tissue specific transcript signatures of ion channel genes in the non-diseased human heart," *The Journal of Physiology*, vol. 582, no. 2, pp. 675–693, 2007.

[71] J. Kuusela, V. J. Kujala, A. Kiviaho, *et al.*, "Effects of cardioactive drugs on human induced pluripotent stem cell derived long qt syndrome cardiomyocytes," *Springerplus*, vol. 5, no. 1, pp. 1–13, 2016.

[72] A. O. Grant, "Cardiac ion channels," *Circulation: Arrhythmia and Electrophysiology*, vol. 2, no. 2, pp. 185–194, 2009.

[73] J. M. Nerbonne and R. S. Kass, "Molecular physiology of cardiac repolarization," *Physiological Reviews*, vol. 85, no. 4, pp. 1205–1253, 2005.

[74] B. G. Kornreich, "The patch clamp technique: Principles and technical considerations," *Journal of Veterinary Cardiology*, vol. 9, no. 1, pp. 25–37, 2007.

[75] J. Kuusela, "Modelling Long QT Syndrome in patient-specific cardiomyocytes," *Tampere University Press*, 2016.

[76] P. Pradhapan, J. Kuusela, J. Viik, K. Aalto-Setälä, and J. Hyttinen, "Cardiomyocyte mea data analysis (cardiomda)–a novel field potential data analysis software for pluripotent stem cell derived cardiomyocytes," *PLOS One*, vol. 8, no. 9, e73637, 2013.

[77] L. Guo, J.-Y. Qian, R. Abrams, *et al.*, "The electrophysiological effects of cardiac glycosides in human iPSC-derived cardiomyocytes and in guinea pig isolated hearts," *Cellular Physiology and Biochemistry*, vol. 27, no. 5, pp. 453–462, 2011.

[78] K. Harris, M. Aylott, Y. Cui, J. B. Louttit, N. C. McMahon, and A. Sridhar, "Comparison of electrophysiological data from human-induced pluripotent stem cell–derived cardiomyocytes to functional preclinical safety assays," *Toxicological Sciences*, vol. 134, no. 2, pp. 412–426, 2013.

[79] C. C. Veerman, G. Kosmidis, C. L. Mummery, S. Casini, A. O. Verkerk, and M. Bellin, "Immaturity of human stem-cell-derived cardiomyocytes in culture: Fatal flaw or soluble problem?" *Stem Cells and Development*, vol. 24, no. 9, pp. 1035–1052, 2015.

[80] M. Bellin, M. C. Marchetto, F. H. Gage, and C. L. Mummery, "Induced pluripotent stem cells: The new patient?" *Nature Reviews Molecular Cell Biology*, vol. 13, no. 11, pp. 713–726, 2012.

[81] N. Cao, Y. Huang, J. Zheng, *et al.*, "Conversion of human fibroblasts into functional cardiomyocytes by small molecules," *Science*, vol. 352, no. 6290, pp. 1216–1220, 2016.

[82] S. I. Protze, J. Liu, U. Nussinovitch, *et al.*, "Sinoatrial node cardiomyocytes derived from human pluripotent cells function as a biological pacemaker," *Nature Biotechnology*, vol. 35, no. 1, pp. 56–68, 2017.

[83] S. Chauveau, E. P. Anyukhovsky, M. Ben-Ari, *et al.*, "Induced pluripotent stem cell–derived cardiomyocytes provide in vivo biological pacemaker function," *Circulation: Arrhythmia and Electrophysiology*, vol. 10, no. 5, e004508, 2017.

[84] P. Ovics, D. Regev, P. Baskin, *et al.*, "Drug development and the use of induced pluripotent stem cell-derived cardiomyocytes for disease modeling and drug toxicity screening," *International Journal of Molecular Sciences*, vol. 21, no. 19, p. 7320, 2020.

[85] M. Yoneyama and K. Kawahara, "Coupled oscillator systems of cultured cardiac myocytes: fluctuation and scaling properties," *Physical Review E*, vol. 70, no. 2, p. 021 904, 2004.

[86] M. Ben-Ari, R. Schick, L. Barad, *et al.*, "From beat rate variability in induced pluripotent stem cell–derived pacemaker cells to heart rate variability in human subjects," *Heart Rhythm*, vol. 11, no. 10, pp. 1808–1818, 2014.

[87] O. Binah, A. Weissman, J. Itskovitz-Eldor, and M. R. Rosen, "Integrating beat rate variability: From single cells to hearts," *Heart Rhythm*, vol. 10, no. 6, pp. 928–932, 2013.

[88] Y. Yaniv, I. Ahmet, J. Liu, *et al.*, "Synchronization of sinoatrial node pacemaker cell clocks and its autonomic modulation impart complexity to heart beating intervals," *Heart Rhythm*, vol. 11, no. 7, pp. 1210–1219, 2014.

[89] Y. Soen and E. Braun, "Scale-invariant fluctuations at different levels of organization in developing heart cell networks," *Physical Review E*, vol. 61, no. 3, R2216, 2000.

[90] C. Chatfield, *The analysis of time series: an introduction*. Chapman and Hall, CRC, 2003.

[91] H. Kantz and T. Schreiber, *Nonlinear time series analysis*. Cambridge University Press, 2004, vol. 7.

[92] J. W. Kantelhardt, E. Koscielny-Bunde, H. H. Rego, S. Havlin, and A. Bunde, "Detecting long-range correlations with detrended fluctuation analysis," *Physica A: Statistical Mechanics and its Applications*, vol. 295, no. 3-4, pp. 441–454, 2001.

[93] N. Iyengar, C. Peng, R. Morin, A. L. Goldberger, and L. A. Lipsitz, "Age-related alterations in the fractal scaling of cardiac interbeat interval dynamics," *American Journal of Physiology-Regulatory, Integrative and Comparative Physiology*, vol. 271, no. 4, R1078–R1084, 1996.

[94] E. Koscielny–Bunde, H. Eduardo Roman, A. Bunde, S. Havlin, and H.-.-J. Schellnhuber, "Long-range power-law correlations in local daily temperature fluctuations," *Philosophical Magazine B*, vol. 77, no. 5, pp. 1331–1340, 1998.

[95] Y. Liu, P. Cizeau, M. Meyer, C.-K. Peng, and H. E. Stanley, "Correlations in economic time series," *Physica A: Statistical Mechanics and its Applications*, vol. 245, no. 3-4, pp. 437–440, 1997.

[96] J. W. Kantelhardt, R. Berkovits, S. Havlin, and A. Bunde, "Are the phases in the anderson model long-range correlated?" *Physica A: Statistical Mechanics and its Applications*, vol. 266, no. 1-4, pp. 461–464, 1999.

[97] D. Maraun, H. Rust, and J. Timmer, "Tempting long-memory-on the interpretation of DFA results," *Nonlinear Processes in Geophysics*, vol. 11, no. 4, pp. 495–503, 2004.

[98] Z. Chen, P. C. Ivanov, K. Hu, and H. E. Stanley, "Effect of nonstationarities on detrended fluctuation analysis," *Physical Review E*, vol. 65, no. 4, p. 041 107, 2002.

[99] K. Hu, P. C. Ivanov, Z. Chen, P. Carpena, and H. E. Stanley, "Effect of trends on detrended fluctuation analysis," *Physical Review E*, vol. 64, no. 1, p. 011 114, 2001.

[100] R. Bryce and K. Sprague, "Revisiting detrended fluctuation analysis," *Scientific Reports*, vol. 2, no. 1, pp. 1–6, 2012.

[101] M. Höll and H. Kantz, "The relationship between the detrendend fluctuation analysis and the autocorrelation function of a signal," *The European Physical Journal B*, vol. 88, no. 12, pp. 1–7, 2015.

[102] K. Kiyono and Y. Tsujimoto, "Nonlinear filtering properties of detrended fluctuation analysis," *Physica A: Statistical Mechanics and its Applications*, vol. 462, pp. 807–815, 2016.

[103] O. Løvsletten, "Consistency of detrended fluctuation analysis," *Physical Review E*, vol. 96, no. 1, p. 012 141, 2017.

[104] M. Höll, K. Kiyono, and H. Kantz, "Theoretical foundation of detrending methods for fluctuation analysis such as detrended fluctuation analysis and detrending moving average," *Physical Review E*, vol. 99, no. 3, p. 033 305, 2019.

[105] J. W. Kantelhardt, S. A. Zschiegner, E. Koscielny-Bunde, S. Havlin, A. Bunde, and H. E. Stanley, "Multifractal detrended fluctuation analysis of nonstationary time series," *Physica A: Statistical Mechanics and its Applications*, vol. 316, no. 1-4, pp. 87–114, 2002.

[106] B. Podobnik and H. E. Stanley, "Detrended cross-correlation analysis: A new method for analyzing two nonstationary time series," *Physical Review Letters*, vol. 100, no. 8, p. 084 102, 2008.

[107] J. Echeverria, M. Woolfson, J. Crowe, B. Hayes-Gill, G. Croaker, and H. Vyas, "Interpretation of heart rate variability via detrended fluctuation analysis and $\alpha\beta$ filter," *Chaos: An Interdisciplinary Journal of Nonlinear Science*, vol. 13, no. 2, pp. 467–475, 2003.

[108] M. P. Tulppo, T. H. Makikallio, T. Takala, T. Seppanen, and H. V. Huikuri, "Quantitative beat-to-beat analysis of heart rate dynamics during exercise," *American Journal of Physiology-Heart and Circulatory Physiology*, vol. 271, no. 1, H244–H252, 1996.

[109] S. M. Pincus, "Approximate entropy as a measure of system complexity.," *Proceedings of the National Academy of Sciences*, vol. 88, no. 6, pp. 2297–2301, 1991.

[110] J. S. Richman and J. R. Moorman, "Physiological time-series analysis using approximate entropy and sample entropy," *American Journal of Physiology-Heart and Circulatory Physiology*, vol. 278, no. 6, H2039–H2049, 2000.

[111] M. Costa, A. L. Goldberger, and C.-K. Peng, "Multiscale entropy analysis of biological signals," *Physical Review E*, vol. 71, no. 2, p. 021 906, 2005.

[112] M. Baumert, M. Javorka, A. Seeck, R. Faber, P. Sanders, and A. Voss, "Multiscale entropy and detrended fluctuation analysis of QT interval and heart rate variability during normal pregnancy," *Computers in Biology and Medicine*, vol. 42, no. 3, pp. 347–352, 2012.

[113] Q. Wang, M. Curran, I. Splawski, *et al.*, "Positional cloning of a novel potassium channel gene: KVLQT1 mutations cause cardiac arrhythmias," *Nature Genetics*, vol. 12, no. 1, pp. 17–23, 1996.

[114] M. C. Sanguinetti, C. Jiang, M. E. Curran, and M. T. Keating, "A mechanistic link between an inherited and an acquird cardiac arrthytmia: Herg encodes the IKr potassium channel," *Cell*, vol. 81, no. 2, pp. 299–307, 1995.

[115] J. Kim, J. Kuusela, K. Aalto-Setälä, and E. Räsänen, "Short-and long-range correlations in beat rate variability of human pluripotent-stem-cell-derived cardiomyocytes," in *2017 Computing in Cardiology (CinC)*, IEEE, 2017, pp. 1–4.

[116] J. S. Perkiömäki, W. Zareba, J.-P. Couderc, and A. J. Moss, "Heart rate variability in patients with congenital long QT syndrome," *Annals of Noninvasive Electrocardiology*, vol. 6, no. 4, pp. 298–304, 2001.

[117] R. E. Ahmed, T. Anzai, N. Chanthra, and H. Uosaki, "A brief review of current maturation methods for human induced pluripotent stem cells-derived cardiomyocytes," *Frontiers in Cell and Developmental Biology*, vol. 8, p. 178, 2020.

[118] A. Hidalgo, N. Glass, D. Ovchinnikov, *et al.*, "Modelling ischemia-reperfusion injury (IRI) in vitro using metabolically matured induced pluripotent stem cell-derived cardiomyocytes," *APL Bioengineering*, vol. 2, no. 2, p. 026 102, 2018.

[119] D. Shah, L. Virtanen, C. Prajapati, *et al.*, "Modeling of LMNA-related dilated cardiomyopathy using human induced pluripotent stem cells," *Cells*, vol. 8, no. 6, p. 594, 2019.

[120] M. Häkli, J. Kreutzer, A.-J. Mäki, *et al.*, "Human induced pluripotent stem cell-based platform for modeling cardiac ischemia," *Scientific Reports*, vol. 11, no. 1, pp. 1–13, 2021.

[121] O. Metsälä, J. Kreutzer, H. Högel, P. Miikkulainen, P. Kallio, and P. M. Jaakkola, "Transportable system enabling multiple irradiation studies under simultaneous hypoxia in vitro," *Radiation Oncology*, vol. 13, no. 1, pp. 1–11, 2018.

[122] J. S. Perkiömäki, J.-P. Courderc, J. P. Daubert, and W. Zareba, "Temporal complexity of repolarization and mortality in patients with implantable cardioverter defibrillators," *Pacing and Clinical Electrophysiology*, vol. 26, no. 10, pp. 1931–1936, 2003.

[123] M. Lewis, A. Short, and J. Suckling, "Multifractal characterisation of electrocardiographic RR and QT time-series before and after progressive exercise," *Computer Methods and Programs in Biomedicine*, vol. 108, no. 1, pp. 176–185, 2012.

[124] M. Baumert, A. Porta, M. A. Vos, *et al.*, "QT interval variability in body surface ECG: measurement, physiological basis, and clinical value: position statement and consensus guidance endorsed by the European Heart Rhythm Association jointly with the ESC Working Group on Cardiac Cellular Electrophysiology," *Europace*, vol. 18, no. 6, pp. 925–944, 2016.

[125] A. Cabasson, O. Meste, and J.-M. Vesin, "Estimation and modeling of QT-interval adaptation to heart rate changes," *IEEE Transactions on Biomedical Engineering*, vol. 59, no. 4, pp. 956–965, 2011.

[126] I. Potapov, J. Latukka, J. Kim, P. Luukko, K. Aalto-Setälä, and E. Räsänen, "Information transfer in QT-RR dynamics: Application to QT-correction," *Scientific Reports*, vol. 8, no. 1, pp. 1–9, 2018.

[127] O. Monfredi, A. E. Lyashkov, A.-B. Johnsen, *et al.*, "Biophysical characterization of the underappreciated and important relationship between heart rate variability and heart rate," *Hypertension*, vol. 64, no. 6, pp. 1334–1343, 2014.

[128] E. J. de Geus, P. J. Gianaros, R. C. Brindle, J. R. Jennings, and G. G. Berntson, "Should heart rate variability be "corrected" for heart rate? Biological, quantitative, and interpretive considerations," *Psychophysiology*, vol. 56, no. 2, e13287, 2019.

[129] J. Sacha, "Interaction between heart rate and heart rate variability," *Annals of Noninvasive Electrocardiology*, vol. 19, no. 3, pp. 207–216, 2014.

[130] A. M. Van Roon, H. Snieder, J. D. Lefrandt, E. J. De Geus, and H. Riese, "Parsimonious correction of heart rate variability for its dependency on heart rate," *Hypertension*, vol. 68, no. 5, e63–e65, 2016.

[131] A. L. Goldberger, L. A. Amaral, L. Glass, *et al.*, "PhysioBank, PhysioToolkit, and PhysioNet: components of a new research resource for complex physiologic signals," *Circulation*, vol. 101, no. 23, e215–e220, 2000.

PUBLICATIONS

PUBLICATION
I

The effects of pharmacological compounds on beat rate variations in human long QT-syndrome cardiomyocytes

J. Kuusela, J. Kim, E. Räsänen, and K. Aalto-Setälä

Stem Cell Reviews and Reports, vol. 12, no. 6, pp. 698–707
DOI: 10.1007/s12015-016-9686-0

Stem Cell Rev and Rep (2016) 12:698–707
DOI 10.1007/s12015-016-9686-0

The Effects of Pharmacological Compounds on Beat Rate Variations in Human Long QT-Syndrome Cardiomyocytes

Jukka Kuusela[1,2] · **Jiyeong Kim**[3] · **Esa Räsänen**[3] · **Katriina Aalto-Setälä**[1,2,4,5]

Published online: 19 September 2016

Abstract Healthy human heart rate fluctuates overtime showing long-range fractal correlations. In contrast, various cardiac diseases and normal aging show the breakdown of fractal complexity. Recently, it was shown that human induced pluripotent stem cell-derived cardiomyocytes (hiPSC-CMs) intrinsically exhibit fractal behavior as in humans. Here, we investigated the fractal complexity of hiPSC-derived long QT-cardiomyocytes (LQT-CMs). We recorded extracellular field potentials from hiPSC-CMs at baseline and under the effect of various compounds including β-blocker bisoprolol, ML277, a specific and potent I_{Ks} current activator, as well as JNJ303, a specific I_{Ks} blocker. From the peak-to-peak-intervals, we determined the long-range fractal correlations by using detrended fluctuation analysis. Electrophysiologically, the baseline corrected field potential durations (cFPDs) were more prolonged in LQT-CMs than in wildtype (WT)-CMs. Bisoprolol did not have significant effects to the cFPD in any CMs. ML277 shortened cFPD in a dose-dependent fashion by 11 % and 5–11 % in WT- and LQT-CMs, respectively. JNJ303 prolonged cFPD in a dose-dependent fashion by 22 % and 7–13 % in WT- and LQT-CMs, respectively. At baseline, all CMs showed fractal correlations as determined by short-term scaling exponent α. However, in all CMs, the α was increased when pharmacological compounds were applied indicating of breakdown of fractal complexity. These findings suggest that the intrinsic mechanisms contributing to the fractal complexity are not altered in LQT-CMs. The modulation of I_{Ks} channel and β1-adrenoreceptors by pharmacological compounds may affect the fractal complexity of the hiPSC-CMs.

Keywords Induced pluripotent stem cell · Long QT syndrome · Cardiomyocytes · Multielectrode array · Detrended fluctuation analysis · Fractals · Nonlinear dynamics

Electronic supplementary material The online version of this article (doi:10.1007/s12015-016-9686-0) contains supplementary material, which is available to authorized users.

✉ Katriina Aalto-Setälä
katriina.aalto-setala@uta.fi

Jukka Kuusela
jukka.kuusela@uta.fi

Esa Räsänen
esa.rasanen@tut.fi

[1] Institute of Biomedical Technology, University of Tampere, Tampere, Finland

[2] BioMediTech, Tampere, Finland

[3] Department of Physics, Tampere University of Technology, Tampere, Finland

[4] School of Medicine, University of Tampere and Tampere University Hospital, Finn-Medi 5, Biokatu 12, FI-33014 Tampere, Finland

[5] Heart Hospital, Tampere University Hospital, Tampere, Finland

Introduction

Heart rate dynamics have been previously analyzed using conventional linear and newer nonlinear methods in healthy and diseased states (for review see Perkiömäki [1]). The nonlinear indices of the RR variations include fractals, which are geometrically defined as objects composed of subunits (and sub-subunits) that sustain self-similarity on different measurement scales [2]. The characteristic feature of fractals is 1/f-like fluctuations, which has been shown to be present in a healthy human heartbeat [3–6]. Such fluctuations possess long-range correlations indicative of a memory effect, which means that the heart rate is not only related to immediately preceding value but also to values in the remote past [2].

In the heart rate time series, a breakdown of 1/f-like fluctuations may lead into either completely uncorrelated randomness (white noise) or into total correlation resembling random walk (Brownian motion). A number of studies have shown that in various cardiac disease states (e.g. congestive heart failure, myocardial infarction) the fractal 1/f-like long-range correlations of the heartbeat breakdown producing more uncorrelated randomness [7–13]. Furthermore, normal aging has been associated with the breakdown of fractal complexity producing more total correlation in the heartbeat dynamics [6, 14, 15]. Thus, it is thought that the breakdown of fractal complexity in heart rate dynamics may cause the system to be less adaptable and less responsive to unpredictable stimuli and stresses increasing susceptibility to injury and illness [6, 16].

The biological origin of the fractal-like behavior has not been yet fully established and is somewhat contradictory. In the heart, the origin of the fractal-like behavior is thought to result from complex interaction between vagal and sympathetic inputs of the autonomous nervous system [17, 18]. Experimental observations in humans have supported this notion [19–23], although opposing views have been presented [24]. However, evidence suggests that monolayer cultures of rat ventricular cardiomyocytes and human induced pluripotent stem cell-derived cardiomyocytes (hiPSC-CMs) lacking autonomic control exhibit fractal-like complexity, which indicates that the autonomous nervous system input is not necessary for fractal dynamics [25, 26]. It has been further demonstrated that single cardiomyocytes also exhibit fractal-like complexity and that intracellular Ca^{2+}-cycling mechanisms contribute to the fractal complexity of the single cardiomyocytes [27].

Long QT syndrome (LQTS) is a potentially severe life-threatening arrhythmic cardiac disease characterized by prolonged QT interval on the electrocardiogram. LQTS is associated with torsades de pointes, a special type of ventricular tachycardia, which may degenerate into ventricular fibrillation and cause sudden cardiac death [28]. Inherited forms of LQTS are a result of mutations in the cardiac ion channel coding genes. One of the most common LQTS genes is *KCNQ1*, which encodes the α-subunit of the voltage-gated potassium channel responsible for the slow delayed rectifier K^+ current (I_{Ks}) [29, 30]. In Finland, the prevalence of gene mutations associated with LQTS is high (0.4 % of Finnish population), which has been explained to be caused by four founder mutations with one of them being C-terminal G589D missense mutation in *KCNQ1* gene [31, 32]. The hiPSCs represent excellent research tool to study the pathophysiology of inherited cardiac diseases [33–41]. Until now, the fractal dynamics of hiPSC-LQT-CMs have not been investigated.

Here, we utilize patient-specific LQTS disease model [41] to study the fractal dynamics in the symptomatic and asymptomatic LQTS type 1 (LQT1)-specific CMs carrying Finnish founder mutation G589D. The aim of this study was to investigate the fractal dynamics of LQT-CMs in unmedicated and medicated conditions as compared to healthy control and under the effect of various compounds affecting cardiac action potential.

Material & Methods

ECG Recordings and Human Induced Pluripotent Stem Cell Generation

The study was approved by the ethical committee of Pirkanmaa Hospital District (R08070). Participants who volunteered for the study gave their consent. The ECGs were recorded using MARS-Holter from a healthy individual, asymptomatic LQT-mutation carrier and symptomatic LQT-patient. The LQT-patients are on bisoprolol medication. The healthy individual has no medication. Human iPSCs were generated as described earlier [42]. The LQT1-specific hiPSCs were derived from patients' skin fibroblasts carrying G589D missense mutation in *KCNQ1* [41, 43].

Patient Characteristics

Skin biopsies with LQT1 mutation were obtained from a symptomatic 41-year old female patient (QTc interval, 456 ms) and from an asymptomatic 28-year old female mutation carrier (QTc interval, 428 ms). Both carry the *KCNQ1* G589D mutation. The symptomatic 41-year old patient had experienced seizures, episodes of unconsciousness and syncope before β-blocker (bisoprolol) medication. The healthy control human iPS cells were derived from skin fibroblasts of a healthy 55-year old female (QTc interval, 406 ms) [44].

Human Induced Pluripotent Stem Cell Culture, Differentiation and Characterization

Human iPS cells were cultured and differentiated as previously described [43]. All the hiPSC lines (UTA.04602.WT, UTA.00208.LQT1, UTA.00211.LQT1, UTA.00303.LQT1 and UTA.00313.LQT1) and the differentiated CMs from them have been previously characterized elsewhere [41, 43, 44].

Multielectrode Array Recordings and Data Analysis

In this study, 30–45 days old hiPSC-CMs were used for the experiments. Spontaneously beating cardiomyocyte clusters were manually dissected and plated on 6-well MEAs (6-well MEA 200/30iR-Ti-tcr, Multichannel Systems, Reutlingen, Germany), which were first coated with fetal bovine serum (FBS, Invitrogen) for 30 min at room temperature and then with 0.1 % gelatine (Sigma Aldrich) for 1 h at room temperature. The cardiomyocyte clusters were cultured in EB-medium: KO-DMEM with 20 % FBS, NEAA, Glutamax and penicillin/streptomycin. The experiments were conducted in 5 %

FBS containing EB-medium (5 % EB-medium). Before drug tests, the field potentials originating from the spontaneously beating cardiomyocytes were recorded for 30 min (baseline) at +37 °C with the MEA platform (MEA2100-2 × 60–2, Multichannel Systems, Reutlingen, Germany) using 10 kHz sampling frequency and MC_Rack (Multichannel Systems, Reutlingen, Germany) software. After the 30-min baseline measurement, the MEA plate was put on +37 °C thermal plate (Tokai Hit, Japan) for keeping the temperature stable while adding drugs. The following drugs were used in the study: Bisoprolol (Sigma-Aldrich), ML277 (Tocris Bioscience) and JNJ303 (Tocris Bioscience). The drugs were dissolved in dimethyl sulfoxide (DMSO, Sigma-Aldrich) according to manufacturer's instructions. The bisoprolol concentrations were chosen based on its therapeutic blood serum concentration range [45]. For bisoprolol, 260 nM (upper limit of the therapeutic serum concentration) and 520 nM (twice the upper limit of the therapeutic concentration) concentrations were used. ML277 (I_{Ks} channel activator) concentrations of 1 μM and 2 μM were chosen based on previous reports [46, 47]. The concentrations of I_{Ks} blocker JNJ303 (300 nM and 1000 nM) were chosen based on our previous study [41]. After drug addition, the MEA plates were incubated for 5 min at +37 °C thermal plate before the 30-min measurement (first drug concentration). After this, we added more drugs to the cells (second drug concentration) and similarly as before, recorded the field potentials for 30 min. We also conducted vehicle control experiments with similar protocol as described above, with the exception that no drugs but only DMSO (0.1 %) was added to the cells. The recording time for baseline and for each drug concentration was 30 min. The data obtained from MEA was analyzed by our in-house developed CardioMDA software, which averages field potential signals using cross correlation algorithms [48]. From each recording, the last 2 min from the 30-min recording were chosen for averaging the field potential signals. For determining the field potential duration (FPD), the onset was determined as the beginning of depolarizing peak and the offset as T_{max} of the repolarizing wave. The Bazett's and Fridericia's formula were used to calculate the corrected field potential duration (cFPD).

Detrended Fluctuation Analysis

We applied detrended fluctuation analysis (DFA) to the RR-intervals. DFA is one of the most used time-series analysis methods that gives a reliable estimate for the existence and the characteristics of long-range correlations in the data [7]. DFA has been applied in various fields of science ranging from physiological signals such as heartbeat and gait [49] to, for example, musical rhythms [50, 51], rainfall statistics [52], structural properties of DNA [53], and electronic quantum transport [54].

A detailed description of DFA can be found in the above-listed references and here we only summarize the main steps. First, we take the peak-to-peak intervals of the hiPSC-CM or ECG data set and subtract the mean value, so that we consider the *fluctuations* around the mean. Next, we integrate the series by taking a cumulative sum of the fluctuations. The time axis is then divided into non-overlapping windows, and in each window, a least-squares line (trend) is fit to the data. The root-mean-square deviations from the trend (residuals) are averaged through the whole data set. This procedure is repeated for different window sizes. As a result, we get relationship between the window size and the average fluctuation (within that window size). The slope in this plot in a log-log scale corresponds to the DFA exponent α. White noise with no correlation between consecutive values has $\alpha = 0.5$, whereas Brownian motion with strongly correlated values generated by uncorrelated consecutive *increments* has $\alpha = 1.5$. In general, intermediate predictability between these limits with $0.5 < \alpha \leq 1.5$ indicates long-range (fractal) correlations. Anti-correlations are characterized by $-0.5 < \alpha < 0.5$. The special case of pink noise $\alpha = 1$ corresponds to 1/f behavior.

Statistical Analyses

From MEA data, one-way ANOVA followed by Dunnet's post hoc test was performed to test differences in baseline values between control and LQT cell lines (IBM version 22.0; SPSS Inc., Chicago, USA). If datasets did not meet ANOVA requirements (normal distribution, equal variances), nonparametric test Mann-Whitney U followed by alpha correction was employed to compare control cell line and LQT cell lines. In drug experiments, the baseline and the effect of drug concentrations were compared using paired sample t-test. Similarly, if datasets did not meet the requirements for t-test, nonparametric Wilcoxon test was employed. From DFA data, paired sample t-test was employed to determine the statistical differences between baseline and each drug concentration. The $p < 0.05$ was considered statistically significant. The levels of significance are represented as (*) $p < 0.05$, (**) $p < 0.01$ and (***) $p < 0.001$. The cFPD prolongations of >10 % are considered physiologically significant. The data is presented as mean ± standard deviation (SD).

Results

The Effect of Pharmacological Compounds to the hiPSC-CM Clusters

The 208.LQT1 and 211.LQT1 were derived from symptomatic patient whereas 303.LQT1 and 313.LQT1 were derived from asymptomatic mutation carrier. The baseline cFPDs (Fridericia's correction) were significantly more prolonged in hiPSC-LQT-CMs than in healthy WT-CMs (Fig. 1b, d, f).

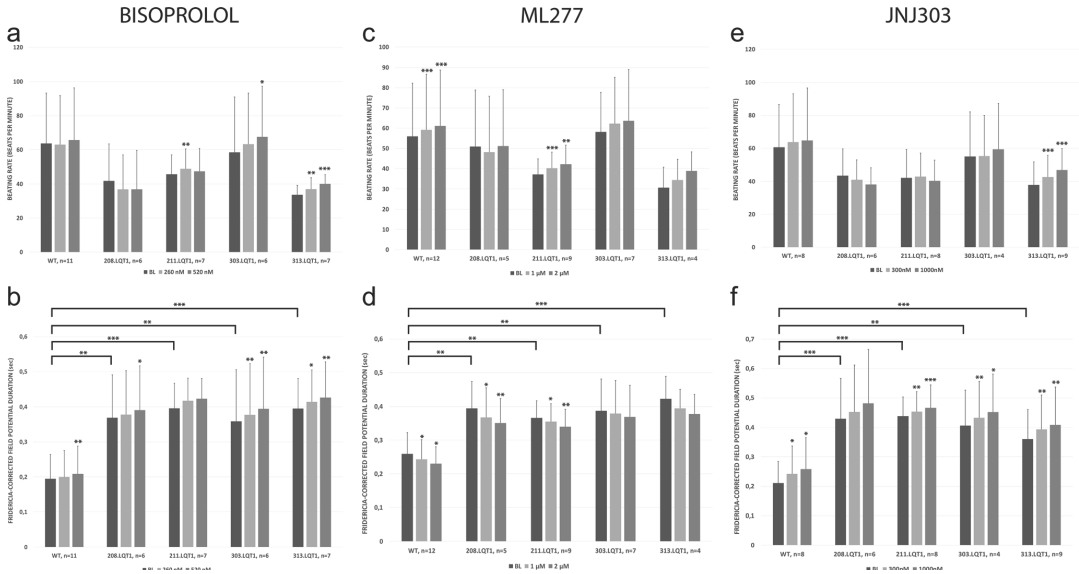

Fig. 1 The effects of various compounds to the human induced pluripotent stem cell (hiPSC)-derived cardiomyocytes' field potential parameters. The upper row depicts the beating rate (BR) and the lower row Fridericia-corrected field potential duration (cFPD). The baseline cFPDs of long QT-specific cardiomyocytes were significantly more prolonged than in healthy wild type-cardiomyocytes. The asterisks on top of the bars depict the statistical significance for mean BR or cFPD change compared to baseline values. Significance levels are indicated by (*) $p < 0.05$, (**) $p < 0.01$ and (***) $p < 0.001$, respectively

Similar results were obtained when Bazett's FPD correction was used (Supplemental Fig. 1). In contrast, we did not find any significant differences in the beating rates (BRs) between WT- and LQT-CMs (Fig. 1 a, c, e).

β-Blocker Bisoprolol The bisoprolol did not cause any major differences in the BRs of the hiPSC-CMs (Fig. 1a). We noted a slightly increasing trend of BR with increasing bisoprolol concentration in the hiPSC-CMs from asymptomatic mutation carrier (15 % for 303.LQT1 and 19 % for 313.LQT1). As for the cFPD, bisoprolol caused only mild cFPD prolongation in the WT-CMs (3–7 %) at the concentration range of 260–520 nM. Similar cFPD prolongations were seen in LQT-CMs from symptomatic patient (2–6 % for 208.LQT1 and 5–7 % for 211.LQT1) and from asymptomatic mutation carrier (5–10 % for 303.LQT1 and 5–8 % for 313.LQT1) at the concentration range of 260-520 nM (Fig. 1b). The representative bisoprolol traces for WT- and LQT-CMs are illustrated in Fig. 2a.

I_{Ks} Activator ML277 The ML277 caused significant increase in the BRs of WT and 211.LQT1, 9 % and 14 %, respectively (Fig. 1c). Overall, the trend of increasing BR with increasing ML277 concentration was observed although statistical significance was not found for all the cell lines. As expected, the ML277 shortened the cFPD in a dose-dependent manner, although the cFPD shortening was relatively mild (Fig. 1d). In the WT, the shortening of cFPD was 11 % whereas in the LQTs it ranged from 5 to 11 % at the concentration range of 1-2 μM. The representative ML277 traces for WT- and LQT-CMs are illustrated in Fig. 2b.

I_{Ks} Blocker JNJ303 Blocking the I_{Ks} channel with JNJ303 did not significantly change the BRs of the WT- or LQT-CMs except in 313.LQT1, in which the 23 % increase in the BR was observed (Fig. 1e). JNJ303 showed a dose-dependent cFPD prolongation in the WT- and LQT-CMs (Fig. 1f). The most increment in cFPD was seen in the WT (22 %) whereas in the LQTs, the cFPD increase was around 7–13 % at the highest concentration (1000 nM). The representative JNJ303 traces for WT- and LQT-CMs are illustrated in Fig. 2c.

Detrended Fluctuation Analysis (DFA) of Healthy Control- and LQT-Specific Cardiomyocytes and ECG Data

We first determined the fractal scaling exponent α from human subjects who participated to the study ($n = 3$). Results are shown in Table 1. Next, we determined the scaling exponent α from hiPSC-CMs derived from the same human subjects participating to the study. In Fig. 3 we show the DFA results of the peak-to-peak fluctuations for healthy control- (WT) and LQT-specific CMs when exposed to bisoprolol (Fig. 3 a),

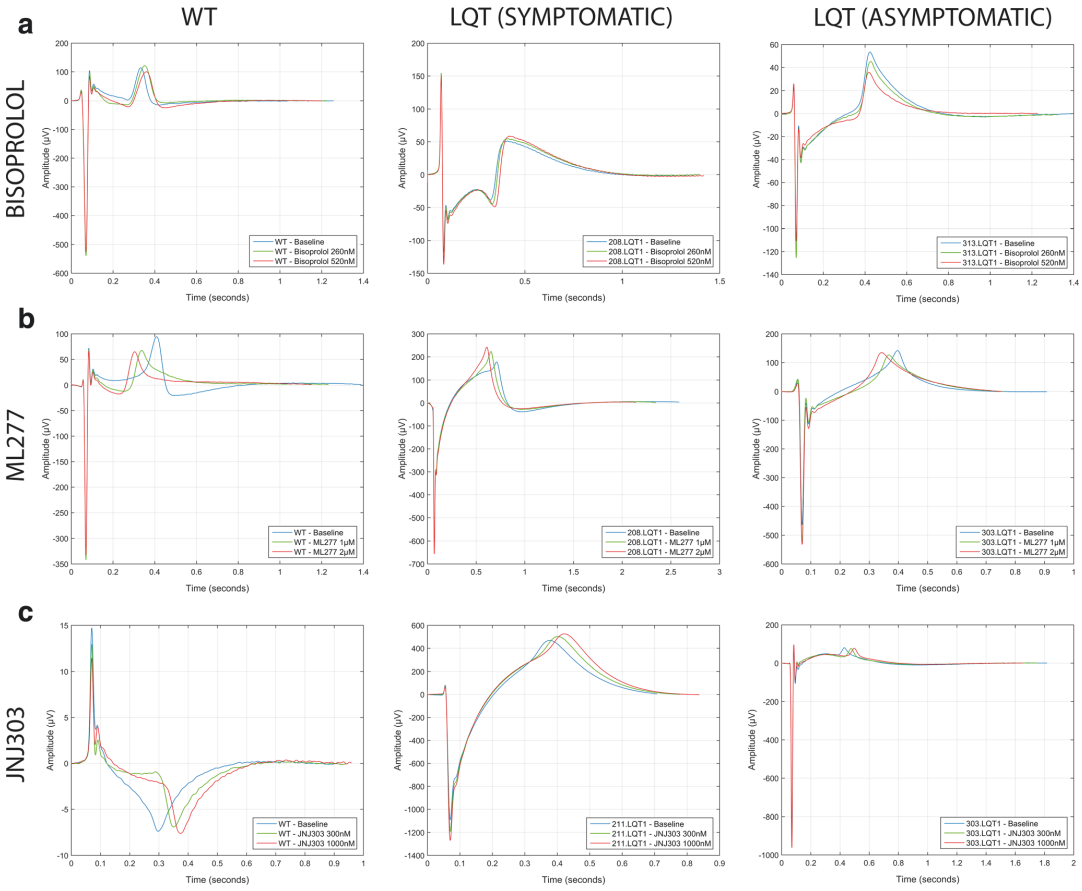

Fig. 2 The representative traces of the human induced pluripotent stem cell (hiPSC)-derived wild type- and long QT (LQT)-specific cardiomyocytes under the effect of various compounds. The LQTs are grouped according to symptomatic (208.LQT1, 211.LQT1) and asymptomatic cases (303.LQT1, 313.LQT1) shown in the middle and in the right column, respectively. **a**) β-blocker Bisoprolol, **b**) I_{Ks} activator ML277 **c**) I_{Ks} blocker JNJ303. Notice, how the T_{max} of the repolarization wave is relatively unchanged between baseline and different bisoprolol concentrations depicting marginal effect of the β-blocker to the corrected field potential duration (cFPD). However, I_{Ks} activator ML277 shows clear shortening of cFPD seen by shift in the T_{max}. Similarly, but conversely to ML277, I_{Ks} blocker JNJ303 shows clear prolongation of cFPD assessed by the shift in the T_{max}

ML277 (Fig. 3 b), or JNJ303 (Fig. 3c). The first bar in all the subplots corresponds to the baseline with zero drug concentration. The LQT data is grouped according to symptomatic (208.LQT1, 211.LQT1) and asymptomatic cases (303.LQT1, 313.LQT1) shown in the middle and in the right column, respectively.

We found that all the average baseline values for the DFA scaling exponent are close to one, i.e., $\alpha \sim 0.9$–1.1. There was

Table 1 The patient characteristics and detrended fluctuation analysis from ECG data

	Healthy individual	LQT1-patient (symptomatic)	LQT1-patient (asymptomatic)
Age	55	41	28
Medication	-	Bisoprolol	Bisoprolol
QTc (ms)	406	456	428
α	1.21 ± 0.03	1.08 ± 0.02	1.07 ± 0.02

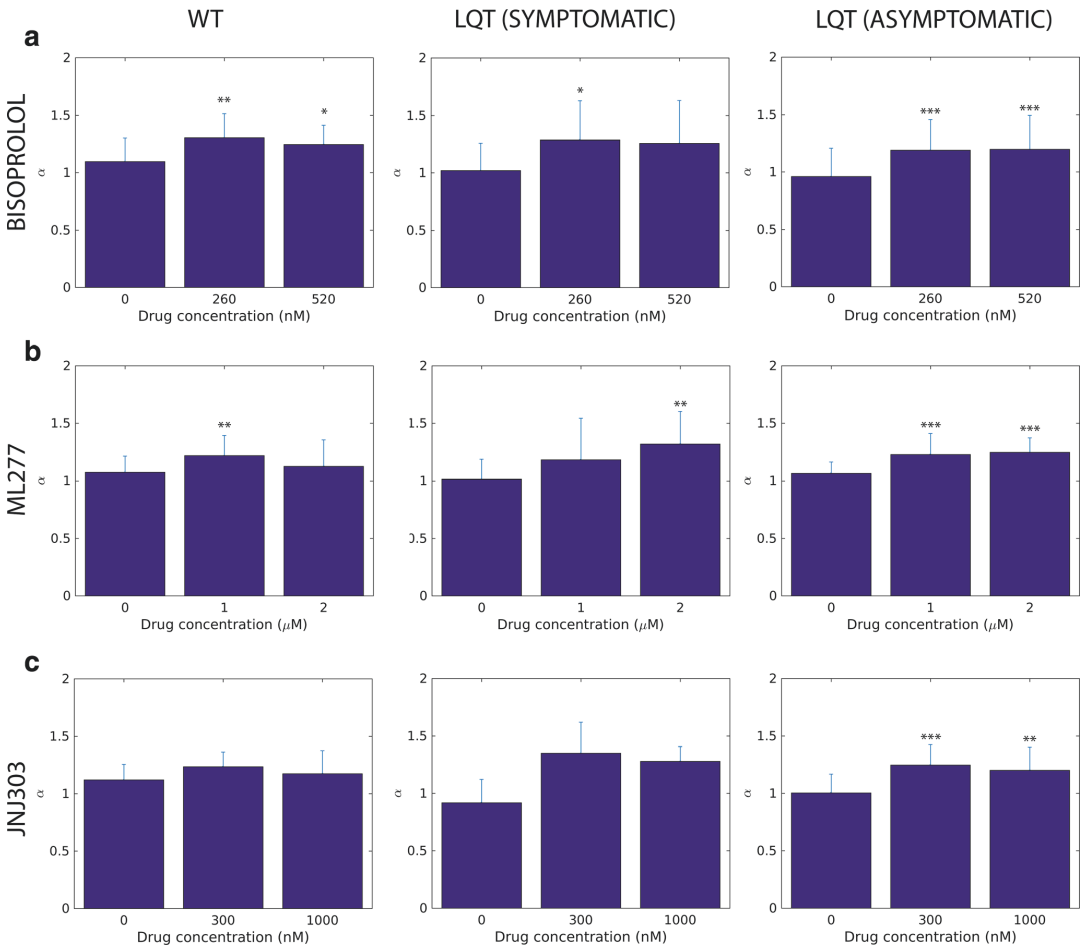

Fig. 3 The detrended fluctuation analysis (DFA) α scaling exponents of the human induced pluripotent stem cell (hiPSC)-derived wild type- and long QT (LQT)-specific cardiomyocytes. The LQTs are grouped according to symptomatic (208.LQT1, 211.LQT1) and asymptomatic cases (303.LQT1, 313.LQT1) shown in the middle and in the right column, respectively. **a**) (row) β-blocker Bisoprolol, **b**) I_{Ks} activator ML277 **c**) I_{Ks} blocker JNJ303. At baseline, the α scaling exponents are close to 1 in all hiPSC-CMs. The addition of various compounds to the hiPSC-CMs increased the α scaling exponent closer to Brownian motion (α = 1.5). The asterisks on top of the bars depict the statistical significance for mean α scaling exponent change compared to baseline values. Significance levels are indicated by (*) $p < 0.05$, (**) $p < 0.01$ and (***) $p < 0.001$, respectively

no notable difference in the baseline α values between the WT and the LQTs. This is in line with our ECG data, which shows α of 1.08, 1.07 and 1.21 for symptomatic and asymptomatic LQT patient as well as for healthy individual, respectively (Table 1). However, all the pharmacological compounds lead to an increase in the DFA scaling exponent α toward Brownian motion (α = 1.5) when compared to the baseline (Fig. 3). The trend is visible both in the WT and in the LQTs. In most cases a further increase in the concentration does not affect α. When comparing all the α values of WT and LQTs, we did not find any statistical difference between the groups. We also conducted vehicle control experiments in which no pharmacological compounds but only DMSO (0.1 %) was added to the CMs. We did not observe any significant changes in the α scaling exponent during these recordings. The α was 1.024 ± 0.13 at baseline, 1.00 ± 0.12 (first DMSO addition) and 1.03 ± 0.13 (second DMSO addition) ($n = 6$). Thus, the change seen in α scaling exponent with various pharmacological compounds reflect the intrinsic properties of the pharmacological compounds themselves.

Discussion

In human hearts, the fractal dynamics is thought to result from complex interaction between vagal and sympathetic inputs of autonomous nervous system [17, 18]. However, evidence suggest that the hiPSC-CMs also exhibit fractal-like complexity indicating intrinsic mechanisms of the CMs contributing to fractal dynamics [26, 27]. This study further supports the concept that healthy hiPSC-CMs lacking autonomous nervous system input exhibit fractal-like complexity at baseline condition. We also observed that the untreated (without any pharmacological intervention) hiPSC-LQT-CMs also appear to exhibit fractal-like complexity at baseline condition. This result is in line with the previous study in untreated patients with congenital LQTS [55]. Thus, our results further expand this concept suggesting that the intrinsic mechanisms contributing to the fractal-like complexity is not altered in hiPSC-LQT-CMs. However, it is of note that the results obtained were from 2 LQTS patients only and further studies on a larger population would be needed to definitely conclude the matter.

The Electrophysiological Properties of the hiPSC-CMs The baseline behavior of hiPSC-CMs is in line with our previous studies [41, 43]. Results obtained from this study clearly show that the cFPDs, corrected with either Bazett's or Fridericia's formulae, are more prolonged in LQT-CMs than in healthy WT-CMs. We also investigated the healthy and LQT-specific hiPSC-CMs under the effect of β-blocker bisoprolol and pharmacological compounds affecting specifically to cardiac ion channel I_{Ks}. Overall, the drug effects in LQT-CMs appeared to be of similar magnitude to those of WT-CMs, similar to our previous findings [43].

The Effect of Bisoprolol to the Fractal Complexity of hiPSC-CMs The β-blockers are the standard and currently, the only treatment of choice for LQTS patients [56]. Here, in order for valid comparisons between cellular and whole heart data, we chose to study bisoprolol in hiPSC-CMs because the LQTS patients volunteered for this study were on bisoprolol medication. Bisoprolol, a β1-adrenoreceptor selective β-blocker, did not have physiological significance to the field potential parameters (>10 % cFPD prolongation) in any of the hiPSC-CMs at clinically relevant concentration. It is important to notice that we did not activate β-receptors with β-agonists prior to β-blocker application. However, the acute application of bisoprolol increased the α scaling exponent toward Brownian motion (α = 1.5) in all hiPSC-CMs at the upper limit of therapeutic concentration (260 nM). At 520 nM, the effect was attenuated. Although the baseline α data from hiPSC-LQT-CMs correlated with the ECG data (α ~ 1.0), bisoprolol α data did not correlate with the ECG data. The discrepancy between cellular and heart α data remains yet unclear but it may be attributed to e.g. acute application of the bisoprolol or in the absence of autonomous nervous system in hiPSC-LQT-CMs, which may affect to fractal complexity upon drug application. Previous human study has shown that the fractal complexity (α ~ 1.0) was unaltered in patients with congenital LQTS treated or untreated with β-blockers [55]. Thus, the β-blockers may not have significant effect on the α of the whole LQTS hearts. On the other hand, there is evidence from the human studies that the β-blocker treatment improves fractal dynamics of the heart in advanced congestive heart failure patients by increasing the α scaling exponent during 1–3-month therapy period [21–23]. It is completely unknown whether such differences result from the different disease states, the type of β-blocker used or treatment periods among other things. However, this study clearly shows that although the field potential parameters were not significantly changed, the intrinsic mechanisms contributing to fractal-like complexity were altered during acute β-blocker treatment. On the other hand, further studies would be needed to answer what the effect would be in long-term (chronic) situation and what the mechanism behind of this phenomenon is.

The significance of the fractal complexity resembling Brownian motion in the heart is unclear. The loss of fractality toward white noise (α = 0.5) has been found to predispose to severe life-threatening arrhythmias and cardiac death [9, 10, 13]. However, very little is known when the fractal dynamics of the heart become more correlated resembling Brownian motion (α = 1.5). Such phenomenon has been observed in healthy elderly subjects implying decrease of fractal complexity with age [6, 14, 15] and, although not yet proven, it has been suggested that such system would be more susceptible to injury and illness in the elderly [6, 16].

The Effect of I_{Ks} Affecting Pharmacological Compounds to the Fractal Complexity of hiPSC-CMs Next, we investigated the effects of the other two pharmacological compounds (ML277 and JNJ303) to hiPSC-CMs. The ion channel activator ML277 has been shown to augment specifically I_{Ks} current and shorten the action potential duration in both healthy and LQT-CMs [46, 47]. Similarly, in this study, the ML277 shortened the cFPD although the effect was relatively mild in these hiPSC-CM clusters at 1-2 μM concentration. Similarly, as was seen with bisoprolol, also ML277 resulted in the dysfunction of regulatory mechanisms contributing to fractal complexity as the α scaling exponent was increased toward Brownian motion in all hiPSC-CMs at 1 μM. However, at 2 μM a small difference was seen that in the WT-CMs α exponent decreased to baseline level whereas the LQT-CMs α exponents continued to increase from 1 μM, which was most prominently seen in CMs derived from symptomatic patient (208.LQT1 and 00,211.LQT1). Furthermore, the effect of JNJ303, a potent and specific I_{Ks} blocker [57] known to evoke torsades de pointes, was assessed in hiPSC-CMs. The WT-CMs appeared to be more sensitive to JNJ303 than LQT-CMs as measured by

cFPD prolongation. This result is in line with our previous findings from single WT- and LQT-CMs measured with patch clamp using the same cell lines [41]. Although not yet proven in the experimental setting, this indicates that the I_{Ks} current is diminished in the LQT1-CMs harboring G589D missense mutation compared to healthy WT-CMs. Contradictory to our expectations, also the JNJ303 resulted in similar alterations of fractal complexity in hiPSC-CMs as ML277 by increasing the α scaling exponent. Taken together, these evidence imply that the modulation of the ion channel generating I_{Ks} current with pharmacological compounds may result in the dysfunction of the intrinsic mechanisms contributing to fractal complexity. Indeed, rhythmic ion channel activation and inactivation in pacemaker cells has been thought to contribute to the ultradian rhythmicity in addition to spontaneous Ca^{2+}-cycling [58]. Previous study has shown that the disruption of intracellular Ca^{2+} handling causes alterations in the scaling exponent α, mostly by decreasing it [27]. Here, we have shown that at baseline, the rhythmicity of hiPSC-CMs is sustained as determined by long-range fractal correlations. Furthermore, the modulation of the ion channel generating I_{Ks} current with specific pharmacological compounds disrupts CM rhythmicity and fractal complexity.

Potential Limitation of the Study

In this study, only the acute effects of the various compounds to the fractal-like complexity were assessed in hiPSC-CMs. Further studies would be needed to show the chronic, long-term effects of the compounds. Moreover, the mechanisms behind the alterations in fractal complexity were not studied. We did not investigate in detail the effect of β-adrenergic agonist to the long-range fractal correlations of hiPSC-CMs. Also, with this model we could not take into account the continuous exposure of sympathetic and parasympathetic stimuli affecting CMs in vivo. This study does not answer to what would be the implications of altered fractality toward Brownian motion in hiPSC-CMs in terms of long-term health, adaptability and responsiveness to unpredictable stimuli.

Conclusions

In conclusion, the hiPSC-LQT-CMs appear to exhibit fractal-like complexity at baseline condition suggesting that the intrinsic mechanisms of LQT-CMs contributing to the fractal complexity are not altered. Although the effects of various compounds to the field potential parameters were as expected, the fractal-like complexity of the hiPSC-CMs was significantly altered in healthy as well as LQT-specific CMs. No significant differences in the α scaling exponent were found between WT- and LQT-CMs. These findings may suggest that the cardiac ion channel generating I_{Ks} current as well as the modulation of β1-adrenoreceptors by β-blocker bisoprolol may contribute to the fractal-like complexity of the hiPSC-CMs.

Acknowledgments We kindly thank Markus Haponen and Henna Venäläinen for their excellent technical expertise with the stem cell culture and cardiac differentiation. We also kindly thank Anna Kiviaho for generating the iPS cell lines, The END-2 cells were a kind gift from Christine Mummery. On the computational side, we thank Mika Sarvilahti, and Perttu Luukko for assistance with DFA analysis. This study was funded by grants from the Finnish Funding Agency for Technology and Innovation (TEKES), Finnish Foundation for Cardiovascular Research, Finnish Cultural Foundation and the Academy of Finland.

Compliance with Ethical Standards

Author Contributions JK designed and performed MEA experiments, analyzed MEA data, performed statistical analyses and wrote the manuscript, JKim performed detrended fluctuation analysis, analyzed the numerical results and wrote the manuscript, ER designed experiments, performed detrended fluctuation analysis and wrote the manuscript, KA conceived the study, designed experiments and wrote the manuscript. All authors read and approved the final manuscript.

Conflict of Interest The authors declare no potential conflicts of interests.

References

1. Perkiömäki, J. S. (2011). Heart rate variability and non-linear dynamics in risk stratification. *Frontiers in Physiology, 2*, 81.
2. Goldberger, A. L. (1996). Non-linear dynamics for clinicians: chaos theory, fractals, and complexity at the bedside. *Lancet, 347*(9011), 1312–1314.
3. Kobayashi, M., & Musha, T. (1982). 1/f Fluctuation of Heartbeat Period. *I.E.E.E. Transactions on Bio-Medical Engineering, BME-29*(6), 456–457.
4. Peng, C., Mietus, J., Hausdorff, J. M., Havlin, S., Stanley, H. E., & Goldberger, A. L. (1993). Long-range anticorrelations and non-Gaussian behavior of the heartbeat. *Physical Review Letters, 70*(9), 1343–1346.
5. Pikkujämsä, S. M., Mäkikallio, T. H., Juhani Airaksinen, K. E., & Huikuri, H. V. (2001). Determinants and interindividual variation of R-R interval dynamics in healthy middle-aged subjects. *American Journal of Physiology. Heart and Circulatory Physiology, 280*(3 49–3), H1400–H1406.
6. Goldberger, A. L., Amaral, L. A. N., Hausdorff, J. M., Ivanov, P. C., Peng, C., & Stanley, H. E. (2002). Fractal dynamics in physiology: alterations with disease and aging. *Proceedings of the National Academy of Sciences of the United States of America, 99*(Suppl. 1), 2466–2472.

7. Peng, C., Havlin, S., Stanley, H. E., & Goldberger, A. L. (1995). Quantification of scaling exponents and crossover phenomena in nonstationary heartbeat time series. *Chaos, 5*(1), 82–87.
8. Ho, K. K. L., Moody, G. B., Peng, C., et al. (1997). Predicting survival in heart failure case and control subjects by use of fully automated methods for deriving nonlinear and conventional indices of heart rate dynamics. *Circulation, 96*(3), 842–848.
9. Mäkikallio, T. H., Seppänen, T., Airaksinen, K. E. J., et al. (1997). Dynamic analysis of heart rate may predict subsequent ventricular tachycardia after myocardial infarction. *The American Journal of Cardiology, 80*(6), 779–783.
10. Mäkikallio, T. H., Koistinen, J., Jordaens, L., et al. (1999). Heart rate dynamics before spontaneous onset of ventricular fibrillation in patients with healed myocardial infarcts. *The American Journal of Cardiology, 83*(6), 880–884.
11. Vikman, S., Mäkikallio, T. H., Yli-Mäyry, S., et al. (1999). Altered complexity and correlation properties of R-R interval dynamics before the spontaneous onset of paroxysmal atrial fibrillation. *Circulation, 100*(20), 2079–2084.
12. Huikuri, H. V., Poutiainen, A., Mäkikallio, T. H., et al. (1999). Dynamic behavior and autonomic regulation of ectopic atrial pacemakers. *Circulation, 100*(13), 1416–1422.
13. Huikuri, H. V., Mäkikallio, T. H., Peng, C., Goldberger, A. L., Hintze, U., & Møller, M. (2000). Fractal correlation properties of R-R interval dynamics and mortality in patients with depressed left ventricular function after an acute myocardial infarction. *Circulation, 101*(1), 47–53.
14. Iyengar N, Peng C-, Morin R, Goldberger AL, Lipsitz LA. (1996). Age-related alterations in the fractal scaling of cardiac interbeat interval dynamics. American Journal of Physiology. Regulatory, Integrative and Comparative Physiology, 271(4 40–4):R1078–84.
15. Pikkujämsä, S. M., Mäkikallio, T. H., Sourander, L. B., et al. (1999). Cardiac interbeat interval dynamics from childhood to senescence: comparison of conventional and new measures based on fractals and chaos theory. *Circulation, 100*(4), 393–399.
16. Lipsitz, L. A., & Goldberger, A. L. (1992). Loss of 'complexity' and aging: potential applications of fractals and chaos theory to senescence. *JAMA, 267*(13), 1806–1809.
17. Goldberger, A. L., & West, B. J. (1987). Fractals in physiology and medicine. *The Yale Journal of Biology and Medicine, 60*(5), 421–435.
18. West, B. J., & Goldberger, A. L. (1987). Physiology in fractal dimensions. *American Scientist, 75*(4), 354–365.
19. Tulppo, M. P., Mäkikallio, T. H., Seppänen, T., et al. (2001). Effects of pharmacological adrenergic and vagal modulation on fractal heart rate dynamics. *Clinical Physiology, 21*(5), 515–523.
20. Tulppo, M. P., Kiviniemi, A. M., Hautala, A. J., et al. (2005). Physiological background of the loss of fractal heart rate dynamics. *Circulation, 112*(3), 314–319.
21. Lin, L., Lin, J., C-, D., Lai, L., Tseng, Y., & Huang, S. K. S. (2001). Reversal of deteriorated fractal behavior of heart rate variability by beta-blocker therapy in patients with advanced congestive heart failure. *Journal of Cardiovascular Electrophysiology, 12*(1), 26–32.
22. Ridha, M., Makikallio, T. H., Lopera, G., et al. (2002). Effects of carvedilol on heart rate dynamics in patients with congestive heart failure. *Annals of Noninvasive Electrocardiology, 7*(2), 133–138.
23. Chiu, K., Chan, H., Chu, S., & Lin, T. (2007). Carvedilol can restore the multifractal properties of heart beat dynamics in patients with advanced congestive heart failure. *Autonomic Neuroscience Basic Clinical, 132*(1–2), 76–80.
24. Tan, C. O., Cohen, M. A., Eckberg, D. L., & Taylor, J. A. (2009). Fractal properties of human heart period variability: physiological and methodological implications. *The Journal of Physiology, 587*(15), 3929–3941.
25. Kucera, J. P., Heuschkel, M. O., Renaud, P., & Rohr, S. (2000). Power-law behavior of beat-rate variability in monolayer cultures of neonatal rat ventricular myocytes. *Circulation Research, 86*(11), 1140–1145.
26. Mandel, Y., Weissman, A., Schick, R., et al. (2012). Human embryonic and induced pluripotent stem cell-derived cardiomyocytes exhibit beat rate variability and power-law behavior. *Circulation, 125*(7), 883–893.
27. Ben-Ari, M., Schick, R., Barad, L., et al. (2014). From beat rate variability in induced pluripotent stem cell-derived pacemaker cells to heart rate variability in human subjects. *Heart Rhythm, 11*(10), 1808–1818.
28. Schwartz, P. J., Crotti, L., & Insolia, R. (2012). Long-QT syndrome from genetics to management. *Circulation. Arrhythmia and Electrophysiology, 5*(4), 868–877.
29. Barhanin, J., Lesage, F., Guillemare, E., Fink, M., Lazdunski, M., & Romey, G. (1996). K(V)LQT1 and lsK (minK) proteins associate to form the I(Ks) cardiac potassium current. *Nature, 384*(6604), 78–80.
30. Sanguinetti, M. C., Curran, M. E., Zou, A., et al. (1996). Coassembly of K(V)LQT1 and minK (IsK) proteins to form cardiac I(Ks) potassium channel. *Nature, 384*(6604), 80–83.
31. Marjamaa, A., Salomaa, V., Newton-Cheh, C., et al. (2009). High prevalence of four long QT syndrome founder mutations in the Finnish population. *Annals of Medicine, 41*(3), 234–240.
32. Piippo, K., Swan, H., Pasternack, M., et al. (2001). A founder mutation of the potassium channel KCNQ1 in long QT syndrome: implications for estimation of disease prevalence and molecular diagnostics. *Journal of the American College of Cardiology, 37*(2), 562–568.
33. Egashira, T., Yuasa, S., Suzuki, T., et al. (2012). Disease characterization using LQTS-specific induced pluripotent stem cells. *Cardiovascular Research, 95*(4), 419–429.
34. Bellin, M., Casini, S., Davis, R. P., et al. (2013). Isogenic human pluripotent stem cell pairs reveal the role of a KCNH2 mutation in long-QT syndrome. *The EMBO Journal, 32*(24), 3161–3175.
35. Moretti, A., Bellin, M., Welling, A., et al. (2010). Patient-specific induced pluripotent stem-cell models for long-QT syndrome. *New England Journal of Medicine, 363*(15), 1397–1409.
36. Itzhaki, I., Maizels, L., Huber, I., et al. (2011). Modelling the long QT syndrome with induced pluripotent stem cells. *Nature, 471*(7337), 225–229.
37. Lahti, A. L., Kujala, V. J., Chapman, H., et al. (2012). Model for long QT syndrome type 2 using human iPS cells demonstrates arrhythmogenic characteristics in cell culture. *Disease Models & Mechanisms, 5*(2), 220–230.
38. Matsa, E., Rajamohan, D., Dick, E., et al. (2011). Drug evaluation in cardiomyocytes derived from human induced pluripotent stem cells carrying a long QT syndrome type 2 mutation. *European Heart Journal, 32*(8), 952–962.
39. Ma, D., Wei, H., Zhao, Y., et al. (2013). Modeling type 3 long QT syndrome with cardiomyocytes derived from patient-specific induced pluripotent stem cells. *International Journal of Cardiology, 168*(6), 5277–5286.
40. Yazawa, M., Hsueh, B., Jia, X., et al. (2011). Using induced pluripotent stem cells to investigate cardiac phenotypes in Timothy syndrome. *Nature, 471*(7337), 230–236.
41. Kiviaho, A. L., Ahola, A., Larsson, K., et al. (2015). Distinct electrophysiological and mechanical beating phenotypes of long QT syndrome type 1-specific cardiomyocytes carrying different mutations. *IJC Heart & Vasculature, 8*, 19–31.
42. Takahashi, K., Tanabe, K., Ohnuki, M., et al. (2007). Induction of pluripotent stem cells from adult human fibroblasts by defined factors. *Cell, 131*(5), 861–872.
43. Kuusela, J., Kujala, V. J., Kiviaho, A., et al. (2016). Effects of cardioactive drugs on human induced pluripotent stem cell derived long QT syndrome cardiomyocytes. *SpringerPlus, 5*(1), 1–13.

44. Ahola, A., Kiviaho, A. L., Larsson, K., Honkanen, M., Aalto-Setälä, K., & Hyttinen, J. (2014). Video image-based analysis of single human induced pluripotent stem cell derived cardiomyocyte beating dynamics using digital image correlation. *Biomedical Engineering Online, 13*, 39.
45. Schulz, M., & Schmoldt, A. (2003). Therapeutic and toxic blood concentrations of more than 800 drugs and other xenobiotics. *Pharmacogenetics, 58*(7), 447–474.
46. Yu, H., Lin, Z., Mattmann, M. E., et al. (2013). Dynamic subunit stoichiometry confers a progressive continuum of pharmacological sensitivity by KCNQ potassium channels. *Proceedings of the National Academy of Sciences of the United States of America, 110*(21), 8732–8737.
47. Ma, D., Wei, H., Lu, J., et al. (2015). Characterization of a novel KCNQ1 mutation for type 1 long QT syndrome and assessment of the therapeutic potential of a novel IKs activator using patient-specific induced pluripotent stem cell-derived cardiomyocytes. *Stem Cell Research & Therapy, 6*, 39,015–0027-z.
48. Pradhapan, P., Kuusela, J., Viik, J., Aalto-Setala, K., & Hyttinen, J. (2013). Cardiomyocyte MEA data analysis (CardioMDA)–a novel field potential data analysis software for pluripotent stem cell derived cardiomyocytes. *PloS One, 8*(9), e73637.
49. Peng, C., Hausdorff, J. M., & Goldberger, A. L. (1999). Fractal mechanisms in neural control: Human heartbeat and gait dynamics in health and disease. In J. Walleczek (Ed.), *Nonlinear Dynamics, Self-Organization, and Biomedicine*. Cambridge University Press.
50. Räsänen, E., Pulkkinen, O., Virtanen, T., Zollner, M., & Hennig, H. (2015). Fluctuations of hi-hat timing and dynamics in a virtuoso drum track of a popular music recording. *PloS One, 10*(6), e0127902.
51. Hennig, H., Fleischmann, R., Fredebohm, A., et al. (2011). The nature and perception of fluctuations in human musical rhythms. *PloS One, 6*(10), e26457.
52. Matsoukas, C. (2000). Detrended fluctuation analysis of rainfall and streamflow time series. *Journal of Geophysical Research, D: Atmospheres, 105*(D23), 29165–29172.
53. Peng, C., Buldyrev, S. V., Havlin, S., Simons, M., Stanley, H. E., & Goldberger, A. L. (1994). Mosaic organization of DNA nucleotides. *Physical Review E, 49*(2), 1685–1689.
54. Kotimäki, V., Räsänen, E., Hennig, H., & Heller, E. J. (2013). Fractal dynamics in chaotic quantum transport. *Physical Review E - Statistical, Nonlinear, and Soft Matter Physics, 88*(2). doi:10.1103/PhysRevE.88.022913.
55. Perkiömäki, J. S., Zareba, W., Couderc, J., & Moss, A. J. (2001). Heart rate variability in patients with congenital long QT syndrome. *Annals of Noninvasive Electrocardiology, 6*(4), 298–304.
56. Schwartz, P. J., Ackerman, M. J., George Jr., A. L., & Wilde, A. A. (2013). Impact of genetics on the clinical management of channelopathies. *Journal of the American College of Cardiology, 62*(3), 169–180.
57. Towart, R., Linders, J. T. M., Hermans, A. N., et al. (2009). Blockade of the IKs potassium channel: an overlooked cardiovascular liability in drug safety screening? *Journal of Pharmacological and Toxicological Methods, 60*(1), 1–10.
58. Yaniv, Y., & Lakatta, E. G. (2015). The end effector of circadian heart rate variation: the sinoatrial node pacemaker cell. *BMB Reports, 48*(12), 677–684.

PUBLICATION
II

Intrinsic complexity of RR and QT intervals at the cellular level

J. Kim, I. Potapov, D. Shah, J. Kuusela, K. Aalto-Setälä, and E. Räsänen

In *Computing in Cardiology*, C. Pickett, Ed., vol. 45, IEEE, 2018, pp. 1–4
DOI: 10.22489/CinC.2018.179

Intrinsic Complexity of RR and QT Intervals at the Cellular Level

Jiyeong Kim[1], Ilya Potapov[1], Disheet Shah[2], Jukka Kuusela[2], Katriina Aalto-Setälä[2,3], Esa Räsänen[1]

[1]Tampere University of Technology, Tampere, Finland
[2]BioMediTech, University of Tampere, Tampere, Finland
[3]Heart Hospital, Tampere University Hospital, Tampere, Finland

Abstract

We characterize the complexity of interbeat intervals (IBIs) and field potential durations (FPDs) of human-induced pluripotent stem cell-derived cardiomyocytes (hiPSC-CMs). The complexity is assessed using the multiscale entropy (MSE) method up to the scale of ten beats. The MSE profiles of healthy and diseased (long-QT syndrome) hiPSC-CMs show important differences, which demonstrate the usefulness of the method in the characterization of the cells and in the analysis of hereditary cardiac diseases. We show that the intrinsic complexity is possibly altered by the differentiation methods, as well as the age and mutations of the cells.

1. Introduction

The complexity of heart rate variability (HRV) has been well established as an important measure in cardiac health, as it reflects the heart's ability to adapt to sudden perturbations. Multiscale entropy (MSE) [1] is one of the measures assessing the complexity of long-range correlated signals. In HRV studies, MSE curves often have distinguishable profiles under different conditions, such as age and cardiac diseases [2]. QT intervals also exhibit spontaneous beat-to-beat variability, which is useful in monitoring increased risks of fatal ventricular arrhythmias. Only few studies have quantified QT variability (QTV) using MSE [3] and related measures, such as sample entropy [4] and revised MSE [5]. In essence, QT intervals have a MSE profile distinctly different from those of RR intervals [3].

To the best of our knowledge, entropy-based measures have not yet been reported for beat rate dynamics at the *cellular level*. In this study, we apply the MSE method to quantify the complexity of field potential signals, generated by clusters of human-induced pluripotent stem-cell-derived cardiomyocytes (hiPSC-CMs). For this purpose, we extract the interbeat intervals (IBIs) and field potential durations (FPDs) from the field potential. These quantities correspond to the RR and QT intervals of the electrocardiogram (ECG), respectively. The observed effects of age and differentiation methods of hiPSC-CMs on the IBI entropies contribute important information for the characterization of the cell aggregates as an *in vitro* model of a heart. We demonstrate the ability of the MSE method to distinguish the diseased state of the cell aggregates, which is useful in the study of hereditary cardiac diseases modeled by hiPSC-CMs.

2. Data and Methods

2.1. Electrocardiogram data

Raw ECG recordings were obtained from the MIT-BIH Normal Sinus Rhythm database of PhysioNet [6]. RR and QT intervals were extracted using the PhysioNet algorithm [6] and other software [7, 8]. Low quality signals and ectopic beats were discarded. The final set of the ECG data contains 15 RR and QT interval time series of 24 hours from healthy individuals of 11 women (age from 20 to 45 years) and 4 men (age from 26 to 45 years).

2.2. Cellular data

Healthy control hiPSCs were derived from skin fibroblasts of a 55-year-old female and a 44-year-old male. The LQT1-specific hiPSCs were derived from a symptomatic 41-year-old female long QT syndrome (LQTS) patient and an asymptomatic 28-year-old LQT-mutation carrier, both carrying G589D missense mutation in KCNQ1 [9,10]. The study was performed under the volunteers' informed consent and approved by the Ethical Committee of Pirkanmaa Hospital District (R08070). The hiPSCs were generated as described in Ref. [11], and cultured and differentiated with the small molecule (SM) [12] and the mouse visceral endoderm-like (END2) cell co-culture method, as previously described in Ref. [10]. The field potential signals of hiPSC-CMs were measured with a six-well multielectrode array. The signals displaying the highest amplitudes, low signal-to-noise ratios, and clear repolarization phases were chosen for the analysis. Two parameters that were extracted were IBIs and FPDs; an IBI is defined as the time

 ISSN: 2325-887X DOI: 10.22489/CinC.2018.179

period between two consecutive depolarization peaks. A FPD is defined as the time period between the depolarization peak and the end of the repolarization peak. The extracted IBI and FPD time series have a length of 1000-3000 beats.

2.3. Multiscale entropy analysis

Entropy-based algorithms measure the degree of regularity to quantify complexity. The multiscale entropy (MSE) method overcomes the limitations of traditional entropy-based algorithms by considering nature of complexity at various scales [2]. The complexity at each scale is quantified by the sample entropy (SampEn) [13], which is obtained from a set of time series that are coarse-grained by scale factors τ. The SampEn values are then plotted over the scale factors to produce a MSE curve. Due to the finite length of real-world data, it is not feasible to assign a single complexity value from the MSE curves, but the curve profiles can be compared between normalized time series.

In this study, we use the same MSE parameters as in the previous studies [2, 3], i.e., the epoch length $m = 2$ and tolerance level $r = 0.15$. For hiPSC-CM aggregates we apply scale factors $1 \leq \tau \leq 10$.

3. Results and Discussion

3.1. ECG vs. cellular level

For healthy adults, our MSE analysis of RR intervals (from ECG) in Fig. 1(a) is in line with the previous studies. In particular, the result resembles the MSE profile (both the shape and magnitude) of healthy young subjects during sleep [2]. The MSE of the corresponding QT intervals in Fig. 1(a) is significantly smaller than that of RR for scales greater than five ($p<0.05$ by independent t-test). This reflects the deterministic components of the QT variability (QTV), possibly driven by HRV as a major physiological source of the QTV in the resting condition. A comparable result has been reported in Ref. [3]. The MSE curve of the QT intervals consists of two different regimes. At small scales (<5 in particular), the curve resembles that of the shuffled QT, indicating highly irregular QTV. At larger scales (>10), on the other hand, the profile of the curve is very similar to that of RR. The observation suggests that similar control mechanisms regulating HRV may be assumed for QTV at large scales.

The MSE analysis of IBIs and FPDs for healthy hiPSC-CM aggregates is shown in Fig. 1(b). At small scales (<5), the entropy values of IBI and FPD decrease monotonically, forming similar profiles as those of the shuffled series. The white noise-like irregularity may be due to hiPSC-CMs' immaturity and divergent expression levels of atrial, nodal, and ventricular cardiomyocytes [14]. Other factors such as differentiation techniques, age of the cells, and environmental variations may also introduce erratic variability in their beat rates. For scales larger than five beats, the IBI has a constant entropy over the scale, which is a characteristic for the "fractal" $1/f$ noise. Even though the entropy values are lower than those of the shuffled IBI, we expect an overturn at a larger scale, as long-range correlated IBIs would retain a constant entropy value, while uncorrelated shuffled series would have monotonically decreasing entropy over the scale. On the other hand, the MSE curve of FPDs closely follows that of the shuffled series over the scales up to ten beats. The result agrees well with our previous report [15], in which FPDs of hiPSC-CM aggregates were observed to have scaling exponents comparable to that of white noise at relatively small scales (<20 beats).

3.2. hiPSC-CMs by age and differentiation methods

The age and differentiation methods of hiPSC-CMs are factors that may affect the cell aggregates' beat rate dynamics. Figure 2 shows the MSE curves for IBI and FPD data, classified by those factors. The difference between the MSE curves is pronounced for IBIs. In particular, the IBI entropies of 26-day-old hiPSC-CM aggregates are significantly larger than the others ($p<0.05$ for scales >3 beats). The observation suggests that the complexity of the IBIs is higher for younger hiPSC-CMs, though no statistically significant difference is found in the entropy values between 47- and 70-day-old hiPSC-CMs.

Two older hiPSC-CM groups are differentiated with the END2 method. Both exhibit monotonically decreasing MSE profiles at short scales, contrary to that of 26-day-old hiPSC-CMs, which are differentiated with the SM method. Therefore, the significant difference in the entropy values may be due to different differentiation methods of the hiPSC-CMs. More systematic investigation is required to determine which factor is more responsible in determining the MSE profile and entropy values.

On the other hand, FPDs show no significant differences between different groups. The MSE profile follows that of the shuffled FPD, as already seen in Fig. 1(b). Therefore, neither age nor differentiation method affects the dynamics of FPDs in the defined scale.

3.3. Healthy vs. diseased hiPSC-CMs

The MSE is also evaluated for hiPSC-CMs derived from type-1 long-QT syndrome patients (LQT1-CMs) carrying the KCNQ1 (G589D) mutation. Figure 3 shows three cell groups of (i) healthy wild type (WT) and (ii) symptomatic and (iii) asymptomatic LQT1 cells. Here we use only the IBIs as they contain more interesting information than

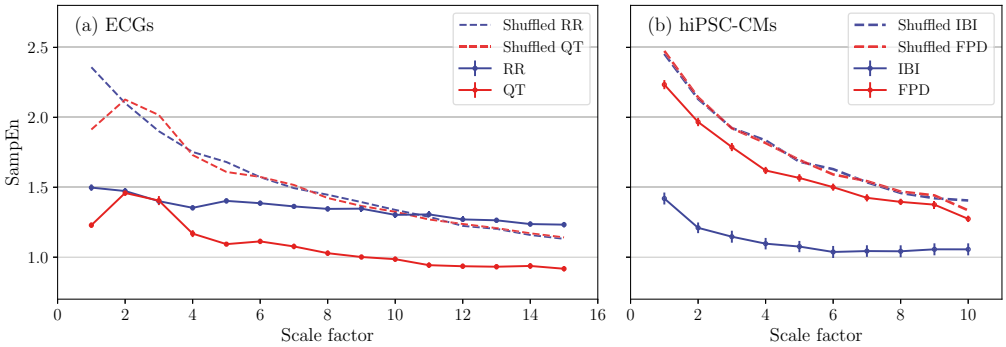

Figure 1. MSE analysis of (a) RR and QT intervals of ECGs and (b) IBIs and FPDs of hiPSC-CM aggregates. MSE analysis of shuffled, i.e., uncorrelated, times series (dashed lines) are included as references.

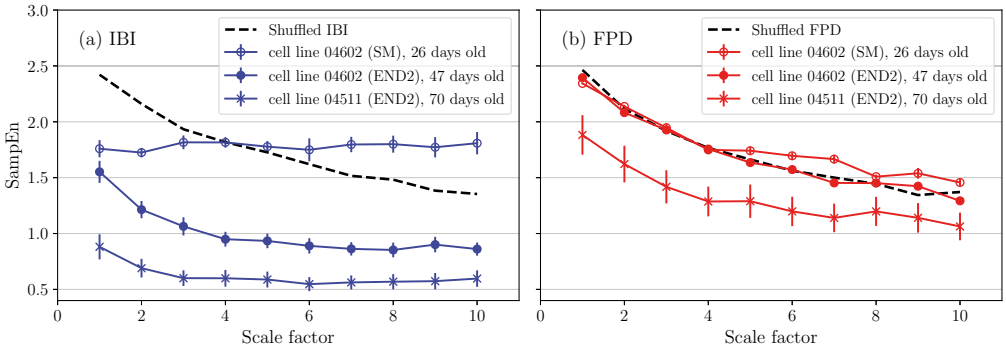

Figure 2. MSE curves of (a) IBI and (b) FPD, classified by their cell lines, differentiation methods, and age of the cells. The MSE curve of shuffled data is added in each plot as a reference. The averages of the curves are shown in Fig. 1 (b).

FPDs in the defined scale regime of fewer than ten beats. The hiPSC-CMs of all three groups are differentiated with the END2 method and have comparable ages ranging 30-45 days. Similar to the MSE profiles of 47- and 70-day-old hiPSC-CMs in Fig. 2 (a), all three curves in Fig. 3 share a common feature of monotonically decreasing entropy values over small scales (<5).

For scales larger than five beats, the entropy of symptomatic LQT1-CMs continues to decrease, while those of healthy and asymptomatic LQT1-CMs reach constant values. Thus, the beat rate dynamics of symptomatic LQT1-CMs seems to be less complex than that of healthy or asymptomatic LQT1-CMs at scales $5 \ldots 10$ beats. However, the MSE of symptomatic LQT1-CMs still contains a structure that persists over the scale, as it is clearly different from that of uncorrelated noise, represented by the shuffled series (dashed line in Fig. 3). The result indicates that the intrinsic complexity of the hiPSC-CMs can be altered by a diseased state of hiPSC-CMs. It is also in line with our previous study [16], which showed that symptomatic LQT1-CMs exhibit reduced short-term scaling exponents, while healthy and asymptomatic LQT1-CMs have scaling exponents close to $1/f$ noise throughout the scale.

4. Conclusion

We have characterized the complexity of beat rates and beat durations of hiPSC-CM aggregates using the MSE method. While RR-equivalent IBIs exhibit scale-invariant entropy values, especially for large scales greater than five consecutive beats, the MSE profiles of QT-equivalent

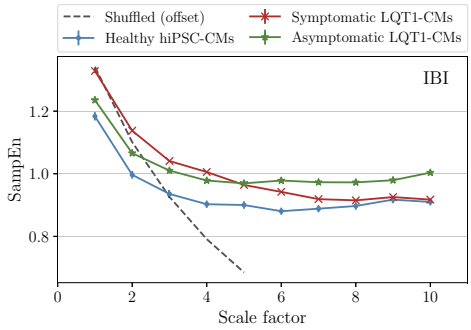

Figure 3. MSE analysis of IBIs of healthy, symptomatic and asymptomatic LQT1-CMs. All hiPSC-CMs are differentiated with the END2 method and aged 30-45 days. The reference MSE of shuffled data (dashed line) is offset to the overlap with other curves for easier comparison.

FPDs follow those of uncorrelated noise. This reflects the irregular nature of FPDs at small scales ($<$10 beats). We suggest that the age and differentiation method of hiPSC-CMs possibly affect the entropy values and profile of IBIs at short scales, though these factors do not affect the FPD results. The MSE analysis of healthy and LQT1 cells also shows that the diseased state of hiPSC-CMs leads to reduced complexity at short scales. The result suggests that the usefulness of the MSE method in studying other hereditary cardiac diseases that can be modeled by hiPSC-CMs.

References

[1] Costa M, Goldberger AL, Peng CK. Multiscale Entropy Analysis of Complex Physiologic Time Series. Physical Review Letters 2002;89(6):068102.

[2] Costa M, Goldberger AL, Peng CK. Multiscale Entropy Analysis of Biological Signals. Physical Review E 2005; 71(2):021906.

[3] Baumert M, Javorka M, Seeck A, Faber R, Sanders P, Voss A. Multiscale Entropy and Detrended Fluctuation Analysis of QT Interval and Heart Rate Variability During Normal Pregnancy. Computers in Biology and Medicine 2012; 42(3):347–352.

[4] Lewis M, Short A. Sample Entropy of Electrocardiographic RR and QT Time-Series Data During Rest and Exercise. Physiological Measurement 2007;28(6):731.

[5] Bari V, Valencia JF, Vallverdú M, Girardengo G, Marchi A, Bassani T, Caminal P, Cerutti S, George Jr AL, Brink PA, et al. Multiscale Complexity Analysis of the Cardiac Control Identifies Asymptomatic and Symptomatic Patients in Long QT Syndrome Type 1. PLoS One 2014;9(4):e93808.

[6] Goldberger AL, Amaral LA, Glass L, Hausdorff JM, Ivanov PC, Mark RG, Mietus JE, Moody GB, Peng CK, Stanley HE. Physiobank, Physiotoolkit, and Physionet: Components of a New Research Resource for Complex Physiologic Signals. Circulation 2000;101(23):e215–e220.

[7] Silva I, Moody GB. An Open-Source Toolbox for Analysing and Processing Physionet Databases in Matlab and Octave. Journal of Open Research Software 2014;2(1).

[8] Pan J, Tompkins WJ. A Real-Time QRS Detection Algorithm. IEEE Trans Biomed Eng 1985;32(3):230–236.

[9] Kiviaho AL, Ahola A, Larsson K, Penttinen K, Swan H, Pekkanen-Mattila M, Venäläinen H, Paavola K, Hyttinen J, Aalto-Setälä K. Distinct Electrophysiological and Mechanical Beating Phenotypes of Long QT Syndrome Type 1-Specific Cardiomyocytes Carrying Different Mutations. IJC Heart Vasculature 2015;8:19–31.

[10] Kuusela J, Kujala VJ, Kiviaho A, Ojala M, Swan H, Kontula K, Aalto-Setälä K. Effects of Cardioactive Drugs on Human Induced Pluripotent Stem Cell Derived Long QT Syndrome Cardiomyocytes. SpringerPlus 2016;5(1):234.

[11] Takahashi K, Tanabe K, Ohnuki M, Narita M, Ichisaka T, Tomoda K, Yamanaka S. Induction of Pluripotent Stem Cells from Adult Human Fibroblasts by Defined Factors. Cell 2007;131(5):861–872.

[12] Lian X, Zhang J, Azarin SM, Zhu K, Hazeltine LB, Bao X, Hsiao C, Kamp TJ, Palecek SP. Directed Cardiomyocyte Differentiation from Human Pluripotent Stem Cells by Modulating Wnt/β-Catenin Signaling Under Fully Defined Conditions. Nature Protocols 2013;8(1):162.

[13] Richman JS, Moorman JR. Physiological Time-Series Analysis Using Approximate Entropy and Sample Entropy. American Journal of Physiology Heart and Circulatory Physiology 2000;278(6):H2039–H2049.

[14] Altomare C, Pianezzi E, Cervio E, Bolis S, Biemmi V, Benzoni P, Camici GG, Moccetti T, Barile L, Vassalli G. Human-Induced Pluripotent Stem Cell-Derived Cardiomyocytes from Cardiac Progenitor Cells: Effects of Selective Ion Channel Blockade. EP Europace 2016; 18(suppl_4):iv67–iv76.

[15] Kim J, Shah D, Potapov I, Latukka J, Aalto-Setälä K, Räsänen E. Scaling and Correlation Properties of RR and QT Intervals at the Cellular Level. Scientific Reports 2018; Submitted.

[16] Kim J, Kuusela J, Aalto-Setälä K, Räsänen E. Short- and Long- Range Correlations in Beat Rate Variability of Human Pluripotent-Stem-Cell-Derived Cardiomyocytes. Computing 2017;44:1.

Address for correspondence:

Jiyeong Kim
Laboratory of Physics, Tampere University of Technology
Korkeakoulunkatu 10, 33720 Tampere
jiyeong.kim@tut.fi

PUBLICATION III

Scaling and correlation properties of RR and QT intervals at the cellular level

J. Kim, D. Shah, I. Potapov, J. Latukka, K. Aalto-Setälä, and E. Räsänen

Scientific Reports, vol. 9, no. 1, pp. 1–9
DOI: 10.1038/s41598-019-40247-9

SCIENTIFIC REPORTS

OPEN

Scaling and correlation properties of RR and QT intervals at the cellular level

Received: 5 September 2018
Accepted: 6 February 2019
Published online: 06 March 2019

Jiyeong Kim[1], Disheet Shah[2], Ilya Potapov[1], Joonas Latukka[1], Katriina Aalto-Setälä[2,3] & Esa Räsänen[1]

We study complex scaling properties of RR and QT intervals of electrocardiograms (ECGs) with their equivalences at the cellular level, that is, inter-beat intervals (IBI) and field potential durations (FPD) of spontaneously beating human-induced pluripotent stem cell-derived cardiomyocyte (hiPSC-CM) aggregates. Our detrended fluctuation analysis and Poincaré plots reveal remarkable similarities between the ECG and hiPSC-CM data. In particular, no statistically significant difference was found in the short- and long-term scaling exponents α_1 and α_2 of RR and QT intervals and their cellular equivalences. Previously unknown scaling properties of FPDs of hiPSC-CM aggregates reveal that the increasing scaling exponent of QT intervals as a function of the time scale, is an intrinsic feature at the cellular level.

In the last few decades, it has been shown that a healthy heart commonly exhibits fractal scaling (long-range correlations) in heart rate variability, i.e., variations in beat-to-beat RR intervals in electrocardiograms (ECGs)[1]. Alterations in the scaling properties have been observed in the case of cardiac diseases, such as congestive heart failure[2,3], myocardial infarction[4,5], atrial fibrillation[6], and dilated cardiomyopathy[7]. QT intervals also exhibit spontaneous beat-to-beat fluctuations[8] and QT variability has been an important measure in cardiac safety and drug development, because prolongation of QT intervals increases the risk of ventricular arrhythmias, such as Torsade de Pointes[9,10], and repolarisation lability[11]. On the other hand, relatively few studies have characterised the long-range scaling properties of QT intervals under different physical conditions[12–14].

Less is known about the beat-to-beat scaling properties at the cellular level. With the rise of human-induced pluripotent stem cell (hiPSC) technology[15], it is now possible to study the complex non-linear properties at the cellular level. Spontaneous contraction of hiPSC-derived cardiomyocyte (hiPSC-CM) aggregates produces a field potential comparable to an ECG waveform. In particular, peak-to-peak intervals in the field potential denoted here as interbeat intervals (IBIs) correspond to RR intervals, and field potential durations (FPDs) are equivalent to QT intervals[16–20].

Recently intrinsic power-law behaviour of IBIs of the isolated clusters of cardiomyocytes (CMs) has been characterised with one or two scaling exponents over predefined scale ranges[21–23]. In this study, we assess complex variabilities of IBI as well as FPD times series more in depth. To the best of our knowledge, scaling properties of FPDs of isolated CMs have never been investigated. Complex variabilities of RR and QT intervals of *in vivo* heart are also evaluated. Understanding the complex dynamics of IBIs and FPDs in comparison to the RR and QT variabilities is important in establishing hiPSC-CM aggregates as an ideal *in vitro* model of the human heart. Moreover, these studies provide new insights into the intrinsic QT-RR dynamics in the absence of the autonomic nervous system.

Methods

ECG recordings. Raw ECG recordings are obtained from the MIT-BIH Normal Sinus Rhythm database of PhysioNet[24]. RR and QT intervals are extracted using the PhysioNet algorithm[24] and other software[25–27]. Low quality signals and ectopic beats have been discarded (see Preprocessing). The final set of ECG data contain 18 RR and QT interval time series of 24 hours from healthy individuals of 13 women (age from 20 to 50 years) and 5 men (age from 26 to 45 years). The average length of RR and QT intervals is around 9800 beats.

[1]Computational Physics Laboratory, Tampere University, Tampere, Finland. [2]Heart Group, Faculty of Medicine and Health Technology, Tampere University, Tampere, Finland. [3]Heart Hospital, Tampere University Hospital, Tampere, Finland. Correspondence and requests for materials should be addressed to J.K. (email: jiyeong.kim@tuni.fi)

Cell culture and differentiation. Oral and written information of the study has been provided and a signed informed consent has been obtained from the participants. The study has been approved by the ethics committee of Pirkanmaa Hospital District to establish, culture, and differentiate the hiPSC lines (R08070). All experiments were carried out in accordance with following all relevant rules and regulations set by Tampere University. Healthy control hiPSCs were derived from skin fibroblasts of a 55-year-old female and a 44-year-old male (hiPSC lines UTA.04602.WT, UTA.04511.WT). Both subjects showed no detectable cardiac diseases when the skin biopsy was taken. The hiPSCs were generated and characterised as described by Takahashi *et al.*[28]. The hiPSCs were cultured and differentiated as previously described[29]. All the hiPSCs were genotyped to ensure that no major cardiac genetic disease mutations were present. A normality test on Graphpad Prism 8 software (GraphPad Software, Inc., USA) was conducted on the beating frequency and field potential duration of each sample to ensure the normally distributed population.

Multi-electrode array (MEA) measurements. Spontaneously beating cardiomyocyte (CM) aggregates (day 30–70) were manually dissected and plated on 1% gelatin-coated 6-well MEAs (Multichannel Systems, Reutlingen, Germany). Field potential signals were recorded from the CM aggregates under serum-free EB medium (knock-out DMEM, non-essential amino acids, GlutaMAX and penicilin/streptomycin) at 36 ± 1 °C at 10 kHz sampling frequency using MEA 1060-Inv-BC and MC_Rack software (Multichannel Systems, Reutlingen, Germany). The field potentials were continuously recorded for 30 minutes at the baseline. The data obtained from MEA were analysed using a custom-made analysis module in Origin2018 software (OriginLab Corporation, USA). The signals displaying the highest amplitudes, low signal-to-noise ratios, and clear repolarisation phases were chosen for the analysis.

Two parameters that were extracted were IBIs and FPDs. An IBI is defined as the time period between two consecutive depolarisation peaks. A FPD is defined as the time period measured from the first upstroke of the depolarisation wave to the baseline of the repolarisation wave. FPDs have been shown to correlate with APD90 from action potential measurements[16,20]. Both IBIs and FPDs were extracted using a custom-developed analysis module in Origin 2017 (MicroCal Origin™, USA), in which each upstroke of the depolarisation wave is detected as the start of a field potential, and the end of the field potential is calculated semi-automatically by detecting where the repolarisation decay phase intersects with the 0 μV line abscissa. The lengths of IBI and FPD time series range from 900 to 3000 beats with the average length around 1600 beats. The IBI and FPD data-sets are available from the corresponding author on reasonable request.

Preprocessing. Each time series was filtered before analysis in order to discard any artificial noises and ectopic beats. All the RR and QT intervals or their cellular equivalences below 200 and above 3000 ms were systematically discarded as nonphysical values. Then an appropriate envelope, or lower and upper limit, was selected around a global trend, so that the intervals outside the envelope were filtered out. The trend was calculated with a 5th order polynomial fit and twice the standard deviation of the time series was used for the envelope size, or limits.

Poincaré plot. A Poincaré plot is a standard method to measure and visualise the temporal correlation of a time series at the shortest time scale. For a given time series $\{x_t\}_{t=1,\ldots,N}$, each x_t is plotted against x_{t+1}. To characterise the distribution of the data points on the plane, an ellipse fitting technique[30] is employed. The standard deviation of the data points perpendicular to the line $x_t = x_{t+1}$, denoted as SD1, represents short-term variability of the data[31]. The standard deviation along the line $x_t = x_{t+1}$, denoted as SD2, reflects long-term variability, implied by the relation:

$$\mathrm{SD1}^2 + \mathrm{SD2}^2 = 2\sigma^2, \tag{1}$$

where σ is the standard deviation of the time series[31]. Equation 1 is equivalent to the statement that the sum of short-term and long-term variability is the total variability. SD1 and SD2 are computed from the eigenvalues of the covariance matrix between x_t and x_{t+1}.

A complementary measure to SD1 and SD2 is the Pearson's correlation coefficient r, which represents the linear correlation between time series x_t and x_{t+1}, defined by

$$r = \frac{\mathrm{cov}(x_t, x_{t+1})}{\sigma_{x_t}\,\sigma_{x_{t+1}}},$$

where cov stands for the covariance and σ is the standard deviation. The Pearson r ranges from -1 to 1, where values closer to 1 indicate positive linear correlation, and values closer to -1 indicate negative correlation.

Detrended fluctuation analysis. Detrended fluctuation analysis (DFA), originally introduced by Peng *et al.*[32], has been established as a reliable method to detect long-range correlation in a non-stationary time series. We follow the algorithms as described by Kantelhardt *et al.*[33]. The implementation of the algorithm has been validated against the PhysioNet DFA software package[24]; see section 1 of the supplementary information for more details. For a time series of length N with observations $\{x_t\}_{t=1,\ldots,N}$, the DFA procedure can be summarised in four steps:

1. The profile of the time series is defined by taking an integrated sum of the series:

$$y(k) = \sum_{t=1}^{k} (x_t - \langle x \rangle).$$

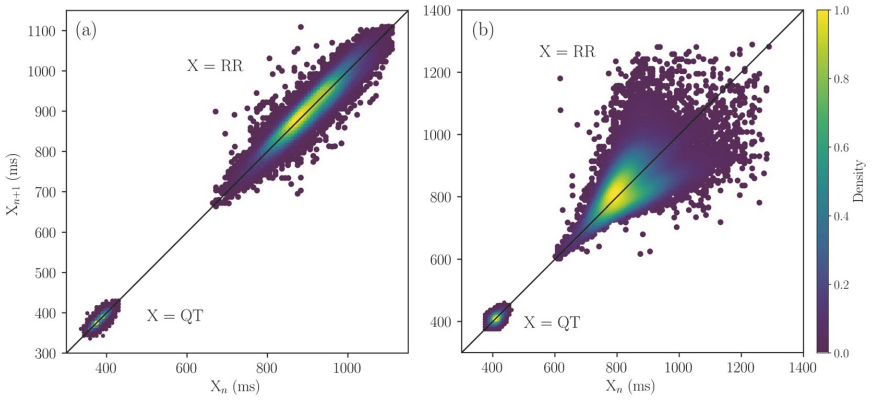

Figure 1. Examples of Poincaré plots of RR and QT intervals. A typical Poincaré plot for RR intervals has an elongated elliptical shape shown in (**a**). A few samples of RR interval time series has a fan-shaped plot shown in (**b**). Poincaré plots of QT intervals have smaller and rounder elliptical shapes, compared to those of RR. The density of the points is shown with a colour bar.

2. The profile is divided into N/s non-overlapping windows of equal length s. In each window, an n-degree polynomial approximation y_{tr} representing a local trend is computed by a least-squares fit. For our analysis we use the first-order DFA, in which a linear trend is eliminated from each window. When the windows does not divide the profile evenly, a reverse ordering of the window is averaged with the original ordering, so that the windows cover the whole profile.
3. The root-mean-square of the average variance of the residuals $(y - y_{tr})$ over all $2N/s$ windows defines the fluctuation F for window size s.

$$F(s) = \sqrt{\frac{1}{2N/s}\sum_{m=1}^{2N/s}\left[\frac{1}{s}\sum_{i=1}^{s}\left[y_m(i) - y_{tr,m}(i)\right]^2\right]} \tag{2}$$

The window sizes range from $s = 4$ to $s = N/4$.

4. In presence of power-law scaling, $F(s) \sim s^{\alpha}$. The scaling exponent α is the slope of $F(s)$ in log-log scale.

The scaling exponent α describes the nature of the correlation present in the data. The white noise with no correlation and Brown noise are characterised by $\alpha = 0.5$ and $\alpha = 1.5$, respectively. Values $0.5 < \alpha < 1.5$ indicate long-range correlation, and values $\alpha < 0.5$ correspond to anti-correlations. The value $\alpha = 1$ corresponds to $1/f$ or "pink" noise, often referred to as fractal.

More than one scaling exponents may be required to describe different correlations at different scales. It is a common practice to define two scaling exponents, α_1 and α_2, to describe short-range and long-range correlations, respectively. It is also possible to calculate the gradient of $F(s)$ as a function of s and define a spectrum $\alpha(s)$, also known as continuous α or local α. Here we use the $\alpha\beta$ filter[34], which is a simplified version of a Kalman filter, to recursively estimate a local least-squares fit for tracking the evolution of the gradient of $F(s)$ in log-log scale. The α spectrum provides a more complete description of complex correlation properties of a given time series than two scaling exponents with predefined scale ranges. Despite possible limitations of the $\alpha\beta$ filter, such as over-smoothing or under-smoothing of the gradient depending on the choice of its parameters, the method is sufficient for our purpose to assess the general scaling patterns of our time series data. The limitations may be overcome by advanced filtering techniques using other types of smoother based on Kalman filters[35].

Statistical analyses. Normality of the measures obtained from Poincaré analysis and DFA was checked with Shapiro-Wilk test. When comparing the measures between ECG and hiPSC-CM data Welch's t-test was employed to determine the statistical differences. If a variable did not meet the normality requirement for t-test, non-parametric Wilcoxon rank-sum test was employed. All the measures are presented in min-max, median, and interquartile range (Q1–Q3). Distributions of the measures are plotted in section 2 of the supplementary information.

Results

Quantitative analysis of Poincaré plots. Figure 1 shows the representative Poincaré plots of RR and QT intervals extracted from ECGs. Most of the RR intervals show a shape of an ellipse, as in Fig. 1(a), but 20% of the samples have a fan-like shape, which is spread out towards larger RR intervals, as shown in Fig. 1(b). Results are in line with the previous studies showing the Poincaré plots of RR intervals are spread along the line of identity[36].

The Poincaré plots of the corresponding QT intervals, also shown in Fig. 1 in the same time scale, have elliptical shapes along the line of identity, but with less eccentricity and variation, compared to those of the RR intervals.

Measures	ECG, RR ($n=18$)	hiPSC-CMs, IBI ($n=21$)	p-value
	min-max, median, (Q1–Q3)	min-max, median, (Q1–Q3)	
Mean (ms)	871–1830	703–2383	0.0207
	1092	**1400**	
	(1044–1232)	(1178–1745)	
SD1/SD2 (n.u)	0.15–0.54	0.03–0.98	0.749
	0.28	**0.28**	
	(0.22–0.33)	(0.16–0.45)	
Pearson's r (n.u)	0.55–0.96	−0.02–1.00	0.483
	0.85	**0.85**	
	(0.80–0.91)	(0.67–0.95)	
Measures	**ECG, QT ($n=18$)**	**hiPSC-CMs, FPD ($n=20$)**	**p-value**
	min-max, median, (Q1–Q3)	**min-max, median, (Q1–Q3)**	
Mean (ms)	377–501	394–1529	<0.001
	419	**902**	
	(406–434)	(764–982)	
SD1/SD2 (n.u)	0.21–0.83	0.13–0.98	0.023
	0.45	**0.72**	
	(0.35–0.67)	0.53–0.88	
Pearson's r (n.u)	0.19–0.92	−0.15–0.97	0.015
	0.66	**0.32**	
	(0.38–0.78)	(0.08–0.56)	

Table 1. Standard measures of the Poincaré plots of RR and QT intervals represented by min-max, median, and interquartile range (Q1–Q3). The values are obtained over $n=18$ ECG samples, and those of IBIs and FPDs of the hiPSC-CM aggregates, obtained over $n=21$ IBI and $n=20$ FPD time series. p-values are computed using independent two-sample t-test.

The standard quantitative measures to characterise the poincaré plots, averaged over 18 control ECG recordings, are listed in Table 1.

Figure 2 and Table 1 show the Poincaré plots and the related measures of IBI and FPD time series of the hiPSC-CM aggregates, which correspond to RR and QT interval times series of ECGs. Each Poincaré plot Fig. 2(a) is plotted for the IBI time series, measured from a cell aggregate in each well, labelled as A, B, C, D, E, and F on a six-well MEA. The Poincaré plots in Fig. 2(b) are plotted for the corresponding FPD time series.

The IBI and FPD values vary considerably among the aggregates. The hiPSC-CM aggregates tend to behave more erratically as they contract spontaneously without any inputs from the autonomous nervous system. Their beat-to-beat variations are also extremely sensitive to small fluctuations in the environment, e.g., in the temperature, pressure, oxygen levels, and ion concentration. Consequently, the absolute measures of SD1 and SD2 have large variances. In order to make the visual comparison of the Poincaré plots among the aggregates easier, we have normalised the data by subtracting the mean offset and scaling by the standard deviation, so that each Poincaré plot in Fig. 2 is centred at zero and comparable with each other in magnitude. Therefore, instead of computing SD1 and SD2 separately, we examine the ratio SD1/SD2 and Pearson's correlation coefficient r between the different groups, which are unaffected by the normalisation. There is a remarkable agreement between RR and IBI in SD1/SD2 and r, while a discrepancy exists between QT and FPD. The significantly larger SD1/SD2 (with statistical significance $p=0.023$) and smaller r ($p=0.015$) of the FPD Poincaré plots suggest that the FPD time series have significantly larger short-term variability with respect to the long-term variability.

Detrended fluctuation analysis. We first quantify two scaling exponents α_1 and α_2, which represent short-range and long-range correlations, respectively. In particular, α_1 is calculated in the time scale of less than 20 beats, α_2 in the scale of more than 30 beats. The α_1 and α_2 values of RR and QT intervals of ECGs and IBIs and FPDs of the hiPSC-CM measurements are visualised in Fig. 3. Each corner of the quadrilaterals corresponds to a scaling exponent. The mean α values are marked with bold lines and the spread of the values is shown in coloured bands. The means and standard deviations of the α_1 and α_2 values are also listed in Table 2.

Figure 3 allows us to compare the relative magnitudes of the α values from the shapes of the quadrilaterals. On the average, the quadrilateral for the hiPSC-CM aggregates resembles that of ECGs. The top sites of the quadrilaterals connecting the α_1 and α_2 of RR intervals and IBIs are flat, i.e., $\alpha_1 \approx \alpha_2 \approx 1$, suggesting that the fractal-like scaling property is invariant over the time scale. On the other hand, QT intervals have significantly different α_1 and α_2. The mean α_2 is close to one, indicating that QT intervals are long-range correlated as the RR intervals, while the mean α_1 is much closer to 0.5, indicating that the correlation properties resemble those of white noise in the short time scale. The scaling behaviour of FPDs is in notable agreement with that of QT intervals, with a small discrepancy in α_2 ($p=0.09$).

In further analysis, we examine the spectra of the scaling exponent α defined over a continuous time scale. The estimation of local α using the $\alpha\beta$ filter[34] produces a smooth spectrum, which depicts the evolution of the

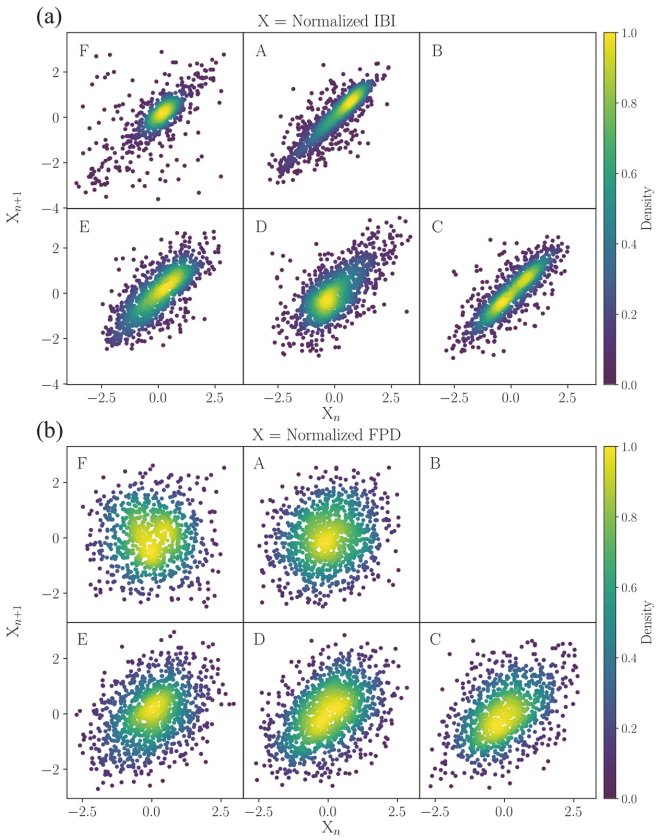

Figure 2. Poincaré plots of (**a**) IBI and (**b**) FPD time series extracted from the field potentials of the hiPSC-CM aggregates. The cell aggregates are plated on a six-well MEA with each well labelled as A, B, C, D, E, and F. Each Poincaré plot is centred at zero and scaled by the standard deviation. The density of the points is shown in colour.

scaling exponents over the scales from short-range to long-range. The left panel of Fig. 4 shows the characteristic scaling patterns of the α spectra of RR and QT intervals. The α spectra of RR intervals approach a constant value with increasing scale resulting $\alpha_1 \approx \alpha_2 \approx 1$. In contrast, the α spectra of QT intervals start at lower values and increase with scale, hence $\alpha_2 > \alpha_1$. Similar results have been shown in the case study of the heart rate variability during pregnancy[12].

Overall, Fig. 4 reveals notable similarities in the scaling patterns of ECGs and the hiPSC-CM aggregates. The hiPSC-CM aggregates tend to behave more erratically. Consequently, their α spectra are not as precise as those of ECGs. However, the scaling patterns observed in ECG, namely, the descending α spectra of RR intervals and the increasing α spectra of QT intervals, are clearly present in the spectra of hiPSC-CM aggregates. Unfortunately, the field potential measurements of the hiPSC-CM aggregates are limited in length to about 1600 intervals, so that the maximum window size in DFA is about 400 (see Methods). Therefore, we are not able to compare the spectra for larger scales than what is shown in Fig. 4. This result, however, already shows that the scaling properties in beat rates of the hiPSC-CM aggregates are well comparable to those of ECGs.

Discussion

Our quantitative analysis reveals that RR intervals and their *in vitro* equivalent from hiPSC-CM aggregates (IBIs) share a common geometry in Poincaré plots with a positive linear correlation between two consecutive beats. Quantitative measures according to the ellipse fitting technique[30] show that the ratio of short-term to long-term variabilities is consistent between the ECGs and the hiPSC-CM data. Therefore, clusters of hiPSC-CMs exhibit beat rate dynamics comparable to a human heart. This has also been confirmed in previous studies[21,22]. On the other hand, there is a significant difference between the hiPSC-CM aggregates and human hearts in variations of the field potential durations, i.e., QT intervals and FPDs. The ratio of short-term to long-term variability is larger in FPDs. This may be due to the erratic and immature nature of the hiPSC-CMs, causing random fluctuations

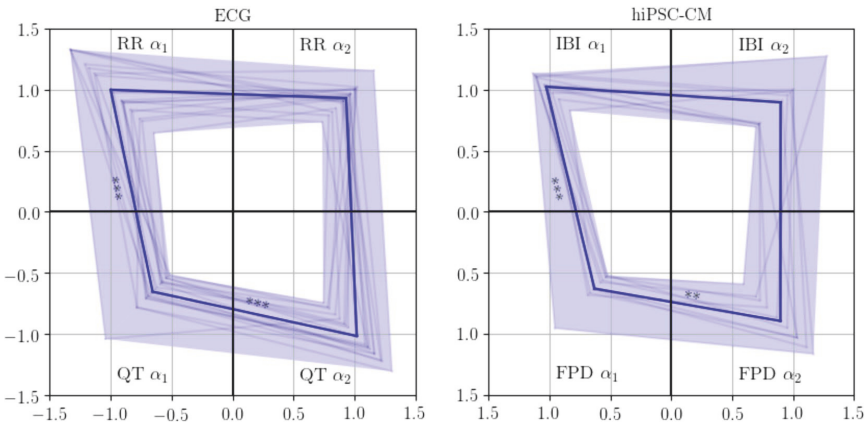

Figure 3. Visualisation of the DFA α_1 in the time scale of beats <20 and α_2 in the scale of beats >30 for ECGs (left panel, $N=18$) and hiPSC-CM aggregates (right panel, $N=10$), respectively. Each corner of the quadrilateral corresponds to an α value. The mean value is marked with bold line, and the statistical significance of the difference in the α values are denoted with asterisks with following significance level: $*p<0.05$, $**p<0.01$, and $***p<0.001$.

ECG ($n=18$)		hiPSC-CMs ($n=10$)		
	min-max, median, (Q1–Q3)		**min-max, median, (Q1–Q3)**	**p-value**
RR α_1	0.64–1.33	IBI α_1	0.83–1.14	0.730
	0.94		**1.03**	
	(0.85–1.17)		(0.98–1.11)	
RR α_2	0.73–1.16	IBI α_2	0.69–1.28	0.516
	0.94		**0.93**	
	(0.90–0.99)		(0.72–0.99)	
QT α_1	0.52–1.04	FPD α_1	0.52–0.96	0.362
	0.63		**0.60**	
	(0.57–0.70)		(0.54–0.66)	
QT α_2	0.74–1.31	FPD α_2	0.59–1.17	0.090
	1.05		**0.91**	
	(0.89–1.15)		(0.74–1.03)	

Table 2. Min-max, median, and interquartile range (Q1–Q3) of the DFA scaling exponents α_1 and α_2 for ECGs ($n=18$) and the hiPSC-CM aggregates ($n=10$). Independent two sample t-tests and Wilcoxon rank-sum test are performed between α values of ECGs and hiPSC-CM aggregates to obtain p-values. High p-values indicate that the values are drawn from a same distribution, hence, similar.

between consecutive beats. However, as it did not affect the IBIs in the same way, the reason may be found in the non-trivial relationship between QT and RR intervals (see below).

The complexity of the RR and QT variabilities and their equivalences at the cellular level is further examined in their longer-range scaling properties. The conventional way to compute short- and long-term scaling exponents α_1 and α_2 in two predefined scales shows a remarkable agreement between RR intervals and IBIs (Fig. 3 and Table 2). The results are in line with previous reports[3,21,22]. Here, more complete descriptions of the scaling properties are given by the full spectra of the scaling exponents. The α spectra of RR and QT in Fig. 4 are in good agreement with results from previous studies[12,34].

The α spectra of IBI and FPD, reported here for the first time, show a notable similarity with the RR and QT intervals of the ECG data. The overall resemblance implies that the distinct scaling patterns of RR and QT intervals are independent of the autonomous regulation of the nervous system, as it is also present in the isolated hiPSC-CM aggregates without any external stimulation. The α spectra of the FPDs stay at low scaling exponents, but the increasing trend towards larger scales–similar to that of the QT intervals–is present. The less prominent long-range correlation may be due to the different QT-RR relationship at the cellular level.

In a normal heart, QT variability is often described in the context of heart rate variability, because the variability in RR intervals is the major physiological source of variability in QT intervals[8]. There is a clear response of QT to the acceleration and deceleration of the heart rate[37]. Moreover, recent studies have shown that there is

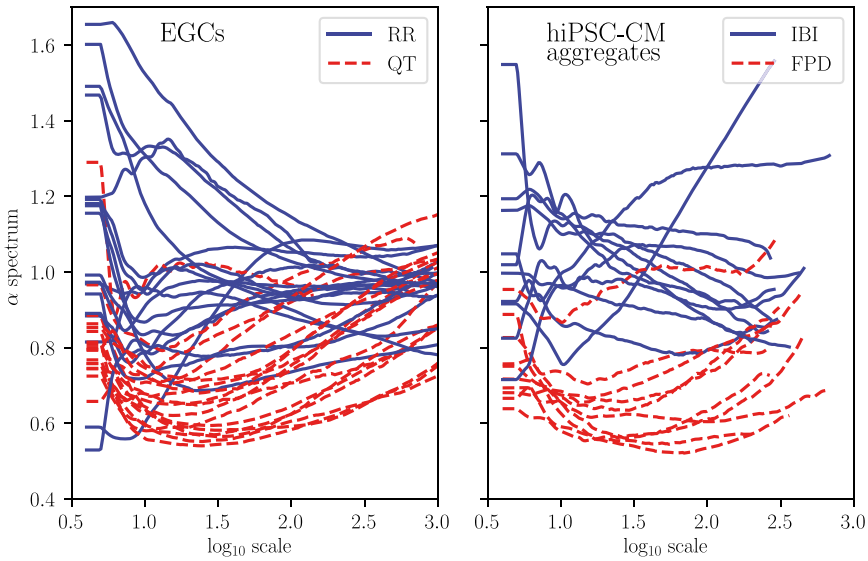

Figure 4. Continuous spectra of α of RR and QT intervals (left) and IBIs and FPDs (right) over the log scales. Local αs are estimated using the $\alpha\beta$ filter[34].

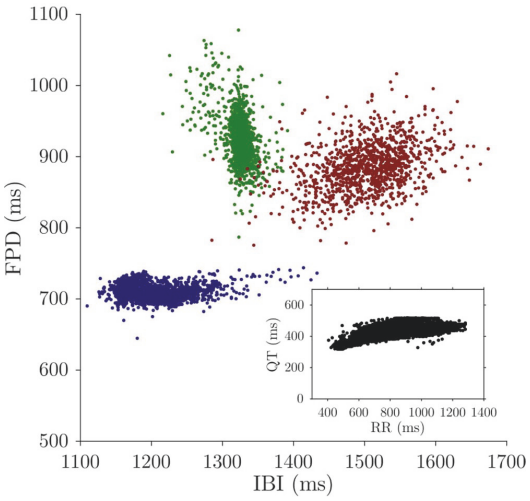

Figure 5. Non-trivial relationship between IBI and FPD. Each colour represents an hiPSC-CM aggregate. FPDs do not necessarily have a positive correlation with IBIs, which is found in a typical QT-RR relationship, shown in the inset.

a non-trivial dynamic relationship in terms of transfer entropy between RR and QT intervals[38]. The relationship is not as clear at the cellular level; FPDs do not necessarily have a positive correlation with IBIs, contrary to the well-known QT-RR relationship (See Fig. 5). Therefore, the discrepancies that appear only for FPDs but not IBIs, such as lower scaling exponents and relatively large short- to long-term variability ratio of FPDs, depicted by the Poincaré plots above, may be due to the less significant influence of IBIs on FPD variability compared to that of RR interval changes on QT variability.

The spontaneously beating hiPSC-CMs are relatively immature cells, which better represent a fetal heart with an underdeveloped contraction machinery and organised structural filaments, when compared to adult cardiomyocytes[39]. Even though the hiPSC-CMs have an expression of similar panel of ion channels as adult

cardiomyocytes, they may have divergent expression levels of atrial, nodal, and ventricular cardiomyocytes[40]. The varying expression levels and other factors, such as differentiation techniques, age of the cells, variations in temperature and ion concentrations in the recording solutions, and recording protocols may introduce erratic variability in the beat rates of hiPSC-CM aggregates. Therefore, the interpretation of the results must be practised with caution. However, our results show that the beating dynamics of the hiPSC-CM aggregates resemble those of *in vivo* heart, despite their relative immaturity and the absence of the autonomic neural input.

Even though the hiPSC-CM aggregates were derived from only two subjects, we assume they are independent, as there are many factors in culture and differentiation process of the hiPSCs that introduce variations among cells, such as passage number, age of the cells, and batch of cultures and differentiation. After the cardiac differentiation, different cell types (nodal, atrial, and ventricular), various sizes and number of beating cells in the culture further give rise to variations among the cell aggregates.

A recent study has suggested that in the presence of inter-cellular connections along with electro-mechanical interactions, intrinsic clock-like signalling of the pacemaker cells in sinoatrial node tissues, which are similar to hiPSC-CM aggregates *in vitro*, adapts and modifies their beat dynamics, contributing to the overall fractal-like behaviour of the heart[41]. Therefore, our findings support the idea that hiPSC-CM aggregates could be an ideal *in vitro* model of a heart, i.e., a suitable platform (i) to model cardiac diseases, (ii) to screen new treatment options, and (iii) to assess cardiac safety of new chemical entities of potential new drug candidates.

Fractality and power-law behaviour of IBIs have been attributed to ion-channel gating and intra-cellular mechanisms that are themselves non-linear processes. In an adult CM, variation in intra-cellular Ca^{2+} is the main trigger for excitation-contraction coupling, which generates mechanical contraction. Due to immaturity, the Ca^{2+} transient is slower and smaller in amplitude for hiPSC-CMs[42], but is clearly present and closely related to the beat rate variability (BRV) of hiPSC-CM aggregates. In particular, the intra-cellular sarcoplasmic reticulum (SR) Ca^{2+} cycling and mitochondrial Ca^{2+} extrusion, and the crosstalk between SR and mitochondria[43] exhibit fractal behaviour, hence contribute to the fractal BRV at the cellular level[22,44].

Intra-cellular Ca^{2+} cycling, among other cellular processes, also contributes to the beat-to-beat variation of the overall repolarisation, which causes variations in QT intervals at a stationary heart rate[8]. Therefore, we may postulate that the fractal behaviour of the intra-cellular Ca^{2+} cycling is also accountable for the intrinsic fractal scaling of FPDs in hiPSC-CM aggregates. There are also other factors, such as stochastic fluctuations in ion currents and inter-cellular interactions that cause variations in QT intervals. Similar effects may be present also in FPDs, which calls for further systematic investigations.

Other standard HRV time- and frequency-domain measures are available in the section 3 of the supplementary information.

References

1. Goldberger, A. L. *et al*. Fractal dynamics in physiology: alterations with disease and aging. *Proc. national academy sciences* **99**, 2466–2472 (2002).
2. Ho, K. K. *et al*. Predicting survival in heart failure case and control subjects by use of fully automated methods for deriving nonlinear and conventional indices of heart rate dynamics. *Circulation* **96**, 842–848 (1997).
3. Peng, C.-K., Havlin, S., Stanley, H. E. & Goldberger, A. L. Quantification of scaling exponents and crossover phenomena in nonstationary heartbeat time series. Chaos: An Interdiscip. *J. Nonlinear Sci.* **5**, 82–87 (1995).
4. Huikuri, H. V. *et al*. Fractal correlation properties of RR interval dynamics and mortality in patients with depressed left ventricular function after an acute myocardial infarction. *Circulation* **101**, 47–53 (2000).
5. Mäkikallio, T. H. *et al*. Heart rate dynamics before spontaneous onset of ventricular fibrillation in patients with healed myocardial infarcts. *The Am. journal cardiology* **83**, 880–884 (1999).
6. Rodriguez, E., Lerma, C., Echeverria, J. & Alvarez-Ramirez, J. ECG scaling properties of cardiac arrhythmias using detrended fluctuation analysis. *Physiol. measurement* **29**, 1255 (2008).
7. Mahon, N. G. *et al*. Fractal correlation properties of R-R interval dynamics in asymptomatic relatives of patients with dilated cardiomyopathy. *Eur. journal heart failure* **4**, 151–158 (2002).
8. Baumert, M. *et al*. QT interval variability in body surface ECG: measurement, physiological basis, and clinical value: position statement and consensus guidance endorsed by the european heart rhythm association jointly with the esc working group on cardiac cellular electrophysiology. *Europace* **18**, 925–944 (2016).
9. Gilmour, R. F. *et al*. Time-and rate-dependent alterations of the QT interval precede the onset of torsade de pointes in patients with acquired QT prolongation. *J. Am. Coll. Cardiol.* **30**, 209–217 (1997).
10. Kay, G. N. *et al*. Torsade de pointes: the long-short initiating sequence and other clinical features: observations in 32 patients. *J. Am. Coll. Cardiol.* **2**, 806–817 (1983).
11. Atiga, W. L. *et al*. Beat-to-beat repolarization lability identifies patients at risk for sudden cardiac death. *J. cardiovascular electrophysiology* **9**, 899–908 (1998).
12. Baumert, M. *et al*. Multiscale entropy and detrended fluctuation analysis of QT interval and heart rate variability during normal pregnancy. *Comput. biology medicine* **42**, 347–352 (2012).
13. Perkiomaki, J. S., Couderc, J.-P., Daubert, J. P. & Zareba, W. Temporal complexity of repolarization and mortality in patients with implantable cardioverter defibrillators. *Pacing clinical electrophysiology* **26**, 1931–1936 (2003).
14. Lewis, M., Short, A. & Suckling, J. Multifractal characterisation of electrocardiographic RR and QT time-series before and after progressive exercise. *Comput. methods programs biomedicine* **108**, 176–185 (2012).
15. Yamanaka, S. Induced pluripotent stem cells: past, present, and future. *Cell stem cell* **10**, 678–684 (2012).
16. Hayakawa, T. *et al*. Image-based evaluation of contraction-relaxation kinetics of human-induced pluripotent stem cellderived cardiomyocytes: Correlation and complementarity with extracellular electrophysiology. *J. molecular cellular cardiology* **77**, 178–191 (2014).
17. Asakura, K. *et al*. Improvement of acquisition and analysis methods in multi-electrode array experiments with iPS cell-derived cardiomyocytes. *J. pharmacological toxicological methods* **75**, 17–26 (2015).
18. Yamamoto, W. *et al*. Electrophysiological characteristics of human iPSC-derived cardiomyocytes for the assessment of drug-induced proarrhythmic potential. *PloS one* **11**, e0167348 (2016).
19. Nozaki, Y. *et al*. Availability of human induced pluripotent stem cell-derived cardiomyocytes in assessment of drug potential for QT prolongation. *Toxicol. applied pharmacology* **278**, 72–77 (2014).
20. Clements, M. & Thomas, N. High-throughput multi-parameter profiling of electrophysiological drug effects in human embryonic stem cell derived cardiomyocytes using multi-electrode arrays. *Toxicol. Sci.* **140**, 445–461 (2014).

21. Mandel, Y. *et al*. Human embryonic and induced pluripotent stem cell–derived cardiomyocytes exhibit beat rate variability and power-law behavior. *Circulation* **125**, 883–893 (2012).
22. Ben-Ari, M. *et al*. From beat rate variability in induced pluripotent stem cell–derived pacemaker cells to heart rate variability in human subjects. *Hear. Rhythm.* **11**, 1808–1818 (2014).
23. Kuusela, J., Kim, J., Räsänen, E. & Aalto-Setälä, K. The effects of pharmacological compounds on beat rate variations in human long QT-syndrome cardiomyocytes. *Stem Cell Rev. Reports* **12**, 698–707 (2016).
24. Goldberger, A. L. *et al*. PhysioBank, PhysioToolkit, and PhysioNet: Components of a new research resource for complex physiologic signals. *Circulation* **101**, e215–e220, https://doi.org/10.1161/01.CIR.101.23.e215 (2000).
25. Silva, I. & Moody, G. B. An open-source toolbox for analysing and processing physionet databases in matlab and octave. *J. open research software* **2** (2014).
26. Pan, J. & Tompkins, W. J. A real-time QRS detection algorithm. *IEEE transactions on biomedical engineering* **32.3**, 230–236 (1985).
27. Laguna, P., Jané, R. & Caminal, P. Automatic detection of wave boundaries in multilead ECG signals: Validation with the cse database. *Comput. biomedical research* **27**, 45–60 (1994).
28. Takahashi, K. *et al*. Induction of pluripotent stem. *cells from adult human fibroblasts by defined factors. cell* **131**, 861–872 (2007).
29. Kuusela, J. *et al*. Effects of cardioactive drugs on human induced pluripotent stem cell derived long QT syndrome cardiomyocytes. *Springerplus* **5**, 234 (2016).
30. Tulppo, M. P., Makikallio, T., Takala, T., Seppanen, T. & Huikuri, H. V. Quantitative beat-to-beat analysis of heart rate dynamics during exercise. *Am. journal physiology-heart circulatory physiology* **271**, H244–H252 (1996).
31. Brennan, M., Palaniswami, M. & Kamen, P. Do existing measures of poincare plot geometry reflect nonlinear features of heart rate variability? *IEEE transactions on biomedical engineering* **48**, 1342–1347 (2001).
32. Peng, C.-K. *et al*. Mosaic organization of DNA nucleotides. *Phys. review e* **49**, 1685 (1994).
33. Kantelhardt, J. W., Koscielny-Bunde, E., Rego, H. H., Havlin, S. & Bunde, A. Detecting long-range correlations with detrended fluctuation analysis. *Phys. A: Stat. Mech. its Appl.* **295**, 441–454 (2001).
34. Echeverria, J. *et al*. Interpretation of heart rate variability via detrended fluctuation analysis and ab filter. Chaos: An Interdiscip. *J. Nonlinear Sci.* **13**, 467–475 (2003).
35. Molkkari, M. *et al*. Robust estimation of the scaling exponent in detrended fluctuation analysis of beat rate variability. *Computing in Cardiology* **45** (2018).
36. Huikuri, H. V. *et al*. Abnormalities in beat-to-beat dynamics of heart rate before the spontaneous onset of life-threatening ventricular tachyarrhythmias in patients with prior myocardial infarction. *Circulation* **93**, 1836–1844 (1996).
37. Cabasson, A., Meste, O. & Vesin, J.-M. Estimation and modeling of QT-interval adaptation to heart rate changes. *IEEE transactions on biomedical engineering* **59**, 956–965 (2012).
38. Potapov, I. *et al*. Information transfer in QT-RR dynamics: Towards a model-free QT correction method. *Sci. Reports* **8**, 14992 (2018).
39. Robertson, C., Tran, D. D. & George, S. C. Concise review: maturation phases of human pluripotent stem cell-derived cardiomyocytes. *Stem cells* **31**, 829–837 (2013).
40. Altomare, C. *et al*. Human-induced pluripotent stem cell-derived cardiomyocytes from cardiac progenitor cells: effects of selective ion channel blockade. *EP Eur.* **18**, iv67–iv76 (2016).
41. Yaniv, Y. *et al*. Synchronization of sinoatrial node pacemaker cell clocks and its autonomic modulation impart complexity to heart beating intervals. *Hear. Rhythm.* **11**, 1210–1219 (2014).
42. Veerman, C. C. *et al*. Immaturity of human stem-cell-derived cardiomyocytes in culture: fatal flaw or soluble problem? *Stem cells development* **24**, 1035–1052 (2015).
43. Yaniv, Y. *et al*. Crosstalk between mitochondrial and sarcoplasmic reticulum Ca2+ cycling modulates cardiac pacemaker cell automaticity. *PloS one* **7**, e37582 (2012).
44. Binah, O., Weissman, A., Itskovitz-Eldor, J. & Rosen, M. R. Integrating beat rate variability: from single cells to hearts. *Hear. Rhythm.* **10**, 928–932 (2013).

Acknowledgements

This project would not have been possible without the kind help form Markus Haponen, Henna Lappi for their technical expertise with the stem cell culture and cardiac differentiation. The project is supported by the Finnish Academy of Science and Letters, Academy of Finland (key project 304458: Health tracking through fractal analysis of complex signals), Aarne Koskelo Foundation, Tampere University of Technology graduate school grant, and University of Tampere graduate school grant. The authors acknowledge the Tampere facility of electrophysiological measurements for their service.

Author Contributions

E.R. and K.A. conceived the project, D.S. performed the experiments, J.K., I.P., and J.L., analysed the results. J.K. wrote the paper and all authors reviewed the manuscript.

Additional Information

Supplementary information accompanies this paper at https://doi.org/10.1038/s41598-019-40247-9.

Competing Interests: The authors declare no competing interests.

Publisher's note: Springer Nature remains neutral with regard to jurisdictional claims in published maps and institutional affiliations.

PUBLICATION IV

Beat rate variability in human cardiomyocytes during hypoxia and reperfusion

J. Kim, D. Shah, M. Molkkari, A. Lönnrot, K. Aalto-Setälä, and E. Räsänen

PLOS One, Submitted